UNIVERSITÀ DEGLI STUDI DI PADOVA

Dipartimento di Fisica e Astronomia "Galileo Galilei"

Corso di Laurea Magistrale in Fisica

Tesi di Laurea

Infrared Production of Gravitinos

Relatore

Dr. Francesco D'Eramo

Controrelatore

Prof. Marco Peloso

Laureando

Andrea Marzo

Anno Accademico 2019/2020

A Ricca

Abstract

According to observations, most matter density of our Universe is dark. Efforts have been done to explain this excess, ranging from alternative theories of gravity, to the introduction of new particles and many other exotic suggestions. Nowadays most of the scientific community agrees on the fact that dark matter is at least partially made of a new particle species, underlying the presence of new physics beyond the Standard Model. In this work we present a possible solution to the dark matter dilemma, showing how *gravitino* can be a good particle candidate solving the problem. Exploiting the properties of this particular particle, we show under what assumptions *freeze-in* mechanism could be the appropriate mechanism for gravitino relic density achievement. We focus on the consequences of a non-instantaneous reheating process on the gravitino relic density production, recovering and extending already existing works, showing under what assumptions this process is still able to solve the dark matter problem.

Contents

Introduction

Recent observations suggest that most matter density of the Universe is non-ordinary, i.e. it is not ascribable to SM particle content. Possible candidates have been proposed to explain this excess of matter density, along with mechanisms that could generate a sufficient relic density of a particular particle species, which although very interesting and promising, did not find any experimental confirmation by far.
In this thesis we explore a possible origin of the excess in matter density as a consequence of the realization of supersymmetry in nature, implying the existence of new particles, with particular interest for the gravitino. We review an alternative infrared dominated mechanism of dark matter production, *freeze-in*, and we show how frozen-in gravitino could in principle account for dark matter relic density.
In chapter 1 we review the experimental observations that since the '30s led to the conclusion that most matter content of the universe must be dark, starting from Zwicky observation of nebulae velocity dispersion, arriving to latest cosmological Planck observations. We list expected properties of dark matter particles, based on observations and general principles. In conclusion we review the long-studied *freeze-out* mechanism for dark matter relic density production.
In chapter 2 we briefly review the basic concepts of supersymmetry, which we'll not take for granted throughout this work. We review the simple case of global supersymmetry, with particular interest to possible ways to break the symmetry so to match observations. We move to local supersymmetry, introducing the gravitational supermultiplets that includes the *gravitino*, and we show how through the super-Higgs mechanism the gravitino acquires mass and two additional helicity modes by 'eating' the goldstino.
In chapter 3 we explore the cosmological implication of the existence of the gravitino, focusing on the case in which it is the LSP, the interesting case for this thesis. We show possible ways of producing gravitinos in the early universe, extending the results to the case of non-instantaneous reheating process. We then explain the main two possible problems arising when gravitino LSP is included in particle spectrum of the theory, namely *gravitino overproduction problem* and the spoilage of BBN results.
In chapter 4 we present the alternative mechanism of dark matter relic density production, freeze-in, showing its general features, focusing only on the case of bath particles decay-produced dark matter, which we'll apply to the gravitino case. In particular, we show the final yield dependence on the parameter of the theory, and set the parameter space region in which freeze-in is active and dominating on other mechanisms. We show the constraints to have an infrared final yield, and we generalize the mechanism to the case of non-instantaneous reheating process.
In chapter 5, we apply the framework we have developed in the previous chapters to show how the freeze-in mechanism, involving sparticles decay to gravitino, could produce the sought-for dark matter relic density. In particular we show the dependence of the final yield on the mass spectra, and we focus on the interesting case of split spectra. We include the possibility of non-instantaneous reheating process, showing how the final result changes depending on the mass spectra of the theory.
In the last chapter we show the main result of this work, namely that gravitino freeze-in can in principle take place in most parameter space regions in the case of extremely split spectra, becoming the main way of gravitino production, independently on the reheating temperature.

Chapter 1

How We Know Dark Matter is There

Observation of the Universe is not a recent development of human knowledge. The first rudimental *cosmological models* are found in ancient Greek and Indian knowledge, depicting the universe as static and geocentric. According to Hindu purainc view, the universe experiences the ciclicity of time, being created, destroyed and re-created during a Brahma's day, lasting 4.32 billion years, which is incredibly comparable to cosmological time. These models though presented some inconsistencies, such as the presence of comets, which clearly couldn't fit the static picture. Such evidences against an *Aristotelian* model were attributed to atmospheric phenomena until 1577, when Tycho Brahe's observation of absence of parallax in comet events, put an end to geocentric static models, and opened the path to heliocentric modern models.
Crucial observations to dismantle Aristotelian model came with Galileo who, among other brilliant discoveries, observed a huge amount of stars like the Sun and four Jupiter satellites, that would have remained unobservable without the development of the telescope.

With the advent of Newtonian dynamics and law of gravitation, two powerful means were added to the observational ability of astronomers.

In 1844, F. Bessel argued the existence of unseen objects just by using the powerful tools of Newtonian gravity, in order to explain anomalies in the motion of Sirius and Procyon stars: for the first time the existence of astronomical objects was inferred by the application of laws of nature.
This was not the only occasion in which the presence of astronomical objects was predicted before their observation: others famous examples are the discovery of Uranus and the observation of the precession of Mercury's perihelion; nevertheless in the latter case the discrepancy was not due to the presence of a perturbing new object, but to our lack of comprehension of gravity, as the solution came with Einstein's general theory of relativity.

Nowadays astronomers and cosmologists have available much more sophisticated meas of observation and the powerful general theory of relativity, therefore deeper regions of the Universe are accessible to observations, and many phenomena they observe can find an explanation. Nevertheless there are still some mysteries that haunt the Universe to be solved. Among them, one is particularly intriguing and fascinating: that of dark matter.

First clues of the presence of non-luminous and hence unseen matter in galaxies, came with Lord Kelvin in his *'Baltimore lectures on molecular dynamics and the wave theory of light'* [1]. In one of these lectures, Lord Kelvin tried to estimate the Milky Way mass

based on velocity dispersion of stars, and he concluded:

'It is nevertheless probable that there may be as many as 1000 millions of stars within the distance $r = 3.09 \cdot 10^{16} km$ but many of them may be extinct and dark,and nine-tenths of them though not all dark may be not bright enough to be seen by us at their actual distance.'

In a later work, Poincaré addressed the missing matter as *dark matter*, although he disagreed with Lord Kelvin's conclusions.

In the last century, astronomical observations got better and better due to the development of new and already existing means of observation, and due to our better comprehension of the laws that govern our universe.
In this chapter we retrace the steps that led to the conclusion that most matter in the universe remains yet unknown.
Hints of the existence of unknown *dark matter* come from observations at all scales, from galactic scales up to clusters and cosmological scale.

1.1 Early observations

It's in 1933 that we have a first indirect evidence of missing matter, in Zwicky famous article [2]. The author analyzed the velocity dispersion of nebulae in the Coma cluster, showing that eight of them exhibit discrepancies with theoretical predictions based on luminous matter alone.

The average recession velocity of the Coma cluster was measured in the context of distance-redshift correlation study, and resulted to be $7500 km/s$.
On the other hand, by measuring the redshift of spectral lines of nebulae (namely the average of at least three, typically H- and K- lines and G-band), since the absorption line are affected by the same amount of redshift independently of their wavelength, one is able to determine the redshift and recession velocity of single nebulae.
In this way Zwicky reports the recession velocities of eight single nebulae in the Coma cluster showing that they range from $5100 km/s$ up to $8100 km/s$ (although it was not clear if one of them is part of the cluster or just projected onto it, in which case the lower velocity is $6000 km/s$, the final result not substantially changing) and he finally evaluated the nebulae velocity dispersion with respect to the average cluster velocity, showing that it it $\mathcal{O}(10^3 km/s)$

In order to explain such a large deviation from the average, Zwicky borrowed the virial theorem that was largely used in thermodynamics, and applied it to the Coma cluster system to come to his conclusions.
The theorem relates the time average of the kinetic and potential energy of a system of N particles, in a mechanically stationary configuration; in its general form it states

$$2\langle K \rangle_t = -\sum_{k=1}^{N} \langle \vec{F}_k \cdot \vec{r}_k \rangle_t, \tag{1.1}$$

where the sum spans over the particles that build the system, $\vec{F}_k$ being the force applied to particle k which is at position $\vec{r}_k$.
In the case of a gravitational potential, eq. (1.1) reduces to

$$\epsilon_k = -\frac{1}{2}\epsilon_p \tag{1.2}$$

where ϵ_k and ϵ_p are the kinetic and gravitational mean energy respectively per unit mass; moreover thanks to Birkhoff ergodic theorem, time averages can be substituted with ensemble averages, avoiding the need to wait for a long time.

With a cluster estimated radius of $R \sim 10^{24} cm$ and 800 single nebulae in the cluster, each of mass $M \sim 10^9 M_\odot$ (as suggested by Hubble), Zwicky estimated the cluster mass as

$$M_{cl} \sim 1.6 \cdot 10^{45} g \tag{1.3}$$

corresponding to a gravitational potential energy

$$\epsilon_p = -\frac{3}{5} G_N \frac{M_{cl}}{R} \sim -6.4 \cdot 10^{13} \frac{cm^2}{s^2}. \tag{1.4}$$

Using the virial theorem, one gets the averaged squared velocity

$$\epsilon_k = \frac{1}{2}\langle v^2 \rangle = -\frac{\epsilon_p}{2} \Rightarrow \sqrt{\langle v^2 \rangle} \sim 80 km/s. \tag{1.5}$$

In order to account for discrepancies of $\mathcal{O}(10^3 km/s)$, Zwicky argued that the Coma cluster average density should be ~ 400 times larger that the observed value so that

'If this should be verified, it would lead to the surprising result that dark matter exists in much greater density than luminous matter.'

Zwicky points out that even if the system is not stationary, but the potential energy is completely stored as kinetic energy, the result differs only by a factor 2, and the need for a larger matter density persists.

At the time, Zwicky used the Hubble constant value of $H_0 \sim 558$ km/s/Mpc, which we now know to be far from the measured value $H_0 = 67.66 \pm 0.42$ km/s/Mpc [14], hence Zwicky result overestimates the mass-to-light ratio by a factor ~ 8.3.

This result has been controversial; the author himself argued that in order to rightly extrapolate a Galaxy mass from the visible matter content, one has to know the microscopic objects, cold stars and gases presence in the Galaxy.

Moreover it was not clear if the virial theorem holds in the Coma cluster case, as the observed nebulae could be not permanent part of the cluster, but just passing-by objects, far from mechanical stationary equilibrium.
However if this was the case, one would expect the cluster to disassemble, resulting in hundreds of nebulae flying apart with large proper speeds. As a consequence one would expect to see such phenomena in the Universe, while velocities of single nebulae do not exceed 200km/s.

Zwicky also considers the effect due to gravitational redshift

$$\frac{\lambda_\infty}{\lambda_e} = \sqrt{\frac{g_{00}(r_\infty)}{g_{00}(r_e)}}$$

which in the weak field limit reduces to

$$\frac{\Delta\lambda}{\lambda} \sim -\frac{\epsilon_p}{c^2} \sim 3.5 \cdot 10^{-8} \tag{1.6}$$

which corresponds via $\frac{\Delta\lambda}{\lambda} = v/c$ to an apparent relative velocity $v \sim \mathcal{O}(10m/s)$ that cannot explain the observed velocity dispersion, and would suggest the presence of a larger amount of dark matter than predicted by virial theorem argument.

The questions about the presence of dark matter in galaxies remained controversial for many years, as for other indirect evidences of its presence we have to wait until the early '70.

1.2 Galaxy rotation curve

In the early '70 the extrapolation of Galaxies masses from luminous matter presence was not a substantial problem anymore, since astronomers could observe the 21 cm line of hydrogen in far galaxies; the mass distribution of galaxies was hence deducible from hydrogen presence. Also the determination of velocities could be inferred from redshift in H_α emission lines.
In the '70, two independent works, Freeman [3] and Rubin and Ford [4], studied the rotation curves, i.e. the orbital velocity of gas and stars as a function of the distance from galactic center, showing that dark matter is needed to stabilize the motion of galaxies (and not only for clusters, as already observed by Zwicky). Moreover thanks to improved spectroscopic measurements it was possible to resolve single stars in far galaxies.

According to keplerian motion and based on the visible matter presence in the galaxy, velocities of stars as a function of their distance from the center should be well approximated by the dynamical equilibrium equation:

$$GM(r) = v^2(r)r$$

where $M(r)$ is the mass encompassed by a sphere of radius r, namely $m(r) = 4\pi \int \rho(r) r^2 dr$. This in turn means that velocities should follow the law

$$v(r) \sim \sqrt{\frac{GM(r)}{r}} \sim \begin{cases} \sqrt{G}r & r \lesssim R \\ \sqrt{\frac{G}{r}} & r > R \end{cases} \tag{1.7}$$

where R denotes the galaxy bulk radius and we assumed a homogeneous matter density inside the bulk . This is a naive approximation of a real galaxy: in fact for instance, the shape of the visible matter distribution is far from being spherical, and a more complex behaviour is expected at small radii. Nevertheless this approximation is useful at large radii, when all the mass is encompassed by a sphere of radius r, as it gives an etimate of the total mass of the galaxy, which is what we'll be interested about.

In Freeman's article [3] observing M35 (*Triangulum Galaxy*) and NGC300 galaxies by means of photometry, the author reports that the peak in velocity is found to be at larger radii than expected assuming that luminous matter accounts for all matter density of the galaxy, without further questioning about the reason of the phenomena.

In their famous article, Rubin and Ford reported the rotation curves of Andromeda galaxy, up to 120 arcminutes (24 kpc) far from the galaxy center (larger radii than that of Freeman's work), aiming to measure the galactic mass.
Surprisingly, they got results in contrast with prediction of eq. (1.7), as shown by figure 1.1: rotation velocities are observed to rapidly increase up to their maximum value at

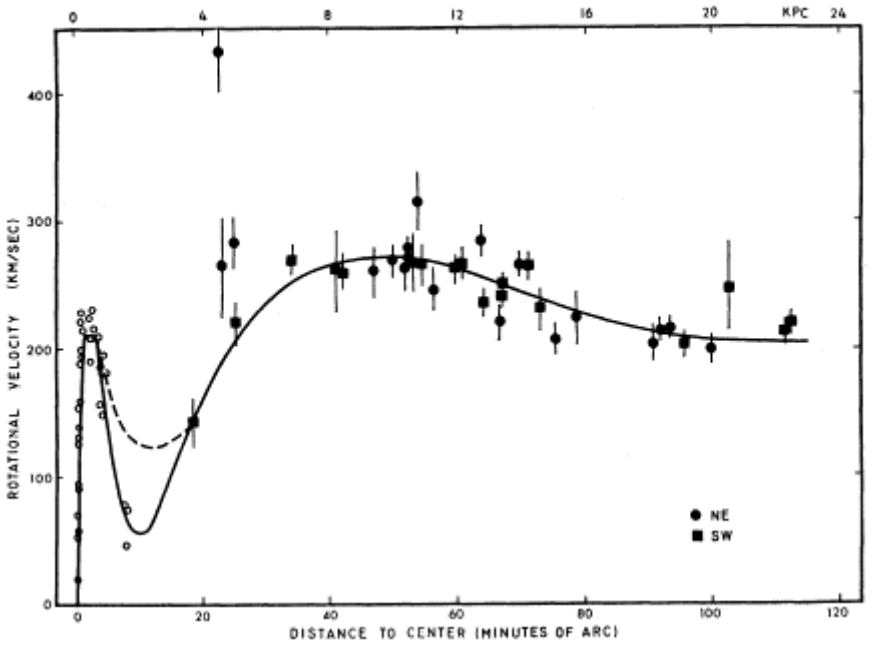

Figure 1.1: Rotation curve for M31 galaxy. The behaviour of the curve shows rapidly increasing velocities for $r \lesssim 400pc$, a minimum at $r \sim 2kpc$, and almost constant velocities up to the farthest observed distance of $24kpc$ from galaxy center. In order for rotation velocities to stay almost constant outside the galaxy bulk, additional matter is needed, whose density should increase approximately linearly with the distance. Empty dots represent measurements of N_{II} line used for the bulk region, while full dots are OB stars measurements outside the bulk. The dashed and solid lines about the minimum show the range of acceptable results, since between distances $1kpc \lesssim r \lesssim 3.6kpc$ there was only one measurement (N_{II} line). Image taken from [4].

$400pc$ from the center, they show a minimum at a distance of $2kpc$ and they remain constant well outside the galaxy bulk up to the farthest observed distance of $24kpc$.
In turn this suggests that beyond a rapidly rotating nucleus, there's a less dense region up to $2kp$ where velocities fall, followed by a farther region where total mass seems to increase linearly with distance from the center up to $14kpc$ and slower up to the observed distance of $24kpc$.
In fact according to eq. (1.7) in order to have a constant rotation velocity outside the bulk, the presence of matter is needed:

$$v(r) = const \Leftrightarrow M(r) \sim r,$$

which correspond to a matter density $\rho(r > r_0) \propto r^{-2}$ where $r_0 \sim 4kpc$ in the case of M31.

In a 1972 work [5], Rogstad and Shostak carried out a similar analysis on five galaxies, observing a flat rotation curve up to the largest observed radius. They used the 21 cm emission line to extrapolate the mass of the galaxies, and concluded that at the Holmberg radius, the surface mass-to-luminosity ratio should be as high as ~ 20. The outcome of the analysis is reported in fig. 1.2. This is credited to be the first uncontroversial indirect proof of dark matter presence in galaxies.

In general, until mid '70, the two observed anomalies, galaxy rotation curves and velocity dispersion in clusters of galaxies, were treated as separated problems, and no common solution (if one was needed, in fact some models could be arranged to repro-

duce the observed results without need for additional mass) was searched. This until the beginning of cosmology as an independent field of study.

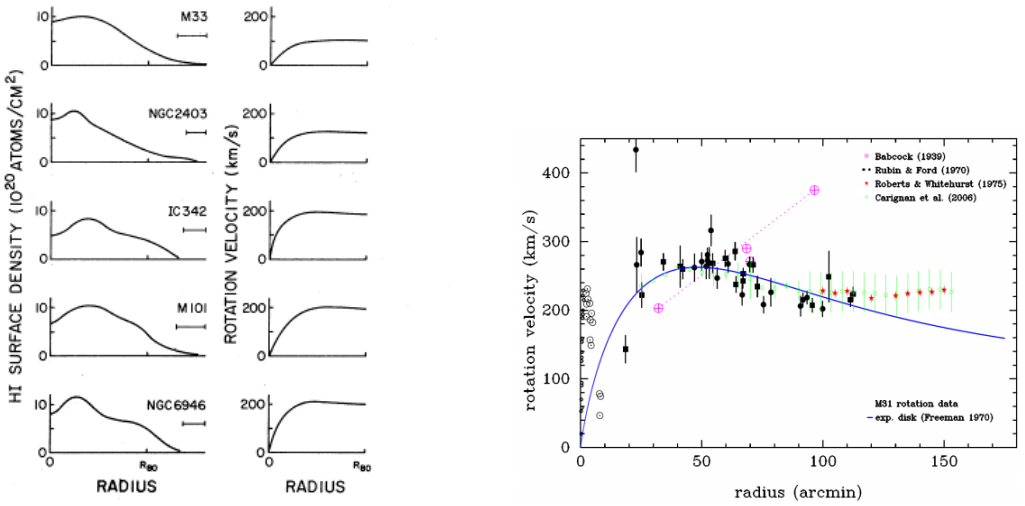

Figure 1.2: The left figure shows the results as reported in [5]. The left panel shows hydrogen presence based in the observation of the 21 cm emission line, R_{80} is the distance within which we find 80% of hydrogen (roughly corresponding to Holmberg radius). On the right panel, the rotation curves. The right image shows the rotation curve for Andromeda galaxy, combining results by various works. Purple crossed points are results from Babcock [7], black filled (empty) circles are results by Rubin and Ford [4] for outer (inner) region, red stars are from Roberts and Whitehurst [6] and green circles from Carignan et al. [8]. It's clear that for all the measurements velocities do not fall as they're expected to without assuming the presence of dark matter.

1.3 X-rays hints on cluster scales

Zwicky results about galaxy clusters was corroborated by new evidences, allowed by means of X-rays emission observation.
It is possible to trace the presence of hot gases inside a cluster by observing the emission of X-rays, and in this way to estimate the cluster matter content.
This result can then be checked with the model-predicted temperature.

In a spherically symmetric system at hydrostatic equilibrium, gravitational force is exactly balanced by pressure, and the equilibrium equation reads

$$\frac{1}{\rho}\frac{dP}{dr} = -\frac{G_N m(r)}{r^2} \tag{1.8}$$

where ρ is the gas density, P the gas pressure and $m(r)$ is the mass encompassed by a sphere of radius r.
If we consider the intracluster gas to be ideal, the equilibrium equation 1.8, con be rewritten as an equation for temperature

$$\frac{dlog\rho}{dlogr} + \frac{dlogT}{dlogr} = -\frac{r}{T}\left(\frac{\mu m_p}{k_B}\right) a(r), \tag{1.9}$$

where m_p is the proton mass, $\mu \sim 0.6$ the average molecular weight, $a(r)$ the gravitational acceleration at radius r and k_B Boltzmann constant. Well outside the galaxy core, the temperature is constant, and the density profile is observed to fall as $r^{-2\sim-1.5}$. Therefore, for large radii, using the observed density profile, eq. 1.9 can be solved for temperature

$$k_B T \approx \frac{2.69}{1.5 \sim 2} keV \left(\frac{m_r}{10^{14} M_\odot}\right) \left(\frac{Mpc}{r}\right). \tag{1.10}$$

The above equation tells us which temperature is needed to balance gravitational attraction of mass m_r at radius r, or conversely, how much mass is needed to balance the pressure of an ideal gas at temperature T, at large radii.
If one tries now to use baryonic mass only to balance the pressure of the gas using eq. 1.10, one finds a great discrepancy with the observed value of $T \sim 10keV$. This means that the baryonic matter alone is not able to bare the pressure of the gas, and hence could not maintain hydrostatic equilibrium.
This suggests that a relevant amount of matter, other than baryonic, should be present in clusters in order to grant equilibrium.

1.4 The birth of modern cosmology

In the decade 1965-1975, publications concerning *cosmology* increased very rapidly, growing of a factor 10 in about 10 years.
New possible observations and theoretical models formulation made it a field of interest itself. The most active and researched subjects aimed to understand if the universe is closed, flat or open and to know the time scale of the Universe. Answering to these questions was a matter of measurement of cosmological parameters, in particular *Hubble parameter* (which gives the time scale of the Universe) and the matter density of the universe (which in case of vanishing cosmological constant tells a closed universe from an open or flat one).
Although at the beginning of the searches there was a 'philosophical' preference for a closed universe, the reasoning remain interesting and valid (the universe is now observed to be very close to flatness).
In order for the universe to be closed, matter density should exceed the critical density $\rho_{c,0} \sim 10^{-29} g/cm^3$, and the willing to observe a closed universe draw the attention of observations to the luminous matter density of the universe.
Several upper bounds to this density were found, and typically luminous matter was found to not exceed $\rho_l \lesssim 10^{-31} g/cm^3$ which is far below the critical density (see for instance [10]).

Suddenly cosmological observations and 'philosophical' motivations (we now know that the matter density has to be very close to the critical density, but this leaves the following unchanged) required additional matter, as did astronomical observations of rotation curves and velocity dispersion in clusters of galaxies.
The joint result of the study of the two apparently independent aspects, led to the conclusion that mass of local giant spiral galaxies grows linearly with radial distance, up to about 300 kpc from the galaxy center, as if they were surrounded by a *'giant halo with a very high mass-to-light ratio'*.
With this assumption, galaxies could account for one fifth of the critical density, which is closer (at least closer than 4 orders of magnitude) to the hypothesis of a closed universe.

1.5 Role of dark matter in structure formation

The observations of the early '70, suggesting the presence of *halos* of faint matter around galaxies somehow brought together all the previous astronomical observations.
Almost in the meanwhile, another discrepancy was found in the study of large-scale structure formation, and surprisingly the presence of this *halos* could also play a role in this independently discovered problem.

Until the mid of last century, our galaxy seemed to be the entire Universe. With the advancing of technological means, observation of further regions of the universe was made possible, and it soon became clear that our universe was much lager than our now relatively small galaxy, and moreover it became clear that the Universe was in evolution. The key observation to come to this conclusion was the discovery of *Quasars* in 1963, which are moving away at relativistic velocities (about 16% of the speed of light). This was a clear evidence that the Universe is not in steady state, and opened the possibility to a dynamical evolution of the structures that build up the Universe at different scales. Among the questions regarding an evolving and dynamical Universe, astronomers and cosmologists also began wondering how the structures we observe today were formed in the beginning.

The largely accepted theory explaining this phenomenon regards the very early stages of the life of our Universe, namely inflation.
The need for an inflationary phase at the very early stage of the universe life span, comes from a different and independent set of problems to be solved, and the widely diffused idea came with 'à la Guth' inflation [11]. Inflation is a period in which the universe experienced an exponential growth (order of 60 e-folds), due to the fact that the energy density was dominated by the potential of a scalar *inflaton* field. This period of exponential growth sets the initial conditions for the thermal evolution of the universe, granting homogeneity, isotropy and flatness. Moreover, the scalar field responsible for inflation is expected to behave like any other quantum field, this means that it will cause vacuum fluctuation: these are the perturbations in the density field of our universe that, after expansion and amplification due to inflation, gave birth (or better, are supposed to have given birth) to the nowadays large-scale and small-scale structures we observe.

The study of how the perturbations evolve in time makes large use of fluid-dynamics equations and theory of gravitation, namely one has to solve continuity, Euler and Poisson coupled equations for matter density, matter velocity and gravitational potential. We'll not show here the detailed calculations for a reason of conciseness, although they can be found in almost any cosmology textbook (we are following here [13]), we only recall that we assume that the primordial fluctuations are a isotropic, homogeneous random gaussian field with zero mean, and that we assume (and this is *a posteriori* verified) that the large structure scales are small compared to the curvature of the universe, which allows us to use Newtonian gravitational dynamics.
Equations for the matter density are equivalent to equations for the density perturbation field

$$\delta(t, \vec{x}) = \frac{\rho(t, \vec{x}) - \bar{\rho}(t)}{\bar{\rho}(t)}, \tag{1.11}$$

where $\bar{\rho}(t)$ is the matter average density at time t. Skipping all the calculations here, we end up with *Jeans equation* for the Fourier transform of the perturbation eq. (1.11)

$$\ddot{\hat{\delta}} + 2H\dot{\hat{\delta}} = \hat{\delta}\left[\frac{1}{2M_{Pl}^2}\bar{\rho} - \left(\frac{c_s a_0 k}{a(t)}\right)^2\right], \tag{1.12}$$

where k is the wave number and c_s is the adiabatic speed of sound. The RHS of eq. (1.12) shows the two opposite effects of the gravitational potential (first term), that tends to make clusters collapse, and pressure (second term), that tends to wash away dishomogeneities, while the LHS shows us that gravity has to deal with universe expansion, which is an important effect when talking about large-scale structures.
At the *jeans wavelength* the two effects exactly balance, and perturbations at this scale will not tend to collapse, nor to be dissolved by pressure

$$\lambda_J = \frac{2\pi}{k_J} = 2\pi\frac{a_0}{a}c_s\sqrt{\frac{2M_{Pl}^2}{\bar{\rho}}}. \tag{1.13}$$

We can now wonder what the solutions to eq. (1.12) are, on scales much smaller or much larger than Jeans wavelength, for relativistic and non relativistic matter.
Solutions to eq (1.12) are

$$\begin{cases} \hat{\delta} \propto t^{2/3} \sim \frac{a}{a_0}\hat{\delta}_0 & large\ structures \\ \hat{\delta} \propto e^{\pm i\omega t} & small\ structures \end{cases} \tag{1.14}$$

for non-relativistic matter and

$$\begin{cases} \hat{\delta} \propto t \sim (\frac{a}{a_0})^2\hat{\delta_0} & large\ structures \\ \hat{\delta} \propto A + B\ logt & small\ structures \end{cases} \tag{1.15}$$

for relativistic matter.
As expected, in the case of relativistic matter the growing of perturbations well below Jeans wavelength is slower than in the non-relativistic case, due to relativistic pressure effects. Hence perturbations well inside the horizon before radiation-matter equality, remained frozen and could not grow due to the counteracting effect of relativistic pressure. When at $z \sim 3600$ matter and radiation came to equivalence, these perturbation were able to grow under the action of gravity and under the weakening of counteraction of relativistic pressure. From the first of eq. 1.14 we learn that perturbations at decoupling time ($z_{dec} \sim 1100$) $\hat{\delta}_{dec} \sim 10^{-5}$ (this comes from CMB observations, better justified in sec. 1.4) grow with the scale factor, yielding a nowadays density perturbation

$$\hat{\delta}_0 \sim z_{dec}\hat{\delta}_{dec} \sim 1\%,$$

which is in strong disagreement with N-bodies simulations (see [12] for instance), which suggest values of δ_0 close to 1. This is a strong evidence that in formation of large-scale structures, the density perturbation due to baryons alone is far from enough to be able to account for the observed distribution of matter on large scales.

Again the same problem shows up: the reproduction of large-scale structures as observed today requires the presence of additional matter in the universe, enhancing gravitational wells that could allow the formation of structures up to *superclusters* and *filaments*.
According to observations, the first objects to form in the history of Universe, were

small-scale structures such as galaxies and clusters of galaxies, and with the passing of time larger structures such as superclusters were formed.

This leads us to another problem, namely if dark matter particles are relativistic or not at the time of decoupling, corresponding respectively to hot and cold dark matter. Jeans equation (1.12) has to be corrected in order to include the different effects of this two kinds of dark matter, namely one has to introduce an effective speed of sound in eq. (1.12).

Without entering the detail of calculations, what happens qualitatively is the following: hot dark matter is relativistic when it decouples, which means that it will be free to steam in the Universe at relativistic speeds after decoupling, while cold dark matter will steam at non-relativistic speeds. In turn, this means that hot dark matter will partially wash away small-scale dishomogeneities, resulting in an overabundance of large-scale structures which form first, to later fragment in smaller structures; conversely cold dark matter will not be energetic enough to escape gravitational wells on small scales, corresponding to the formation of small structures first, and only subsequently of large-scale structures (although non-vanishing velocity dispersion prevents the formations of arbitrary small structures).

Observations suggest a bottom-up formation of structures (namely small first, large then), suggesting that dark matter is cold and collisionless, nevertheless N-bodies simulations with cold collisionless dark matter reveal the presence of small structures in much larger abundance than observed in the form of sub-dwarf galaxies. This suggest an intermediate nature of dark matter and allows the presence of *warm* dark matter, that could wash away this overabundance of non observed small-scale structures, while maintaining a bottom-up pattern for structures formation.

The observed distribution of structures in the universe is contained in the observed two-points correlation function of density fluctuations, or equivalently in its Fourier transform *power spectrum*

$$\langle \hat{\delta}(\vec{k})^* \hat{\delta}(\vec{k}') \rangle = (2\pi)^3 \delta(\vec{k} - \vec{k}') \mathcal{P}(k), \tag{1.16}$$

where $\mathcal{P}(k)$ is the matter power spectrum, and we used the properties of the density perturbation field. The experimental measured matter power spectrum (CMB and galaxy surveys for large scales, Lyman-α forest for smaller scales) is reported in fig. 1.3, and is expected to be of the form

$$\mathcal{P}(k) = k^n \quad , \qquad n = 0.9665 \pm 0.0038 \quad ([14], 68\% C.L.), \tag{1.17}$$

The deviation from this spectrum is due to the *Meszaros effect*, namely the power spectrum has to be corrected by a factor $(a_{enter}/a_{eq})^2$, where a_{enter} is the scale factor at the time of the entrance of scale k in the horizon and a_{eq} is the scale factor at matter-radiation equivalence. Adding this correction factor gives a good theoretical agreement with fig. 1.3.

1.6 *Planck* observation and cosmological parameters

In the past twenty years, observational cosmology and astronomy went steps further, allowing the observation of different phenomena, and among other important discoveries, finding other indirect proofs of dark matter existence and constraining its abundance in

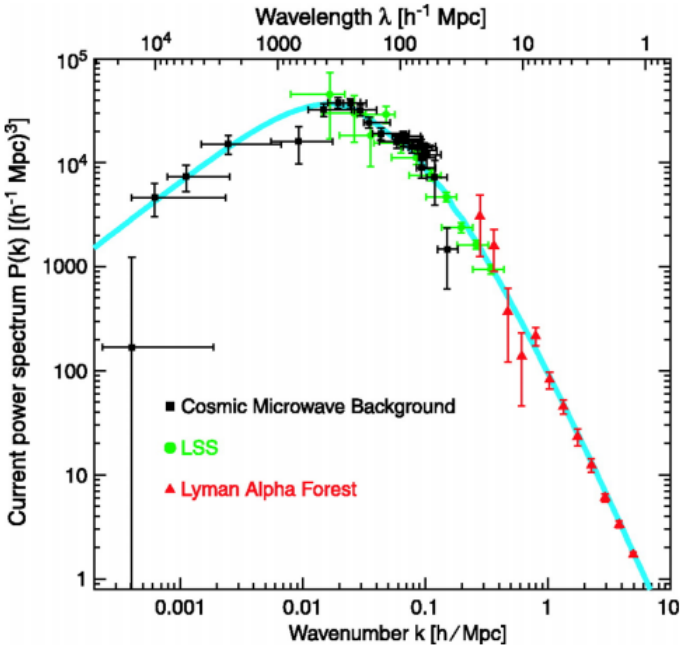

Figure 1.3: Matter power spectrum as reported in [13]. The peak at $\lambda \sim 120 Mpc$ corresponds to the transition between matter-dominated and radiation-dominated era and is due to *Meszaros effect*. At this scale the scaling of the power spectrum changes from $\sim k$ to $\sim k^{-3}$ due to suppressed growing of small-scales perturbations, which is postponed to matter-dominated era. Large-scale perturbations (compared to horizon distance at equivalence) never stopped growing as they grew with the scale factor out of the horizon before radiation-matter equivalence, resulting in an enhanced power spectrum.

the Universe.

The latest results and constraints on cosmological parameters came with ESA's *Planck* CMB anisotropies observations.
During the early stages of its evolution, the universe was opaque, since photons were interacting with free electrons via Thompson scattering. As temperature dropped, protons were able to capture electrons to form neutral hydrogen during so-called *recombination*; this happened at a redshift $z \sim 1100$. At this point photons were not able to scatter against electrons anymore, and they started streaming freely around the Universe, forming CMB. The now free photons keep the footprints of previous inhomogeneity, which we can now measure as anisotropy in CMB temperature on different scales.
These anisotropies are mainly driven by two effects

- *BAO*: Baryon acoustic oscillations are the sound waves due to the evolution of density perturbations on small scales (see eq. 1.14). When photons decoupled they kept track of them as peaks in the power spectrum.

- Sachs-Wolfe effect: this effect is responsible for photons redshift during their travel to Earth due to general relativistic effects. Non integrated Sachs-Wolfe effect takes place immediately at the surface of last scattering, while the integrated effect keeps into account photons travel to Earth; it is particularly important during dark-energy dominated era.

The mean CMB temperature is observed to be $\bar{T} = 2.725K$, with anisotropy $\mathcal{O}(10^{-5})$ due to the effects listed above, which are parametrized as

$$T(\vec{p}) = \bar{T}(1 + \Theta(\vec{p})), \tag{1.18}$$

where $\vec{p}$ defines the direction of observation, and the fluctuations $\Theta(\vec{p})$ can be expanded in spherical harmonic functions

$$\Theta(\vec{p}) = \sum_{l=0}^{\infty} \sum_{m=-l}^{l} a(l,m) Y_{lm}(\vec{p}). \tag{1.19}$$

Assuming absence of non-gaussianity in the primordial perturbation density field, we can use the empirical power spectrum

$$\hat{\mathcal{C}}_l = \frac{1}{2l+1} \sum_m |a(l,m)|^2 \tag{1.20}$$

as an estimator of the CMB angular power spectrum, reported in the famous fig. 1.4.
The position of the first peak in the power spectrum is directly correlated to the angle under which we see the horizon distance at the time of recombination, which is a hint about the spatial geometry of the universe (once we know the distance from recombination and the horizon distance at $z \sim 1100$).
Moreover, odd peaks correspond to maximal compression during an oscillation, while even peaks correspond to maximal expansion.
Nevertheless, only baryons are affected by relativistic pressure, while cold dark matter is not as it interacts only gravitationally. Hence, from the ratio of first-second peaks and first-third peaks, we can deduce the baryon and cold dark matter density of the universe. Further peaks follow the exponential damping of the power spectrum and are less useful for this purpose.

Thanks to Planck results [14], we now have the following density parameters for cold dark matter and baryonic matter

$$\Omega_{dm} h^2 = 0.11933 \pm 0.00091, \qquad \Omega_b h^2 = 0.02242 \pm 0.00014, \tag{1.21}$$

at 68% C.L..

1.7 Constraints on dark matter particles properties

Once we agree on the fact that about five sixths of the matter density of the Universe is not ascribable to ordinary matter, the next natural question is: what is the rest of matter density made of?

Some argued that similarly to the case of precession of Mercury's perihelion, the observed discrepancy is due to our lack of comprehension of gravity. If Newtonian gravity does not act as we know it on cosmological scales, than it can be modified in order to explain the observed phenomena. Such theories named *MOND, modified Newtonian dynamics* are strongly discredited by nowadays observations (for instance by *bullet cluster* collision).

Other possible candidates for dark matter are *massive astrophysical compact halo objects*, *macho*s, which are basically ordinary braryonic objects which emit little or no

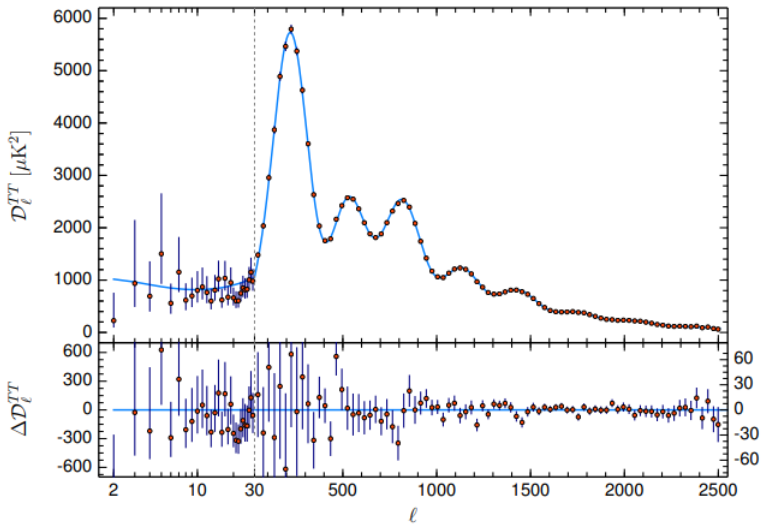

Figure 1.4: CMB angular power spectrum as measured in [14]. on y-axis we have $l(l+1)/2\pi\bar{\mathcal{C}}_l$, for a given multipole l. The position of the first peak gives information about the curvature of the universe, while the ratio of the heights of the second and first peaks gives information abount the baryonic content of the Universe. The dark matter abundance can be inferred from the ratio of the third and first peaks height. Numerical results are in eq. (1.21). The lower panel shows residuals with respect to the ΛCDM theoretical model.

light, such as black holes, brown dwarfs and neutron stars, that could be responsible for the apparent presence of dark matter halos. Machos could be detected via gravitational microlensing effects, though the trial in detection in the Magellanic clouds have excluded a vast range of macho masses ($0.6 \cdot 10^{-7} \lesssim M_{macho}/M_\odot \lesssim 15$[15]).
Moreover from *Big Bang nucleosynthesis* model, we get a constraint on the total baryonic density in the Universe [33]

$$0.019 \leq \Omega_b h^2 \leq 0.025 \quad (95\% C.L.), \tag{1.22}$$

which is in agreement with *Planck* result eq. (1.21), and basically excludes *macho* nature of dark matter.

The largely accepted hypothesis is that of particle nature of dark matter, namely dark matter is made of particles (typically other than standard model particles) which interact very weakly with standard model particles, and surely carry no electric charge.

If we want to stay within the standard model framework, neutrinos could be the only reasonable candidate for dark matter, since they share only weak and gravitational interactions with the other SM particles, and they decoupled at $T \sim 1MeV$.One of the latest upper bound on left-handed SM neutrino masses is given in [16] and reads $m_\nu < 1.1eV$ (90% C.L.).
By entropy conservation at neutrino decoupling time, we know that the temperature of a cosmic neutrino background has a temperature

$$T_{0\nu} = \left(\frac{g^*_{after}}{g^*_{before}}\right)^{1/3} T_{0\gamma} = \left(\frac{4}{11}\right)^{1/3} T_{0\gamma} \sim 1.95K,$$

where g^*_{before} and g^*_{after} are the effective relativistic degrees of freedom of the bath before and after decoupling.

In turn, the total abundance of neutrinos is

$$\Omega_\nu h^2 \sim \frac{\sum_i m_{\nu_i}}{91.5eV},$$

which makes left-handed neutrino incapable of accounting for all dark matter density. Moreover, even if a fourth neutrino species existed (which is however very unlikely) massive enough to account for all DM relic density, since neutrinos are still relativistic at decoupling ($T \sim 1Mev$), they would be candidate for hot dark matter, in contrast with observed bottom-up structure formation.

It is clear that we need to extend our theory in order to include new particles that could account for dark matter, and many exotic candidates were considered as component of particle dark matter.
However all the considered possible candidates need to share some common properties to be coherent with observations, namely with unobserved results in laboratories and with observed astronomical properties.
Here we list those properties

- *dark and long lived*: first of all dark matter should be indeed dark, hence neutral under $U_{em}(1)$. Moreover, even if it is not necessary that dark matter is absolutely stable, it is compulsory that its lifetime is longer than the age of the universe $\tau_U \sim 4 \cdot 10^{17}s$, in order for it to survive until now. More severe bound could follow from astronomical observations: for instance, search for gamma-ray emission the Perseus cluster [23] bounds the lifetime of DM (decaying in SM pairs) in mass range $200GeV \lesssim m_{DM} \lesssim 200TeV$ to $\tau_{DM} \gtrsim 10^{26}s$. Assuming only that DM would decay in relativistic particles, a lower bound is obtained [24] , based on cosmological observations, $\tau_{DM} \gtrsim 6 \cdot 10^{18}s$.

- cold: the adjective *cold* refers to the fact that dark matter should be non-relativistic when it decouples. This follows from astronomical observations: if dark matter is relativistic at decoupling (*hot* dark matter), then it easily escapes gravitational wells on small scales, creating dishomogeneities seeds on large scales only. In turn this means that ordinary matter sees gravitational wells on large scales only, hence large structures are formed first, that later fragment into smaller scale structures such as cluster and galaxies. On the contrary observation suggest that small scale structures merged to form larger scale structures, indicating that dark matter could not easily escape gravitational wells formed on the scale of galaxies, hence its velocity should have been small compared to their mass, favouring cold dark matter. Actually some problems emerge within cold dark matter framework (e.g. *missing satellite problem*: numerical simulations with cold dark matter predict the presence of dwarf galaxies in much larger numbers than observed [17]), and to solve those incompatibilities an intermediate *warm* situation has been considered, so that gravitational wells on dwarf galaxies scales can be easily washed away, reducing the power spectrum in that scale range and finding a better agreement with simulations. The lower bound on thermal produced warm dark matter mass is $m_{warm} \gtrsim 6.3keV$ [18].

- not too fuzzy: in order to solve the problem of cusps in low mass galactic cores, various solutions have been proposed, among which we find extremely light scalar cold dark matter, with mass of order $10^{-22}eV$. However, bosonic dark matter with lower masses is unreliable, since its De Broglie wavelength would be larger that the

kpc scale (relevant scale for galaxies), hence $m_{dm} \gtrsim 10^{-22} eV$ is an absolute bound on scalar dark matter mass. However, if dark matter is fermionic, this turns in the more severe constraint [19] $m_{f,dm} \gtrsim 25eV$. On the other hand, if point-like dark matter is too heavy, it could easily destroy galaxy and cluster structures. By studying the matter power spectrum [25] shows how dark matter mass in form of primordial black holes should be $m_{DM} \lesssim 10^3 M_\odot$. In general, we see that the range of possible dark matter mass is extremely wide.

– Self-interacting: although in standard ΛCDM paradigm, dark matter is considered to bu collisionless, many discrepancies between theory and simulations arise, and it is not clear whether DM should be collisionless or non-collisionless. For instance, Tully-Fisher relation relates the intrinsic luminosity of a galaxy to maximum rotation velocity. Models [27] require much less dark matter halo density than observed in simulation. The introduction of dark matter self-interactions ([21], [20]) produces better matches with simulations, and allows to avoid problems such as the discrepancy with the Tully-Fisher relation without introducing exotic explanations. For self-interacting cross section per unit mass in the range $0.45 cm^2/g \lesssim \sigma/m \lesssim 450 cm^2/g$, the problems of over-dense galaxy and cluster cores and overabundance of DM halos predicted by CDM models can be avoided [22]. On the other hand we have upper bound on self-interaction cross section from cluster collision: bullet cluster collision suggest a constraint $\sigma/m \lesssim 2cm^2/g$ [26].

1.8 Freeze-out mechanism: a possible origin for DM relic density

Studies have been made to explain the mechanisms through which it is possible to have a considerable relic density of a particle species, that in this case will be dark matter.
The most credited and studied mechanism has been for long time *freeze-out* mechanism, which we'll briefly review in this section.

In freeze-out framework what happens is the following: consider a particle species X, which is in thermal equilibrium in the early universe. Its number density will hence be the equilibrium one: $n_X^i = n_{X,eq} \propto T^3$ at early stages.
As time goes by, temperature drops, and particle species X is maintained in thermal equilibrium with the bath, and when $T \approx m_X$, processes involving X particle production are Boltzmann suppressed, hence n_x undergoes a sharp fall, due to annihilation and eventually scattering processes, while the inverse processes are exponentially disfavoured. If this could go on indefinitely, n_X would quickly become negligible, and the relic abundance of particle X would vanish.
Nevertheless, something can happen before n_X completely vanish: if the interaction rate Γ, relative to the residual X number-changing interactions (typically pair annihilation), becomes smaller than the Universe expansion rate H, particle X undergoes *decoupling*, as interactions are no longer able to reduce X number density.
Through this mechanism, the comoving number density of particle species X can remain constant at late stages, and eventually until now.

If this happens when T is not much smaller than m_X (in a sense that has to be discussed by further quantitative analysis), the non vanishing comoving number density of particle specie X remains fixed and can eventually account for dark matter relic density; X is

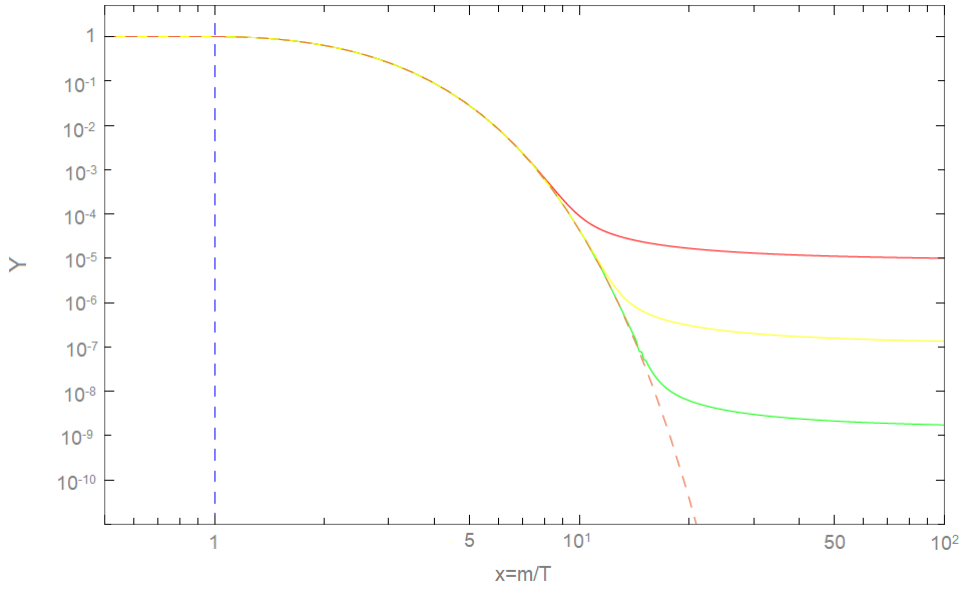

Figure 1.5: Evolution in time of comoving number density of a particle species that undergoes freeze-out. The dashed line tracks the equilibrium number density while the solid (red, green, yellow) lines are freeze-out yield for increasing cross section. We see that the freeze-out temperature is typically $\mathcal{O}(10^{-1}m_X)$

said to be frozen-out.

A schematic representation of the behaviour of X comoving number density is sketched in fig. 1.5.
For the sake of simplicity we'll show a quantitative result in the case in which only one interaction is switched-on for particle X, namely pair self annihilation and its inverse. More complex examples can be found in any cosmology textbook.
In this simple case Boltzmann equation reduces to the form

$$\dot{n}_X + 3Hn_X = -\langle\sigma_{ann}v_{rel}\rangle[n_X^2 - n_{X,eq}^2], \tag{1.23}$$

where n_X^2 accounts for X self annihilation, while $n_{x,eq}^2$ for x pair production.
Assuming that σ_{ann} is temperature independent, which allows us to get an analytical result, the freeze-out condition is

$$\Gamma_{ann} = \langle\sigma_{ann}v_{rel}\rangle n_X = 1.66 g_*^{1/2}\frac{T^2}{M_{PL}} = H. \tag{1.24}$$

Under these assumptions, the freeze-out number density, i.e. the relic number density after decoupling, is

$$Y \simeq \frac{10^{-8}}{(m_X/Gev)(\langle\sigma_{ann}v\rangle/10^{-27}cm^3s^{-1})},$$

corresponding to

$$\Omega_X h^2 \simeq \left(\frac{3\cdot 10^{-27}cm^3s^{-1}}{\langle\sigma_{ann}v\rangle}\right). \tag{1.25}$$

For a weak-scale particle, with $\alpha \simeq 10^{-2}$, the annihilation cross section is $\langle\sigma_{ann}v\rangle \simeq \frac{\alpha^2}{(100Gev)^2} \simeq 10^{-25}cm^3s^{-1}$.

This is a marvellous prediction: if a new particle exists which has only gravitational and weak interactions, it could easily account for dark matter density when it freezes-out.
The exiting aspect of this prediction is that the same weak-scale interaction could make the unknown particle observable at accelerators.
The sought-for particle is called *Weakily Interacting Massive Particle*, or WIMP, due to its interaction properties.
From the above analysis we can underline the main features of the freeze-out mechanism:

- The larger the interaction strenght, the lower the final yield, since decoupling is achieved later in time.

- Freeze-out yield is IR dominated, since it depends mainly on decopling temperature which is tipically $T_{dec} = \mathcal{O}(10^{-1} m_X)$. The final Yield is therefore independent of unknowk UV quantities such as reheating temperature T_{RH}.

Finally the decoupling moment, x_{fo}, is obtained solving eq. 1.24, eventually dropping the assumption of σ_{ann} independence on temperature.

We presented freeze-out mechanism because it has been longly the most credited mechanism for production of a relic density, however this is not the only available possibility, and we'll leave this framework in the following, introducing a different way to get a constant relic number density for a particle species.

Chapter 2

Supersymmetry and its Motivations

The standard model is one of the best verified theory of modern physics. It offers strikingly precise predictions, and it is nowadays a universally accepted theory of nature. Nevertheless we are aware of its limits, as it clearly has to be completed at high energies and it cannot account for gravity. Moreover there are some phenomenological and theoretical problems within the theory of the standard model.

For instance, the observed neutrino oscillation implies non vanishing neutrino masses, which do not fit in the theory, though a simple way to include them could be to extend the theory, encompassing right-handed neutrino, via a *seesaw* mechanism.
Also, within SM there's no way to produce a sufficient baryon-antibaryon asymmetry, nor there's an explanation for the nature of dark matter and dark energy.
Some of these problems could be elegantly solved if one includes a new symmetry in the theory, which is called supersymmetry.
In this chapter we'll explore one of the motivations that led to think that supersymmetry could be a symmetry of nature, namely the solution to the *hierarchy problem*, and we'll later explore supersymmetry in much more detail, providing an explanation of the symmetry breaking process. Lastly we'll promote this new symmetry to a local symmetry and explore its implication, one over all, the existence of the *gravitino*.

2.1 The hierarchy problem

Standard model is a gauge theory encompassing three of the four fundamental forces under the gauge group $\mathcal{G}_{SM} = SU_C(3) \times SU_L(2) \times U_Y(1)$. The symmetry group does not allow mass terms in the lagrangian, for they would explicitly break the symmetry; to overcome this problem a new scalar boson, the Higgs, was added to the theory and particles can now acquire mass via interaction with the Higgs boson. This happens through the spontaneous breaking of the electroweak symmetry, caused by the Higgs acquiring a non-vanishing vacuum expectation value ($v = (\sqrt{2}G_F)^{-1/2} \sim 246GeV$), and breaking the symmetry to

$$SU_C(3) \times SU_L(2) \times U_Y(1) \to SU_C(3) \times U_{em}(1).$$

This happened in the early universe when the energy dropped below the electroweak energy scale, which is $\Lambda_{ew} = \mathcal{O}(10^2 GeV)$, and the Higgs boson was observed at LHC in 2012, reporting a mass of $M_{Higgs} = 124.97 \pm 0.28$GeV [34], fixing the last free parameter of the SM.

Now this theory works brilliantly, but still there's a natural question to ask: why is

the weak scale 10^{17} times smaller than the Planck scale $M_{pl} \sim 1.22 \cdot 10^{19}$ GeV?
Let's see how this can affect SM phenomenology. We know that the SM is UV incomplete, as we expect new physics to arise at energy scales which are typically not far below Planck scale, hence many orders of magnitude larger than Λ_{ew}.
This energy scale at which new physics comes out can be used as an UV cutoff to regularize our divergent integrals.

If we use this procedure here comes the discrepancy: quantum correction to the Higgs mass should be of the same order as the scale at which new physics arises. This can be seen in the following way: Higgs mass at tree level is proportional to v and to a coupling parameter which is fixed once one experimentally measures Higgs mass, nevertheless all massive particles contribute to correct Higgs mass at quantum level. If the Higgs couples to a fermion with an interaction term of the type

$$\mathcal{L}_{int} = -\lambda_f h \bar{f} f,$$

corresponding to a loop diagram as in fig. 2.1, then the Higgs mass gets a one-loop correction which grows quadratically with the UV cutoff Λ_{UV}:

$$\Delta M^2_{h,loop} = -\frac{|\lambda_f|^2}{8\pi^2}\Lambda^2_{UV} + \mathcal{O}\left(m_f^2 ln(\Lambda_{UV}/m_f)\right). \tag{2.1}$$

Since Higgs boson couples to all massive fermions of the standard model, all leptons and quarks contribute to correct the Higgs mass, and if the scale at which new physics arises Λ_{UV} is not far below the Planck mass, then we get a discrepancy of many orders of magnitude on Higgs mass and on all the rest of the standard model masses, since they depend on Higgs VEV.

Within the framework of the standard model, the Higgs bare mass receives one-loop contribution (considering only top quark for fermions)

$$\Delta M^2_{h,SM} = \frac{3}{4\pi^2}\Lambda^2_{UV}\left(-\lambda^2_{top} + \frac{g^2}{4} + \frac{g^2}{4cos^2\theta_W} + \lambda\right), \tag{2.2}$$

where λ_{top} is the top quark Yukawa coupling, λ is the Higgs quartic self-coupling and g is $SU_L(2)$ coupling constant.
This is actually not a problem within SM itself, as one can adjust the bare mass to exactly reproduce the observed mass.
Moreover one could use a dimensional regularization of the integrals, so that the Λ^2_{UV} part of the correction disappears, while one cannot remove the correction proportional to m_f^2 in eq. (2.1).

The problem lies rather in the sensitivity of the Higgs mass to new physics, and it appears as one tries to extend the standard model.
For instance, if the existence of Majorana right-handed neutrinos is the solution to the neutrino mass problem via seesaw mechanism, then the Higgs receives a contribution to its mass which is $\mathcal{O}(M_R)$, where M_R is the right-handed neutrinos Majorana mass, which is typically required to be many orders of magnitude larger than Λ_{ew}.
This means that as we include new particles the problem will show, both in the case in which new particles acquire mass via SSB in the electroweak sector, and in the case in which tree level masses are allowed by symmetry for these particles but they share some

gauge interactions with the Higgs (see diagrams in fig. 2.1).

Therefore a possible solution could be to assume that all new particles do not couple to the Higgs, not even extremely weakly, which seems an unnatural possibility. Only a striking cancellation of the contribution terms to Higgs mass would save us from this problem.

We now come to the possible solution that supersymmetry offers to this problem, namely the sought-for exact cancellation.
Let's now suppose that the Higgs couples to a massive scalar via the interaction term $\mathcal{L}_s = -\lambda_S |h|^2 |s|^2$. Higgs mass will get a contribution also from this interaction (see fig. 2.1)

$$\Delta M^2_{h,loop} = \frac{\lambda_s}{16\pi^2}(\Lambda^2_{UV} - 2m_s^2 ln\frac{\Lambda_{UV}}{m_s} + \cdots). \tag{2.3}$$

Looking at eq. (2.1) and (2.3), we see that the contribution from fermions and scalars exactly cancel if for each fermion there exist two complex scalars that couple to the Higgs with strength $\lambda_s = |\lambda_f|^2$; this means exactly that the realization of supersymmetry would make all the undesired contribution to Higgs mass exactly cancel (it can be shown that this happens to all orders, not only at one loop) solving the naturalness problem.

In the frame of supersymmetry, we can evaluate corrections to Higgs mass that keeps into account the cancellation. The final result makes use of definitions which will be introduced later along this chapter, and requires a quite involved calculation we'll not present here for reasons of conciseness, nevertheless we'll report the final result.
In the limit in which the mass of the *superpartner* of the top quark is much greater than the top quark mass, the largest correction to Higgs mass reads at one-loop order

$$\Delta M^2_H = \frac{3}{4\pi} cos^2\alpha y^2_{top} m^2_{top} \left(ln(m_{\tilde{t}_1} m_{\tilde{t}_2}/m^2_{top}) + \Delta_{threshold}(m_{\tilde{t}_1}, m_{\tilde{t}_2}, m_{top}, \theta_{\tilde{t}}) \right) \tag{2.4}$$

where m_{top} is the usual SM top-quark mass and $m_{\tilde{t}_{1,2}}$ are the masses of the top-like scalar particles mass eigenstates.
What is important is that the final Higgs mass depends only on the mass spectrum of the theory and two angles, while the UV dependence disappeared as wanted.
The first term on the RHS of eq. (2.4) comes from the three diagrams shown in fig. (2.2), while the second term comes from corrections to the running quartic Higgs coupling, considering again only contributions from top-like particles.
It's not difficult to accommodate the mass spectrum so that the result is in agreement with measured value for the Higgs mass. For instance, if superpartner masses do not exceed 1 TeV, one can obtain the upper limit

$$M_H \leq 135 GeV.$$

2.2 A new symmetry

Until the introduction of supersymmetry as a possible symmetry of the theory, the most severe bounds on the possible symmetry group of the lagrangian lied in *Coleman-Mandula theorem.*

The theorem states that in a theory in which (i) the $\mathcal{S}$ matrix is based on a local relativistic field theory, (ii) there is only a finite number of different particles in a one-particle

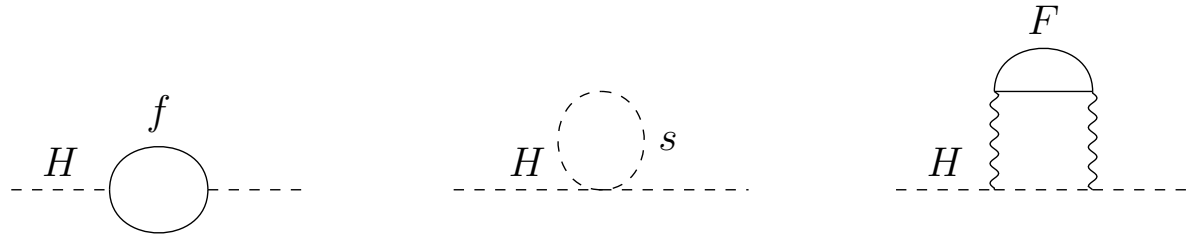

Figure 2.1: Loop contributions to Higgs mass. The first two diagrams represent contributions from fermions and scalar that directly couple to the Higgs, while the third diagram shows a contribution from heavy fermions that couples via gauge interactions to the Higgs.

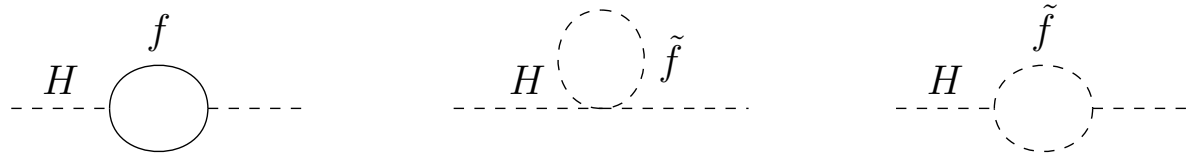

Figure 2.2: Loop contributions to Higgs mass, when we assume the existence of superpartners. The two diagrams involving the scalar $\tilde{f}$ exactly balance the UV sensitive part of the correction due to the fermionic f contribution.

states at a given mass and (iii) there is an energy gap between the vacuum state and one-particle states, then the most general Lie-algebra of symmetries of the $\mathcal{S}$ matrix is generated by P_μ, $M_{\mu\nu}$, and B^a, where B^a are Lorentz scalars and belong a to a compact Lie group $\mathcal{G}$. The algebra is hence defined by the following commutation relations:

$$\begin{aligned}
[P_\mu, P_\nu] =& 0, \\
[M_{\mu\nu}, M_{\lambda\rho}] =& -i\eta_{\nu\lambda}M_{\mu\rho} + i\eta_{\mu\lambda}M_{\nu\rho} + i\eta_{\nu\rho}M_{\mu\lambda} - i\eta_{\mu\rho}M_{\nu\lambda}, \\
[M_{\mu\nu}, P_\rho] =& -i\eta_{\nu\rho}P_\mu + i\eta_{\nu\rho}P_\mu, \\
\left[B^a, B^b\right] =& if_c^{ab}B^c, \\
[B^a, P_\nu] =& 0, \\
[B^a, M_{\mu\nu}] =& 0.
\end{aligned} \tag{2.5}$$

that is , the most general group of symmetry of the $\mathcal{S}$ matrix is $SO(1,3) \otimes \mathcal{G}$.

The idea of supersymmetry appears in the early '70, first in the context of string theory. The basic idea is that for each particle we observe, there are $\mathcal{N}$ companion particles whose spin differs by $\frac{1}{2}$ from the original particle, where $\mathcal{N}$ is the number of supersymmetries in our theory. In our case we'll focus on the $\mathcal{N} = 1$ case, i.e. for each fermion there exists a boson and vice versa.
To achieve this result it's compulsory to extend the algebra (2.5) to include a fermionic generator, to realize the desired transformation:

$$Q|F\rangle \sim |B\rangle; \qquad Q|B\rangle \sim |F\rangle, \tag{2.6}$$

where Q is the fermionic generator and $|F\rangle, |B\rangle$ are a fermionic and bosonic state respectively.
In general, Coleman-Mandula theorem seems to forbid such a symmetry, nevertheless it is possible to extend the theorem to include the possibility of using anticommutators.

This more general no-go theorem that includes anticommutation relations is referred to as *Haag-Łopuszański-Sohnius theorem*, and it states that the general Lie-algebra of symmetry of $\mathcal{S}$ includes the following relations (in the case of $\mathcal{N} = 1$ supersymmetries, useful for this thesis):

$$\begin{aligned} \{P_\mu, Q_\alpha\} =& 0, \\ [M_{\mu\nu}, Q_\alpha] =& -(\Sigma_{\mu\nu})^\beta_\alpha Q_\alpha, \\ [B^a, Q_\alpha] =& (B^a)^i_j Q_\alpha, \\ \{Q_\alpha, \bar{Q}_\beta\} =& 2\gamma^\mu_{\alpha\beta} P_\mu, \end{aligned} \tag{2.7}$$

where $\Sigma_{\mu\nu}$ are the generators of the Lorentz group in spinorial space.
The last of the relations in 2.7 tells us that supersymmetry is not an internal symmetry, rather it is a spacetime symmetry. This makes the resulting algebra a $\mathcal{Z}_2$ graded algebra, where scalar generators B^a are $\mathcal{Z}_2$ even while fermionic generator Q_α is $\mathcal{Z}_2$ odd.

As of today, we have not observed the SM supersymmetric companion particles that, were supersymmetry unbroken, would have exactly the same masses of the SM particles. Therefore if we want supersymmetry to be a symmetry of nature, we need to also accept that it is broken, and eventually include a mechanism providing the desired symmetry breaking.
The motivations that led to accept the idea in the framework of string theory lie out of the aim of this thesis, nevertheless some interesting phenomenological aspect arise after we accept its existence, and we can give some *a posteriori* reasons to believe that SuSy is a symmetry of nature.
One of the marvellous consequence of supersymmetry, is the solution of the *hierarchy problem* of the standard model.

2.3 Global supersymmetry

As anticipated in section 2.2, the basic idea of supersymmetry is to add to gauge invariance another kind of internal symmetry, which relates fermionic fields to bosonic fields. What we're looking for is a transformation that turns a bosonic state into a fermionic one and vice versa, calling Q and $Q^\dagger$ the generators of the symmetry,

$$Q|F\rangle \sim |B\rangle; \qquad Q|B\rangle \sim |F\rangle. \tag{2.8}$$

The generators of the transformation need to carry a fermionic index in order to accomplish this task, and they satisfy the supersymmetry algebra

$$\{Q_\alpha, Q^\dagger_{\dot{\alpha}}\} = -2\sigma^\mu_{\alpha\dot{\alpha}} P_\mu; \qquad \{Q_\alpha, Q_\beta\} = 0 = \{Q^\dagger_{\dot{\alpha}}, Q^\dagger_{\dot{\beta}}\}. \tag{2.9}$$

Fields related via such a symmetry belong to the same *supermultiplet*; that is, a supermultiplet is a collection of fields whose variation under a supersymmetry transformation is proportional to the others.

In building a supersymmetric lagrangian, keeping in mind that we also want to include our old gauge interactions, it turns out that two kind of supermultiplets are needed.
The first one includes a Weyl fermion and two complex scalar fields, one of which is non-propagating. This kind of supermultiplet is called *chiral*, namely

$$\Phi_{chiral} = (\phi, \psi, F).$$

Clearly vector bosons do not fit in chiral supermultiplets, hence we need the so called *gauge* supermultiplets, including a vector boson, a Weyl fermion and a non-propagating real scalar, namely

$$\Phi_{gauge} = (A_\mu, \lambda, D).$$

The two non-propagating scalars, F and D, are needed to close the supersymmetry algebra off-shell, and they also complete the bosonic off-shell degrees of freedom, which we would like to be always equal to fermionic ones.

Fields in the same supermultiplet share the same gauge interactions and the same mass, unless Supersymmetry is broken.
The presence of vector bosons introduces covariant derivatives in the lagrangian, which are responsible for gauge interactions.

Nevertheless, fields belonging to chiral supermultiplets can interact between themselves. These interactions are specified by a single holomorphic complex function of the scalar fields ϕ_i, (i runs over gauge and flavour degrees of freedom), called the *superpotential*. By imposing renormalizability and supersymmetric invariance this function reads:

$$W(\phi) = \frac{1}{2}M^{ij}\phi_i\phi_j + \frac{1}{6}y^{ijk}\phi_i\phi_j\phi_k + L_i\phi^i, \tag{2.10}$$

where M^{ij} and y^{ijk} are totally symmetric under indices exchange.
By defining

$$W_i = \frac{\delta W}{\delta \phi^i}; \qquad W_{ij} = \frac{\delta^2 W}{\delta\phi^i\delta\phi^j}, \tag{2.11}$$

our global supersymmetric lagrangian reads:

$$\begin{aligned}\mathcal{L} = &- \nabla_\mu\phi_i\nabla^\mu\phi^i + i\psi^{\dagger i}\bar\sigma^\mu\nabla_\mu\psi_i - \frac{1}{2}(W^{ij}\psi_i\psi_j + W^*_{ij}\psi^{\dagger i}\psi^{\dagger j}) - W^iW*_i \\ &- \frac{1}{4}F^a_{\mu\nu}F_a^{\mu\nu} + i\lambda^{\dagger a}\bar\sigma^\mu\nabla_\mu\lambda_a + \frac{1}{2}D_aD^a \\ &- \sqrt{2}g(\phi * T^a\psi)\lambda_a - \sqrt{2}g\lambda^\dagger_a(\psi^\dagger T^a\phi) + g(\phi^* T^a\phi)D_a,\end{aligned} \tag{2.12}$$

where covariant derivatives are defined as in usual gauge theories, a runs over the adjoint representation of the gauge group and T^a are the representations of the gauge group under which chiral supermultiplets transform.
The above lagrangian is left invariant up to total derivatives under the supersymmetry transformations:

$$\begin{aligned}&\delta\phi_i = \epsilon\psi_i, && \delta A^a_\mu = -\frac{1}{\sqrt{2}}(\epsilon^\dagger\bar\sigma_\mu\lambda^a + h.c.), \\ &\delta\psi_{i\alpha} = -i(\sigma^\mu\epsilon^\dagger)_\alpha\nabla_\mu\phi_i + \epsilon_\alpha F_i, && \delta\lambda^a_\alpha = \frac{i}{2\sqrt{2}}(\sigma^\mu\bar\sigma^\nu\epsilon)_\alpha F^a_{\mu\nu} + \frac{1}{\sqrt{2}}\epsilon_\alpha D^a, \\ &\delta F_i = -i\epsilon^\dagger\bar\sigma^\mu\nabla_\mu\psi_i + \sqrt{2}g(T^a\phi)_i\epsilon^\dagger\lambda^{\dagger a}; && \delta D^a = \frac{i}{\sqrt{2}}(-\epsilon^\dagger\bar\sigma^\mu\nabla_\mu\lambda^a + h.c.).\end{aligned}$$

In order for lagrangian 2.12 to be supersymmetric, one must also require

$$W^i(T^a\phi)_i = 0.$$

Names	spin 0	spin 1/2	$SU_C(3)$, $SU_L(2)$, $U_Y(1)$
squarks, quarks	$(\tilde{u}_L\ \tilde{d}_L)$	$(u_L\ d_L)$	$(\mathbf{3},\ \mathbf{2},\ \frac{1}{6})$
	$\tilde{u}_R^*$	$u_R^\dagger$	$(\bar{\mathbf{3}},\ \mathbf{1},\ -\frac{2}{3})$
	$\tilde{d}_R^*$	$d_R^\dagger$	$(\bar{\mathbf{3}},\ \mathbf{1},\ \frac{1}{3})$
Sleptons, leptons	$(\tilde{\nu}\ \tilde{e}_L)$	$(\nu\ e_L)$	$(\mathbf{1},\mathbf{2},\ -\frac{1}{2})$
	$\tilde{e}_R^*$	$e_R^\dagger$	$(\mathbf{1},\ \mathbf{1},\ 1)$
Higgs, Higgsinos	$(H_u^+\ H_u^0)$	$(\tilde{H}_u^+\ \tilde{H}_u^0)$	$(\mathbf{1},\ \mathbf{2},\ \frac{1}{2})$
	$(H_d^0\ H_d^-)$	$(\tilde{H}_d^0\ \tilde{H}_d^-)$	$(\mathbf{1},\ \mathbf{2},\ -\frac{1}{2})$

Table 2.1: Chiral supermultiplets and their transformation properties under SM gauge group

The non-propagating fields can be expressed algebraically in terms of the scalar fields of the theory using their equations of motion:

$$F_i = -W_i^*; \qquad D^a = -g\left(\phi^* T^a \phi\right).$$

Using the above expressions one can write the scalar potential of the theory as follows:

$$V(\phi,\phi^*) = F_i^* F^i + \frac{1}{2}\sum_a D^a D^a = W_i^* W^i + \frac{1}{2}\sum_a g_a^2\left(\phi^* T^a \phi\right)^2. \tag{2.13}$$

The supersymmetric lagrangian 2.12 introduces new interactions.
$\mathcal{L}_{chiral}$ adds a scalar-fermion vertex, a quartic interaction for scalars, mass terms for both scalars and fermions and cubic scalar vertex. $\mathcal{L}_{gauge}$restores old gauge interactions and adds gauge boson-gaugino-gaugino and fermion-gaugino-scalar interactions.

Following Noether procedure, one can find the conserved current relative to global supersymmetric invariance, named *supercurrent*. The exact expression for the supercurrent reads:

$$J_\alpha^\mu = (\sigma^\nu\bar{\sigma}^\mu\psi_i)_\alpha \nabla_\nu \phi^{*i} + i(\sigma^\mu\psi^{\dagger i})_\alpha W_i^* - \frac{1}{2\sqrt{2}}(\sigma^\nu\bar{\sigma}^\rho\sigma^\mu\lambda^{\dagger a})_\alpha F^a_{\nu\rho} + \frac{i}{\sqrt{2}} g_a \phi^* T^a \phi (\sigma^\mu\lambda^{\dagger a})_\alpha \tag{2.14}$$

2.4 The minimal supersymmetric standard model

The MSSM is the theory obtained by 'supersymmetrizing' the standard model.
Particle content of the MSSM will include the well-known SM particles plus their superpartners, hence one scalar for each fermion and vice versa. Moreover an additional Higgs chiral doublet is required. This follows from the requirement of the superpotential being holomorphic in the scalar fields, and by gauge anomaly cancellation.
Particle content of MSSM is shown in table 2.1 and table 2.2.

The superpotential reads in this case:

$$W_{MSSM} = \bar{u}\mathcal{Y}_u Q H_u - \bar{d}\mathcal{Y}_d Q H_d - \bar{e}\mathcal{Y}_e L H_d + \mu H_u H_d, \tag{2.15}$$

where $\mathcal{Y}$ are 3x3 matrices, whose indices run over gauge and flavour degrees of freedom. Only scalars appear in 2.15, while we used the ambiguous multiplet notation for simplicity only.

Names	spin 1/2	spin 1	$SU_C(3)$, $SU_L(2)$, $U_Y(1)$
Gluino, gluon	$\tilde{g}$	g	$(\mathbf{8}, \mathbf{1}, 0)$
Winos, W bosons	$(\tilde{W}^{\pm}\ \tilde{W}^0)$	$(W^{\pm}\ W^0)$	$(\mathbf{1}, \mathbf{3}, 0)$
Bino, B boson	$\tilde{B}^0$	B^0	$(\mathbf{1}, \mathbf{1}, 0)$

Table 2.2: Gauge supermultiplets and their transformation properties under SM gauge group

The potential in eq (2.15) introduces a new problem in the theory. In fact, the parameter μ provides both Higgsino masses and scalar Higgs potential:

$$-\mathcal{L}_{H_u,H_d} = \mu(\tilde{H}_u^+\tilde{H}_d^- - \tilde{H}_u^0\tilde{H}_d^0) + h.c. + |\mu|^2(|H_u^+|^2 + |H_u^0|^2 + |H_d^-|^2 + |H_d^0|^2).$$

The scalar part of the lagrangian is positive definite and has a minimum for $|H_u^0|^2 = 0 = |H_d^0|^2$, which prevents electroweak symmetry to be broken. In order to provide a mechanism for electroweak SSB it is necessary therefore to add new terms to the Higgs scalar potential, in order to shift the minimum of the potential along the neutral scalar Higgs directions.
This is actually possible by means of soft breaking terms, which we'll shortly present; it is sufficient to know that scalar masses terms, hence $m_{H,soft}$ too, are allowed (and somehow desirable) as supersymmetry breaking terms.
On the other hand, the minimum of the potential should be around the observed Higgs VEV, hence in absence of striking cancellations it should hold $\mu \sim \mathcal{O}(10^2 - 10^3 GeV)$. Again this insinuates a naturalness problem: why should be μ many oders of magnitude smaller than Planck scale, and why should it be of the same order as the soft mass terms? This is the so called the *μ-problem*. The most studied strategy to solve this problem is to suppose that μ terms are absent in the supersymmetric phase, while being driven by some supersymmetry breaking field's VEV, see e.g. [40, 39].
In this way, it is natural that μ be the same order of magnitude of soft masses, the problem is therefore moved to understand why soft masses are way smaller than Planck mass.

2.5 Supersymmetry breaking

If supersymmetry is realized in nature, then it clearly must be broken. In fact, if that wasn't true, we would have discovered superpartners of SM particles long ago at colliders, since they would share the same messes and interactions of SM particles.
One of the effects of supersymmetry breaking is in fact the splitting of masses of particles in the same supermultiplet, eventually pushing those of superpartners above the experimentally accessible scale.
There are two ways in which supersymmetry can be broken:

Explicitly : the lagrangian of the theory contains terms that explicitly break the symmetry. In this case those terms arise as effective operators of a UV supersymmetric theory, hence the mass dimension of those operators is positive ('*soft*' breaking terms). In this case, when we add soft terms to the lagrangian, no ultraviolet divergences to scalar masses are added.

Spontaneously : SuSy is broken when one or more of the scalar auxiliary fields acquire a non vanishing VEV.

In the case of soft supersymmetry breaking, we expect the symmetry to be actually spontaneously broken in some sector of the theory (other than the MSSM) and to be then communicated to the MSSM sector via some interaction, as we'll better explain later. In this case We will briefly analyze the two cases in more detail.
The latter case happens when one of the F_i or D^a fields acquires a VEV.
In fact, the condition for the vacuum state not to be superymmetric invariant (broken SuSy), via eq. 2.9, translates into $H|0\rangle \neq 0$. Neglecting spacetime dependence and fermionic condensates, this means $\langle 0|V(\phi, \phi^*)|0\rangle \neq 0$, and looking at eq. 2.13, one gets the above condition for SuSy breaking.
Depending on which field(s) (D or F) is responsible for supersymmetric breaking we get different requirements and implications.

- *Feyet-Iliopoulus mechanism* (D-breaking term):
  It is possible when a $U(1)$ factor appears in the gauge group. Such a gauge symmetry allows a $\mathcal{L}_{\mathcal{D}} = -kD$ term, which is also supersymmetric invariant.
  Such a term forces the D field to acquire a VEV and causes mass splitting inside supermultiplets.
  Unfortunately the $U_Y(1)$ factor of the SM gauge group cannot be the sought-for factor, and D-breaking terms cannot provide reasonable masses to MSSM particles.

- *O'Reifeartaigh mechanism* (F-breaking terms):
  these models require at least one gauge singlet among the supermultiplets, allowing a linear term in the relative superfield. Again this linear term forces the auxiliary field to acquire a VEV.
  F-breaking terms are more promising then D-terms, but unfortunately there's no gauge singlet in the MSSM.

Regarding explicit (soft) breaking terms, the general form of the lagrangian that can play that role is:

$$\mathcal{L}_{soft} = -\left(\frac{1}{2}M^a\lambda_a\lambda^a + \frac{1}{6}a^{ijk}\phi_i\phi_j\phi_k + \frac{1}{2}b^{ij}\phi_i\phi_j + t^i\phi_i\right) + h.c. - (m^2)^i_j\phi^{*j}\phi_i. \quad (2.16)$$

Expression 2.16 shows that the general soft breaking terms are gaugino masses, scalar masses and scalar quadratic and cubic interaction terms.
Those terms clearly break supersymmetry since they involve gauginos and scalar fields but not their superpartners.

In all cases there's no MSSM candidate to be responsible for SuSy breaking, hence this process must happen in some '*hidden sector*' and then be communicated to MSSM via some interaction.
The simplest model of 'hidden sector' was proposed by Polonyi in [42], and includes a single chiral supermultiplet.
Once breaking is achieved in the hidden sector, it can be communicated both via gauge interactions or via gravitational interaction.

- Planck-scale mediated SuSy breaking:
  Occurs when gravitational interactions link the two sectors.
  In this case the energy scale (m_{soft}) that enters the soft lagrangian is of order:

  $$m_{soft} \approx \frac{\langle F\rangle}{M_{Pl}}.$$

  Requiring $m_{soft} \approx 1Tev$ one gets $\sqrt{\langle F\rangle} \sim 10^{11}Gev$.

- Gauge-mediated SuSy breaking:
  Occurs when gauge interactions link the two sectors.
  In this case the 'communication' requires at least one loop diagrams and

$$m_{soft} \approx \frac{\alpha_a}{4\pi} \frac{\langle F_a \rangle}{M_{Mess}}.$$

  and the typical mass scale of the interaction mediator M_{Mess} is involved.
  Requiring $m_{soft} \approx 1Tev$ and supposing $\langle F_a \rangle \sim M_{Mess}$, one gets

$$\sqrt{\langle F \rangle} \geq 10^4 Gev$$

As for any case of global broken symmetry, the breaking of supersymmetry implies the presence of a massless Weyl fermion, which in this case is the superpartner of the auxiliary field that acquires a VEV.
This presence of such a fermion can be shown explicitly: the fermion mass matrix derived from eq. 2.12 annihilates the vector

$$\tilde{G} = \frac{\langle D^a \rangle}{\sqrt{2}} \lambda_a + \langle F_i \rangle \psi_i. \tag{2.17}$$

Hence 2.17 is a massless eigenstate of the fermion mass matrix. The goldstino is therefore a linear combination of the other fermion fields of the theory, with coefficients proportional to the VEV of the correspondent auxiliary fields.
The goldstino $\tilde{G}$ interacts with the other supermultiplets, the relative lagrangian reading:

$$\mathcal{L}_{\tilde{G}} = i\tilde{G}^\dagger \bar{\sigma}^\mu \partial_\mu \tilde{G} - \frac{1}{\langle F \rangle} \left(\tilde{G} \partial_\mu j^\mu + h.c. \right) \tag{2.18}$$

where F is the auxiliary filed for the goldstino and j^μ only involves other supermultiplets (so that $\partial_\mu j^\mu \neq 0$).
From expression 2.18 one identifies the interesting *goldstino-scalar-chiral fermion* and *goldstino-gaugino-gauge boson* interactions.

The interaction term of lagrangian 2.18 seems to diverge as SuSy is restored (or equivalently when $\langle F \rangle \to 0$). However, the $\partial_\mu j^\mu$ term contains two derivatives of the other fields, that turn out to be proportional to the on-shell mass splitting inside a supermultiplet, which vanishes as SuSy is restored, granting a non pathological behaviour of interaction terms.

2.6 R-parity

In principle W_{MSSM} could include B and L violating terms. The most general supersymmetric gauge invariant renormalizable terms that violate B and L by one unit are

$$W_{\Delta L=1, \Delta B=1} = \frac{1}{2} \lambda_{ijk} L_i L_j \bar{e}_k + \frac{1}{2} \lambda'_{ijk} L_i Q_j \bar{d}_k + \mu' H_u + \frac{1}{2} \lambda''_{ijk} \bar{u}_i \bar{u}_j \bar{d}_k \tag{2.19}$$

while it is well known that such terms should be highly suppressed or absent at tree level. In fact the last term in equation (2.19) would imply a short proton lifetime, which is the most severe bound on B-violating terms.
In order to preserve already known results about B and L conservation, one could simply postulate conservation in the MSSM or introduce a new symmetry that forbids such

terms.
The simplest symmetry that can be introduced to this end is called *matter parity*, whose quantum number that has to be multiplicatively conserved at each vertex is

$$P_M = (-1)^{3(B-L)}. \tag{2.20}$$

Chiral supermultiplets have $P_M = -1$, except for the Higgs supermultiplets that carry $P_M = +1$. Gauge supermultiplets have $P_M = +1$ since they carry no baryionic or leptonic number.
Matter parity conservation is equivalent to multiplicative conservation of $R-symmetry$, whose quantum number is defined as follows

$$P_R = (-1)^{3(B-L)+2s}, \tag{2.21}$$

where s is the particle spin. It is easy to show that if angular momentum is conserved, the conservation of (2.21) and (2.20) is equivalent.
All standard model particles have $P_R = +1$, while their superpartners have $P_R = -1$.
R-parity is then a $\mathcal{Z}_2$ symmetry between SM particles and superpartners.
Among the implications deriving from the conservation of R-parity, one is of particular interest for this thesis:

The lightest supersymmetric particle (LSP) is completely stable.

2.7 Supersymmetric dark matter

Among the features of supersymmetric models there is an appealing one that provides a natural candidate for dark matter particle. In fact, as we studied in detail throughout the chapter, it is natural to introduce a new $\mathcal{Z}_2$ symmetry, *R-Parity*, in order to forbid tree-level violation of baryonic and leptonic numbers.

If this symmetry is to be exactly conserved the lightest $\mathcal{Z}_2$-odd particles cannot possibly decay into other states, and is hence completely stable; moreover, other $\mathcal{Z}_2$-odd particles will eventually decay in the lightest one.
If we arrange the mass spectrum so that this special particle is also neutral under SM gauge group, then we get a perfect candidate for dark matter. We'll briefly explore possible particles of the MSSM that could be candidates for dark matter.

Sneutrinos are the superpartners of SM neutrinos, and hence share only gravitational and weak interactions with SM particles. Sneutrino LSP is typically underabundant in the MSSM framework, although it could reproduce the wanted relic density for a small mass range [28] [29].However direct detection of DM experiments, i.e. via elastic scattering over detector nuclei, set the most severe constraint on sneutrino DM, typically ruling out mass ranges which are of cosmological interest. Sneutrinos could be good dark matter candidates in extended supersymmetric models such as the BLMMS [30].

Neutralinos are four fermions that compose the MSSM particle spectrum, as they are a linear superposition of the neutral heavy gauginos $\tilde{W}^0$ and $\tilde{B}^0$ and the two neutral Higgsinos. Neutralino masses are obtained diagonalizing the mass matrix of the four sfermions, namely

$$\mathcal{M}_{\tilde{\chi}} = \begin{pmatrix} M_1 & 0 & -g'v_d/\sqrt{2} & g'v_u/\sqrt{2} \\ 0 & M_2 & gv_d/\sqrt{2} & -gv_d/\sqrt{2} \\ -g'v_d/\sqrt{2} & gv_d/\sqrt{2} & 0 & -\mu \\ g'v_u/\sqrt{2} & -gv_d/\sqrt{2} & -\mu & 0 \end{pmatrix} \tag{2.22}$$

where M_1 and M_2 are soft gaugino masses, μ is due to the superpotential (2.15) and v_d, v_u are the VEVs of the down-like and up-like Higgsinos respectively. Neutralinos have been largely studied as possible dark matter particles, and direct detection experiments aim to reduce the available mass range. As of today they're still possible DM candidates.

As a foretaste of what we'll explain in detail in the rest of this chapter, in the framework of local supersymmetry, *gravitino* joins the possible LSP candidates, hence it could constitute dark matter. In unbroken local supersymmetry, gravitino shares only gravitational (therefore extremely weak) interactions with SM particles, and is neutral under the SM symmetry group. Were supersymmetry unbroken, gravitino would be massless, nevertheless as we will show in the following, gravitino can acquire mass via the super-Higgs mechanism when local supersymmetry is broken. In turn gravitino also inherits goldstino interactions that can dramatically boost gravitino production in the early universe. Moreover in the case of gauge-mediated supersymmetry breaking, gravitino can easily be the LSP as it's clear from section 2.9.

2.8 Local supersymmetry

Once we have our global supersymmetric model, we can move a step forward and let the parameter of the SuSy transformation have non vanishing spacetime derivatives.
If ξ_α is the transformation generator,

$$\partial_\mu \xi_\alpha \neq 0. \tag{2.23}$$

This promotes our symmetry to a local one.

Lagrangian 2.12 is invariant (up to total derivatives) under global SuSy, but introducing condition 2.23 will require new terms in order to preserve invariance.
First of all, as in any case of local symmetry, we would like to have a field that mediates local symmetry. In this case, such a field will be a 3/2-spin field carrying both vector and spinorial indices.
We'll refer to it as $\psi_{\mu\alpha}$, often omitting the spinorial index.

The presence of this field partially restores invariance, and belongs to a supermultiplet as all fields (the other field completing invariance restoration).
Surprisingly, the superpartner of ψ_μ is the metric field $g_{\mu\nu}$, and for this reason ψ_μ is called *gravitino*.
For a quick review of spin-3/2 particles see Appendix A.
The implementation of the gravity supermultiplet grants invariance, and the theory obtained is often referred to as *SUperGRAvity*.

A minimal SuGra lagrangian can be found for instance in [37], and we'll not report here it fully for reasons of conciseness.
SUGRA lagrangian depends on two arbitrary functions:

- $f_{ab}(\Phi)$, an arbitrary function of the scalar fields, which affects the scalar kinetic terms. The minimal choice $f_{ab} = \delta_{ab}$ restores the canonical kinetic terms.
- The second function is defined as follows:

$$G(\phi, \phi^*) = K(\phi, \phi^*) + ln|W|^2, \tag{2.24}$$

where W is the superpotential (see eq. 2.10) and K is Kähler function, a real function of the scalar fields.

Kähler function induces a metric on the scalar fields space, namely

$$g_{ij^*} = \frac{\partial^2 K}{\partial \phi^i \partial \phi^{*j}}. \tag{2.25}$$

The minimal choice $K_{min} = \phi^i \phi^{*i}$ translates into $g_{ij^*} = \delta_{ij}$ and restores canonical kinetic terms for spinor fields.
The interesting part of the lagrangian for this thesis is the section that includes interaction operators involving the gravitino:

$$\frac{\mathcal{L}_{\Psi J}}{e} = -\frac{1}{2M} g_{ij^*} \nabla_\nu \phi^{*j} \chi^i \sigma^\mu \bar{\sigma}^\nu \psi_\mu - \frac{i}{2M} \psi_\mu \sigma^{\nu\rho} \sigma^\mu \bar{\lambda}_a F^a_{\nu\rho} + h.c. \tag{2.26}$$

where $e = \sqrt{-g}$ and M is the reduced Planck mass $M = \frac{M_{PL}}{\sqrt{8\pi}}$ In the simple case in which $K(\phi, \phi^*) = \phi^i \phi^{*i}$, covariant derivative takes the usual form

$$\nabla_\mu \phi^i = \partial_\mu \phi^i + i g A^a_\mu T^a_{ij} \phi^j. \tag{2.27}$$

2.9 Spontaneous breaking of local SuSy

As for the case of global supersymmetry, we would like SuGra to be a broken symmetry. Again, after spontaneous breaking of the symmetry, a massless goldstino appears, as previously discussed.
In this case, in analogy to what happens in electroweak SSB, the goldstino gets 'eaten' by the gravitino.
This can be shown writing the quadratic part of the SuGra lagrangian, without derivative couplings, and rearranging it in such a way that massless gravitino ψ_μ mixes with a combination of the other fermions:

$$\eta = -\frac{i}{\sqrt{2}} G_i \chi^i + \frac{1}{2} e^{-\frac{G}{2}} g D^a \lambda^a, \tag{2.28}$$

which is indeed the goldstino.
Subsequent to this process, gravitino acquires two helicity modes, reaching a total of 4. Moreover, gravitino mass term appears.
Gravitino mass $m_{3/2}$ reads

$$m_{3/2} = |e^{\frac{K}{2}} W|. \tag{2.29}$$

Gravitino in broken local suspersymmetry has 4 helicity states, has inherited gravitino interactions and has a non-vanishing mass.

In the case of F-breaking term (as in the minimal Polonyi model [42]), $m_{3/2} \propto \frac{\langle F \rangle}{M}$. This relation is crucial and changes gravitino physics, depending on which interaction mediates symmetry breaking:

- Planck-mediated: Gravitino mass is $\mathcal{O}(Tev)$ and its interactions are mainly gravitational. Its role is mostly confined to cosmological effects (e.g. it could easily overclose the Universe).
- Gauge-mediated: In this case, if $M_{MESS} \ll M_{PL}$ (see Sec. 2.2), gravitino mass can be as low as $\mathcal{O}(10^{-15} Gev)$ and ψ_μ is almost certainly the LSP. The inherited non-gravitational goldstino interactions are dominant over the original gravitational ones, and they can play a relevant role in collider physics.

2.10 Gravitino interactions

The relevant gravitino interaction terms are those of lagrangian 2.26.
The dominant decay processes are $\psi_\mu \to \lambda + A_\mu$ and $\psi_\mu \to \phi^i + \bar{\chi}^i$, if kinematically allowed.
Decay rates for the two processes can be directly evaluated using lagrangian 2.26 and read:

$$\Gamma(\psi_\mu \to \lambda + A_\mu) = \frac{1}{32\pi}\frac{m_{3/2}^3}{M^2}\left(1 - \left(\frac{m_\lambda}{m_{3/2}}\right)^2\right)^3\left(1 + \frac{1}{3}\left(\frac{m_\lambda}{m_{3/2}}\right)^2\right), \tag{2.30}$$

$$\Gamma(\psi_\mu \to \phi^i + \bar{\chi}^i) = \frac{1}{384\pi}\frac{m_{3/2}^3}{M^2}\left(1 - \left(\frac{m_\phi}{m_{3/2}}\right)^2\right)^4. \tag{2.31}$$

where we have assumed zero mass for A_μ and for χ^i.

As pointed out in Sec 2.9, gravitino can be extremely light.
In this case, it is useful to write an effective lagrangian, which is valid for the condition $\sqrt{s} \gg m_{3/2}$. If this holds, the helicity $\pm\frac{1}{2}$ modes of the gravitino, which were inherited by the goldstino, can be written as

$$\psi_\mu \sim \frac{i}{m_{3/2}}\sqrt{\frac{2}{3}}\partial_\mu\psi, \tag{2.32}$$

where ψ is here the spin-1/2 goldstino field.
Substituting relation 2.32 in lagrangian 2.26 one gets an effective lagrangian for light gravitino (equivalently goldstino) interactions (which is of the form of eq. 2.18).

One could expect these effective operators to produce divergences in the UV. In fact, these interaction terms are inherited from the goldstino, which exist only if SuSy is broken, hence the relative terms are proportional to the symmetry breaking order parameter. The order parameter vanishes in the symmetric phase, i.e. at high energies where pathological behaviours are expected to arise. This solves UV problems, and allows us to replace derivatives acting on all the other fields with their respective on-shell masses.

This leaves us with an effective lagrangian for the helicity $\pm\frac{1}{2}$ modes

$$\mathcal{L}_{eff} = -\frac{i(m_\phi^2 - m_\chi^2)}{\sqrt{3}m_{3/2}M}\psi\chi\phi^* - \frac{im_\lambda}{8\sqrt{6}m_{3/2}M}\psi(\bar{\sigma}^\mu\sigma^\nu - \bar{\sigma}^\nu\sigma^\mu)\lambda^a F^a_{\mu\nu} + h.c. \tag{2.33}$$

the feyman diagrams of these interactions are reported in fig. 2.3.
Notice that the gravitino couples to chiral supermultiplets via a marginal operator, while it couples via a non-renormalizable (dimension 5) operator to gauge supermultiplets.
From this lagrangian one can obtain the production rate of goldstinos from a gaugino or scalar particle decay, namely

$$\Gamma(\lambda \to \psi + A_\mu) = \frac{1}{48\pi}\frac{m_\lambda^5}{m_{3/2}^2 M^2}\left(1 - \left(\frac{m_{3/2}}{m_\lambda}\right)^2\right)^3 \tag{2.34}$$

and

$$\Gamma(\phi \to \psi + \chi) = \frac{1}{48\pi} \frac{m_\phi^5}{m_{3/2}^2 M^2} \left(1 - \left(\frac{m_{3/2}}{m_\phi}\right)^2\right)^2 \tag{2.35}$$

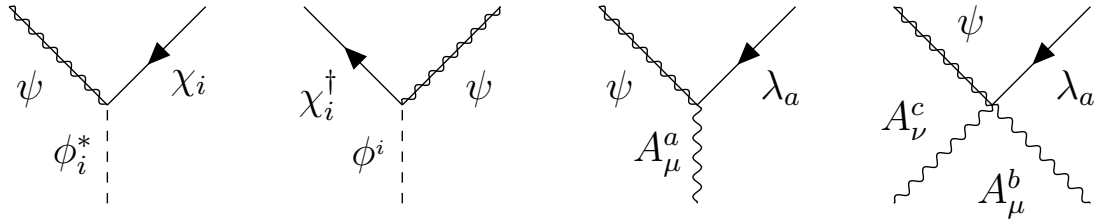

Figure 2.3: The four Feynman diagram arising from interaction terms in lagrangian 2.33. The first two correspond to the marginal chiral operator, while the last two to irrelevant gauge operator.

Chapter 3

Stable gravitino cosmology

As we assume that supersymmetry is a broken symmetry of nature, we need to take into account the effects of the existence of R-odd particles, and among them of the gravitino LSP. The presence of these new particles can largely affect cosmology.

In this chapter we'll first present the gravitino production results as obtained in [46, 49], then we'll add the corrections to these results due to top quark, as shown in [49]. Moreover, we follow the work of [50], dropping the approximation of instantaneous inflaton decay, while keeping the well justified approximation of instantaneous thermalization of decay products.

After getting the right gravitino production rate in the early universe, we review the consequences of gravitino presence in the universe evolution, mainly focusing on unwanted effects [52, 53, 54, 55, 56, 57], showing how the two *cosmological gravitino problems* can be avoided, as shown in [44] and [37].

3.1 Gravitino production in the early universe

In this section we'll be interested in deriving the amount of gravitinos produced in the early universe, namely the evolution of gravitino comoving number density in time.
We know that such a quantity evolves according to the relative Boltzmann equation: in the gravitino case, the ways of production of gravitinos in the early universe are thermal scattering and decay of bath particles.
This in turn gives the following Boltzmann equation for the LSP gravitino comoving number density:

$$\frac{dY_{3/2}}{dT} = -\frac{1}{HT}\left(n_{rad}\langle\sigma_{tot}v_{rel}\rangle + \sum_i \frac{m_i}{\langle E_i\rangle}\Gamma_i Y_i\right), \tag{3.1}$$

where the first term on the RHS stands for scattering production and the second for decay production.
While we know everything about decay production, as Γ_i was obtained in the previous chapter, we miss some information about the scattering term. In particular, we do not know what $\langle\sigma_{tot}v_{rel}\rangle$ is, and its dependence on temperature, hence in the following we'll firstly focus on deriving an explicit expression for that term, while in the following sections we'll focus on cosmological aspects.

The main contribution to gravitino production by scattering comes from QCD processes,

as QCD coupling constant is sensibly larger than the others as the reheating temperature is below GUT scale.
For this reason in the original work [45], the authors focus only on QCD contribution, and later generalize the result to include the other gauge interactions.

Before analyzing in detail the gravitino scattering cross section, we notice that thanks to a general result of thermal field theory, we can derive the total production cross section via evaluating the imaginary part of the gravitino self-energy.
The self-energy is proportional to

$$\Sigma_{3/2}(P) \propto \frac{1}{M_P^2}\left(1+\frac{m_i^2}{3m_{3/2}^2}\right). \tag{3.2}$$

where m_i are gaugino masses.
This factor immediately shows something interesting: the production rate is split into two contributions, one due to $\pm\frac{3}{2}$ modes and one to the $\pm\frac{1}{2}$ goldstino modes.
The former are M_{Pl}^2 suppressed as they should be, while the latter are suppressed by SuSy breaking scale.
This can be shown using the fact that gaugino masses are the explicitly symmetry breaking parameters as shown in section (2.5), hence

$$\frac{1}{M_P^2}\frac{m_i^2}{m_{3/2}^2} \sim \frac{1}{M_P^2}\frac{m_{soft}^2}{(\Lambda_{SuSy}^2/M_P)^2} \sim \frac{1}{\Lambda_{SuSy}^2}\frac{m_{soft}^2}{\Lambda_{SuSy}^2}, \tag{3.3}$$

where $\Lambda_{SuSy} = \sqrt{F}$ is the scale of SuSy breaking in the hidden sector.
In the symmetric case goldstino contributions vanish, but in the non-symmetric phase, if $m_{3/2}^2 \ll m_i^2$ they become largely dominant.
As a last observation, a contribution to gravitino final abundance could come from non-thermal processes during inflaton decay. The relative contribution is typically model-dependent, but it can be shown to be negligible in most cases, as we'll later show.

As a first step we'll try to sum up what is the production rate of a single gravitino due to scattering processes.

For a very light gravitino, interactions are those of lagrangian (2.33) whose resulting vertices are in fig. 2.3. We see that gravitino couples via a non renormalizable operator to gauge supermultiplets and via a renormalizable operator to chiral supermultiplets. When dealing with decay processes, chiral and gauge supermultiplets couple to the gravitino giving comparable widths; on the other hand, when dealing with $2 \to 2$ scattering processes, we get an asymmetric situation, namely since scattering processes will dominate at high energies, processes relative to non-renormalizable operators will be enhanced, with a final yield that exceeds the yield via renormalizable interactions by a factor T. For this reason we will only consider gauge supermultiplets scattering processes. Moreover, processes involving 2 gravitinos in the final state will be Λ_{SuSy}^4 suppressed with respect to the scattering rate involving only one gravitino, where Λ_{SuSy} is the energy scale of SuSy breaking. Hence in the following we will only consider single gravitino gauge scattering, while including chiral supermultiplets when we'll later discuss decay processes.

In considering contribution to gravitino production due to $2 \to 2$ scattering processes, we first focus on the QCD contribution, as the coupling constant g_3 is sensibly larger than the others. Nevertheless, electroweak interaction processes can account for 20% to

process	$\lvert\mathcal{M}\rvert^2/\frac{g^2}{M_P^2}(1+\frac{m_g^2}{3m_{3/2}^2})$	$\lvert\mathcal{A}\rvert^2_{sub}$
$g^a+g^b\to\tilde{g}^c+\tilde{G}$	$4(s+2t+2\frac{t^2}{s})\lvert f^{abc}\rvert^2$	$-2s\lvert f^{abc}\rvert^2$
$g^a+\tilde{g}^b\to g^c+\tilde{G}$	$-4(t+2s+2\frac{s^2}{t})\lvert f^{abc}\rvert^2$	$2t\lvert f^{abc}\rvert^2$
$\tilde{q}_i+g^a\to q_j+\tilde{G}$	$2s\lvert T^a_{ij}\rvert^2$	0
$g^a+q_i\to\tilde{q}_j+\tilde{G}$	$-2t\lvert T^a_{ij}\rvert^2$	0
$\bar{\tilde{q}}_i+q_j\to g^a+\tilde{G}$	$-2t\lvert T^a_{ij}\rvert^2$	0
$\tilde{g}^a+\tilde{g}^b\to\tilde{g}^c+\tilde{G}$	$-8\frac{(s^2+st+t^2)^2}{st(s+t)}\lvert f^{abc}\rvert^2$	0
$q_i+\tilde{g}^a\to q_j+\tilde{G}$	$-4(s+\frac{s^2}{t})\lvert T^a_{ij}\rvert^2$	0
$\tilde{q}_i+\tilde{g}^a\to\tilde{q}_j+\tilde{G}$	$-2(t+2s+2\frac{s^2}{t})\lvert T^a_{ij}\rvert^2$	-t$\lvert$T$^a_{ij}\rvert^2$
$q_i+\bar{q}_j\to\tilde{g}^a+\tilde{G}$	$-4(t+\frac{t^2}{s})\lvert T^a_{ij}\rvert^2$	0
$\tilde{q}_i+\bar{\tilde{q}}_j\to\tilde{g}^a+\tilde{G}$	$2(s+2t+2\frac{t^2}{s})\lvert T^a_{ij}\rvert^2$	$s\lvert T^a_{ij}\rvert^2$

Table 3.1: The ten processes contributing to single gravitino production. f^{abc} and T^a_{ij} are the $SU_C(3)$ color matrices, s and t the usual Mandelstam variables.The third column shows the subtracted matrix element squared divided by the self-energy prefactor.

40% of the total production rate, therefore we'll later generalize the result to all gauge interactions.

Ten tree level processes take part in gravitino scattering production in QCD, as listed in tab. (3.1), four of which are logarithmically divergent as a consequence of massless gluon exchange in t-channel.
These divergences can be avoided moving to finite-temperature theory, where gluons acquire a thermal mass

$$m_g^2=\frac{g^2(T)T^2}{6}(N+n_f), \tag{3.4}$$

where N is the number of colors and n_f is the number of color triplets chiral and anti-chiral supermultiplets; in the MSSM $N=3$ and n_f=6. The acquired thermal mass provides an IR cutoff, that prevents divergence of the full result.

In general, processes listed in tab (3.1) receive a contribution via s,t,u channels, and eventually a contribution via quartic supergravity interactions.
Now, part of these contributions can be obtained using a general result of thermal field theory, i.e. the production rate is proportional to the imaginary part of self-energy via

$$C_{3/2}=-2\int d\Pi f_F(E)Im\Sigma=\int d\Pi\Sigma^<(P), \tag{3.5}$$

where $\Sigma^<$ is the non time-ordered gravitino propagator, summed over polarizations, namely

$$\Sigma^<(P)=\frac{1}{4M_P^2}Tr[\Pi_{\mu\nu}(P)\langle S^\nu(P)\bar{S}^\mu(-P)\rangle_T], \tag{3.6}$$

where S^μ is the supercurrent to which the gravitino couples to.

The diagram that contributes to gravitino production via QCD interaction is reported in fig. (3.1).
This diagram includes an infinite set of multi-loop diagrams, and resummed propagators

that take into account thermal effects: it is important to notice that not only it takes into account $2 \to 2$ scatterings with divergences regularized by thermal effects, but also decays of the type $gluon \to gluino + gravitino$, which are eventually allowed by thermal masses, and become important in some temperature range, as m_g roughly grows as $g \cdot T$.

Hence, one gets a total production which is the sum of diagram (3.1), plus the contribution from processes in tab. (3.1) that are not already included in diagram (3.1). The residual square matrix elements after subtracting those considered in diagram (3.1) are reported in the third column of tab. (3.1).

We're now left to evaluate gravitino self-energy, or equivalently, non time-ordered gravitino propagator.

Now, as already pointed out in chap. 2, in the case of effectively massless gravitino, after spontaneous breaking of supersymmetry, gravitino can be split in two massless fields, the massless gravitino coupled to the supercurrent S^μ, and a massless goldstino that couples to the divergence of the supercurrent (see eq. (2.18)).
Divergence of the supercurrent to which the goldstino couples to reads:

$$\partial_\mu S^\mu = -\sum_{i=1}^{3} \frac{m_i}{4} \mathcal{O}_i, \qquad \mathcal{O}_i = i F^{a,i}_{\mu\nu} (\bar{\sigma}_\mu \sigma_\nu - \bar{\sigma}_\nu \sigma_\mu) \lambda^a, \tag{3.7}$$

where $F_{\mu\nu}$ denotes here the linearized part of the field strength and m_i gaugino masses. Using this facts and recalling eq. (3.6), one gets

$$\Pi^<(P) = \frac{1}{4M_P^2} \left(Tr\langle \bar{S}^\mu \Pi^{3/2}_{\mu\nu} S^\nu \rangle_T - \frac{2}{3m_{3/2}^2} Tr\langle \partial_\mu \bar{S}^\mu \not{P} \partial_\nu S^\nu \rangle_T \right). \tag{3.8}$$

Inserting the massless gravitino polarization tensor given in appendix A, using the gamma identity $\sigma_\mu \bar{\sigma}_\nu \sigma_\mu = -2\sigma_\nu$ and the fact that $\not{\mathcal{S}} = 0$ for vector-gaugino contributions, one gets

$$\Pi^<(P) = \sum_{i=1}^{3} \frac{1}{32 M_P^2} \left(1 + \frac{m_i^2}{3m_{3/2}^2} \right) Tr\langle \bar{\mathcal{O}}_i \not{P} \mathcal{O}_i \rangle_T. \tag{3.9}$$

Finally, integrating eq. (3.9), using the resummed propagator in the trace, and summing the subtracted elements of tab. (3.1) one gets the final result

$$\boldsymbol{C_{3/2}(T) = \sum_{i=1}^{3} \frac{3\zeta(3) T^6}{16\pi^3 M_P^2} \left(1 + \frac{m_i^2}{3m_{3/2}^2} \right) c_i g_i^2 ln \left(\frac{k_i}{g_i} \right)} \tag{3.10}$$

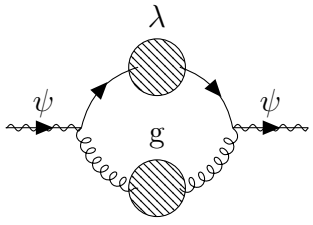

Figure 3.1: Gluon-gluino contribution to gravitino self-energy. The blob denotes a resummed propagator

Gauge group	c_i	k_i
$U_Y(1)$	9.90	1.469
$SU_L(2)$	20.77	2.071
$SU_C(3)$	43.34	3.041

Table 3.2: Values of the parameters k_i and c_i including $2 \to 2$ scattering and decay processes, as reported in [46].

where k_i and c_i are constants, reported in tab. (3.2), and g_i coupling constants.
In eq. (3.10), temperature T provides the energy scale at which gauge couplings and gluino masses have to be evaluated.
Assuming $\alpha = 1/24$ and $m_i = m_{1/2}$ at GUT scale $M_{GUT} = 2 \cdot 10^{16}$ GeV, running of coupling constants and gaugino masses at one loop order are given by:

$$\begin{aligned} g_i^2(T) &= \frac{g_i^2(M_{GUT})}{1 - \frac{b_i}{8\pi^2} g_i^2(M_{GUT}) ln(T/M_{GUT})} \\ m_i(T) &= \left(\frac{g_i(T)}{g_i(M_{GUT})}\right)^2 m_{1/2}, \end{aligned} \tag{3.11}$$

where $b_1 = 11, b_2 = 1, b_3 = -3$.

Authors of [49] also pointed out that a non negligible contribution comes from the top-quark Yukawa coupling.
Looking at the superpotential of MSSM in eq. (2.15) we see that there is a contribution via Higgs production.

The up-like Yukawa parameters in eq. (2.15) read, in the high top mass limit:

$$\mathcal{Y}_u \sim \begin{pmatrix} 0 & 0 & 0 \\ 0 & 0 & 0 \\ 0 & 0 & y_t \end{pmatrix}$$

giving a top Yukawa coupling $y_t \bar{t} T H_u$.

Moreover, a contribution comes from soft breaking terms in eq. (2.16), of the type $\frac{1}{6} a^{ijk} \phi_i \phi_j \phi_k$.

There are four diagrams that give a non vanishing contribution to gravitino production, as shown in fig. 3.2. The top-quark contribution is:

$$\langle \sigma v_{rel} \rangle_{top} = 1.29 \frac{y_t^2}{M_P^2} \left(1 + \frac{\mathcal{A}_t^2}{3 m_{3/2}^2}\right) \tag{3.12}$$

where $\mathcal{A}_t$ is the soft breaking term.

To conclude, the total gravitino production rate including $2 \to 2$ scattering processes, thermal decays of vector bosons, and top soft and Yukawa contribution is:

$$\boldsymbol{\langle \sigma_{tot} v_{rel} \rangle = \langle \sigma_{tot} v_{rel} \rangle_{gauge} + \langle \sigma_{tot} v_{rel} \rangle_{top}} \tag{3.13}$$

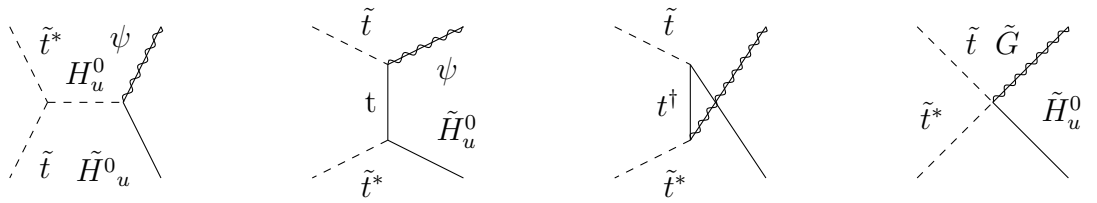

Figure 3.2: The four contribution to gravitino production due to top quark. The first diagram on the left is due to soft breaking term and produces $\pm\frac{1}{2}$ modes, while the others are due to Yukawa coupling and produce $\pm\frac{3}{2}$ modes.

where the first term of RHS is given by eq. (3.10) divided by $n_{rad}^2(T)$, with coefficients in tab. (3.2), while the second is given by eq. (3.12). In the following we'll use $y_t = 0.7$ and negligible $\mathcal{A}_t^2$.

Now that we have all the terms inside the brackets of equation 3.1, we'll make some cosmological considerations to sharpen the accuracy of Boltzmann equation.

3.2 Gravitino production with non-instantaneous reheating

Once we have the thermal average of the total cross section in eq. (3.13), one is tempted to naively solve the Boltzmann equation:

$$\frac{dY_{3/2}}{dT} = -\frac{1}{HT} n_{rad} \langle \sigma_{tot} v_{rel} \rangle \tag{3.14}$$

and integrate it between T_{RH} and T_0 to get the relic gravitino abundance.
Such an integration, assuming negligible g_S dependence on temperature and initial gravitino abundance, would lead to the following result

$$Y_{3/2}(T) = \frac{g_S(T)}{g_S(T_{RH})} \cdot \sqrt{\frac{90}{g^*(T_{RH})}} \cdot \frac{\zeta(3)}{\pi^3} T_{RH} \langle \sigma_{tot} v_{rel} \rangle. \tag{3.15}$$

The above integration has made two implicit assumptions: firstly that the inflaton decay products instantaneously thermalize, and secondly that the reheating process is instantaneous and that at the moment of reheating, the Universe is reheated to a temperature

$$T_{RH} = \left(\frac{40}{g^*(T_{RH})\pi^2} \right)^{1/4} \cdot \left(\frac{\Gamma_\phi M_P}{c} \right)^{1/2}. \tag{3.16}$$

where the $\mathcal{O}(1)$ constant c depends on the definition of reheating moment.
While the assumption of instantaneous thermalization can be kept as justified by [46], the finite duration of the reheating process substantially changes the final result, hence it cannot be neglected.

We now want to drop the hypothesis of instantaneous reheating, letting it be a continuous process.
In fact, right after inflation, the decay of inflaton is not an instantaneous process, rather it must be studied through Boltzmann equation.
For the sake of simplicity, we'll consider only the inflaton field and the radiation that it

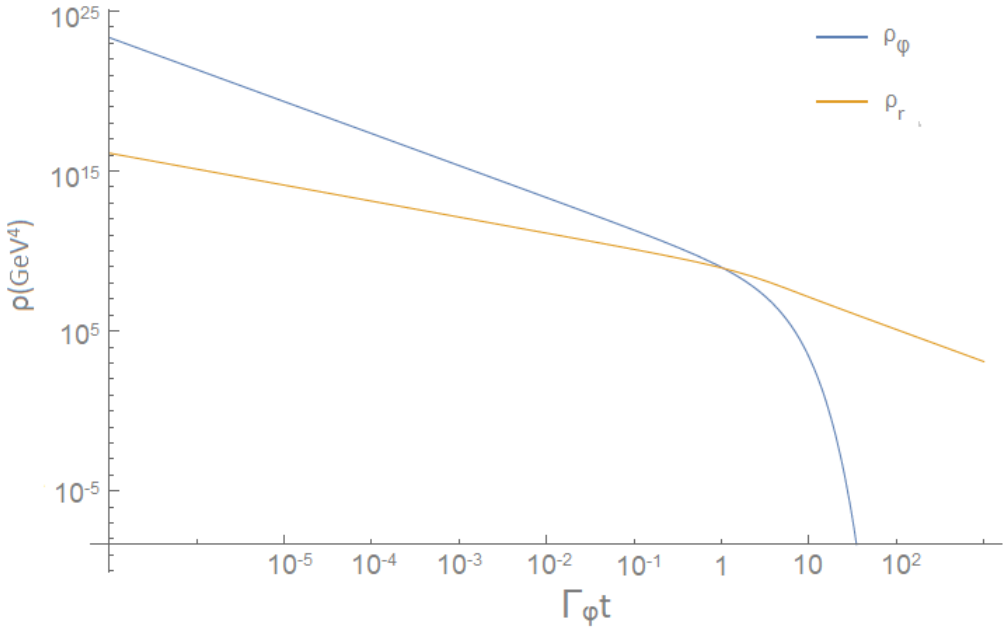

Figure 3.3: Energy densities for radiation and inflaton for a finite duration reheating phase. The initial condition were chosen so that the initial radiation density is negligible, while the inflaton energy density was set to $\rho_\phi = 0.175 M_{Pl}^2 m_\phi^2$ with $m_\phi = 10^{-7} M_{Pl}$.

decays into, which gradually forms the thermal plasma.
The evolution in time of the inflaton energy density can be inferred from its classical equation of motion

$$\ddot{\phi} + (3H + \Gamma_\phi)\dot{\phi} + V'(\phi) = 0. \tag{3.17}$$

After a slow-roll inflationary phase, the inflaton start oscillating around its minimum, producing inflaton particles that will later decay. During this phase, that ends when the reheating temperature is reached and the radiation-dominated phase begins, we're safely allowed to take the average of eq. 3.17 over a complete oscillation

$$\dot{\rho_\phi} + 3H\rho_\phi = -\Gamma_\phi \rho_\phi \tag{3.18}$$

which gives us the first Boltzmann equation for the inflaton energy density.
The radiation content of the Universe originates by inflaton decay, and we'll assume its initial value (i.e. right after inflation ends) to be negligibly small, due to inflation.
The Boltzmann equation for the radiation energy density reads

$$\dot{\rho_r} + 4H\rho_r = \Gamma_\phi \rho_\phi, \tag{3.19}$$

where now we have a production factor on the RHS due to inflaton decay, and the usual dilution factor on the LHS.
The Hubble constant is simply given by Friedmann equation

$$H(\rho_\phi, \rho_r) = \sqrt{\frac{8\pi}{3}} \frac{1}{M_{Pl}} \sqrt{\rho_\phi + \rho_r}. \tag{3.20}$$

In fig. 3.3 we report the behaviour of the energy densities for a continuous reheating process, using the natural unit for time which is $\nu = \Gamma_\phi \cdot t$.

Moreover, the maximum temperature reached during reheating is model-dependent, and we chose here a Starobinsky-like potential, following the work done in [50]:

$$V(\phi) = \frac{3}{4} m_\phi^2 \left(1 - e^{-\sqrt{\frac{2}{3}}\phi}\right)^2, \tag{3.21}$$

During this process, temperatures much higher than T_{RH} can be reached, enhancing gravitino production. At the same time, gravitino produced during inflaton decay due to this temperature jump will be partially washed away, due to the residual entropy production until the end of the reheating phase.

To understand which of the two effects dominates, we have to solve the coupled Boltzmann and Friedmann equations:

$$\begin{aligned} &\dot{\rho}_\phi + 3H\rho_\phi + \Gamma_\phi \rho_\phi = 0 \\ &\dot{\rho}_\gamma + 4H\rho_\gamma - \Gamma_\phi \rho_\phi = 0 \\ &\dot{n}_{3/2} + 3Hn_{3/2} = -\langle \sigma_{tot} v_{rel} \rangle (n_{3/2}^2 - n_{3/2,eq}^2) \\ &\rho_\phi + \rho_\gamma = \frac{3}{8\pi} M_{Pl}^2 H^2 \end{aligned} \tag{3.22}$$

where we have neglected gravitino contribution to the total energy density.
The reheating phase energy density is dominated by the inflaton, which is oscillating around its potential's minimum, hence for all the duration of reheating we can set $w = \frac{P_\phi}{\rho_\phi} = 0$.

Integrating eq.s (3.22), one gets an expression for the scale factor

$$\frac{a(t)}{a(t_{end})} = \left(1 + \frac{v}{A}\right)^{2/3}, \tag{3.23}$$

where $v = \Gamma_\phi \cdot (t - t_{end}) \qquad and \qquad A = \frac{\Gamma_\phi}{m_\phi} \left(\frac{3}{4} \frac{\rho(t_{end})}{m_\phi^2 M^2}\right)^{-1/2}$.
Choosing the potential in eq. 3.21 one gets

$$\frac{\rho(t_{end})}{m_\phi^2 M_P^2} = 0.175, \qquad \rho_\gamma \simeq \rho(t_{end}) \left(\frac{v}{A} + 1\right)^{-8/3} \int_0^v \left(\frac{t}{A} + 1\right)^{2/3} e^{-t} dt.$$

Upon integration one finds the time-temperature relation,which is valid in the limit $A \ll v \ll 1$,

$$T \simeq \left(\frac{24}{\pi^2 g(T)}\right)^{1/4} \sqrt{\Gamma_\phi M_P} v^{-1/4}. \tag{3.24}$$

The behaviour of temperature as a function of time, as $v \ll 1$ is shown in fig. 3.4.

Temperature in finite-duration reheating reaches the value

$$T_{max} = 0.52 \left(\frac{g(T_{RH}) m_\phi}{g(T_{max}) \Gamma_\phi}\right)^{1/4} T_{RH} \tag{3.25}$$

that can be orders of magnitude higher than T_{RH}. The substantial change in the final gravitino yield is driven by relation (3.24).Upon integration of Boltzmann equation for the gravitino yield, using relation (3.24) we get

$$\boldsymbol{\frac{Y_{3/2}^{inst}}{Y_{3/2}(T)} \sim 1.1} \tag{3.26}$$

that is, the instantaneous reheating approximation overestimates the gravitino final yield by a factor ~ 1.1.
Detailed calculation can be found in appendix B.

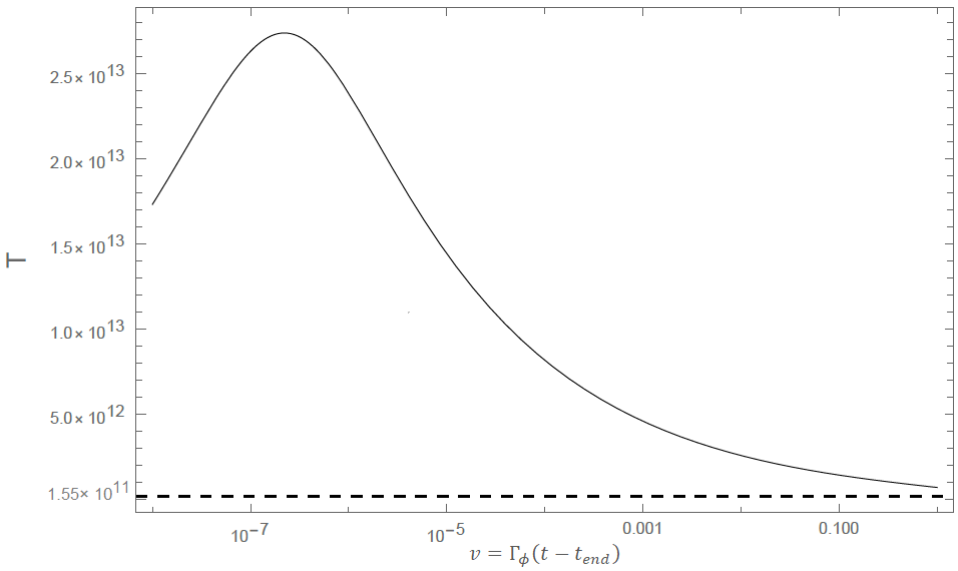

Figure 3.4: Temperature evolution during reheating phase. The dashed line is the reheating temperature defined in eq. (3.16), with the choice $c = 1$. This graphic is obtained by setting $\Gamma_\phi = 10^{-12} M_P = 10^{-7} m$, with a Starobinsky potential.

3.3 Non-thermal production of gravitinos

What we studied above involves only thermal production of gravitino, i.e. via processes that involve thermalized particles.
Nevertheless a non negligible contribution could come from non-thermal processes, as direct inflaton decay or scattering of hard decay products which have not already thermalized.
In the following we'll briefly review this two cases; results are inflation model-dependent, but are typically negligible.

Gravitinos could be produced via scattering of inflaton decay product with momenta $p \sim m_\phi$. If we suppose for instance that inflation mainly decays to gauge bosons via $\phi \to gg$, a subsequent scattering (first line of tab 3.1) could produce a gravitino.
Upon integration of Boltzmann equation considering the first process in tab 3.1, focusing only on the $SU_C(3)$ contribution, we get the following ratio of collision terms

$$\frac{\mathcal{C}_{non-th}}{\mathcal{C}_{th}} \sim \frac{160}{ln(k_3/g_3)} \left(\frac{\Gamma_\phi}{m_\phi}\right)^{1/2} \frac{M_P}{m_\phi}. \tag{3.27}$$

This result would turn in an enhanced production via non-thermal processes if $\Gamma_\phi \gtrsim 10^{-14} m_\phi$.Nevertheless this holds while the decays product are not thermalized, but since thermalization is rapidly achieved, the products of decays would be rapidly washed away by residual entropy production.

The contribution by inflaton decay depend on the *branching ratio* of decays to gravitinos, $\mathcal{B}_{3/2}$.Assuming rapid thermalization, the relative contribution is

$$\frac{Y_{3/2}^{decay}}{Y_{3/2}^{thermal}} \sim 1.6 \cdot 10^3 \mathcal{B}_{3/2} \frac{M_P}{m_\phi}.$$

Branching ratio to gravitinos is again model dependent, but is typically negligibly small, resulting in a vanishing contribution to gravitino final abundance.

3.4 Cosmological gravitino problems

The presence of stable or unstable gravitino during the Universe evolution could easily turn out in unwanted effects [52, 53, 54, 55, 56, 57], that could spoil already tested results, and hence that necessarily have to be avoided. The possible unwanted effects of LSP-gravitino presence are referred to as *cosmological gravitino problems*, and are mainly the following two:

- Sparticles decays can spoil BBN widely accepted results.
- Gravitino can be overproduced hence not matching the expected relic density.

In the following we'll analyze these two effects, and explain how they can be avoided.

3.4.1 Gravitino overproduction problem

One of the two cosmological gravitino problems is that gravitino presence could easily be overproduced, achieving a relic density that exceeds that expected for dark matter, in strong contrast with observations.
Authors of [43] showed that there is a limit to gravitino mass, under which gravitino cannot be overproduced.
In their article they showed that the gravitino number density is today

$$n_{0,3/2} = \frac{3}{4}\frac{g_{3/2}}{22}\frac{43}{g(T_{dec})}n_{0,\gamma}$$

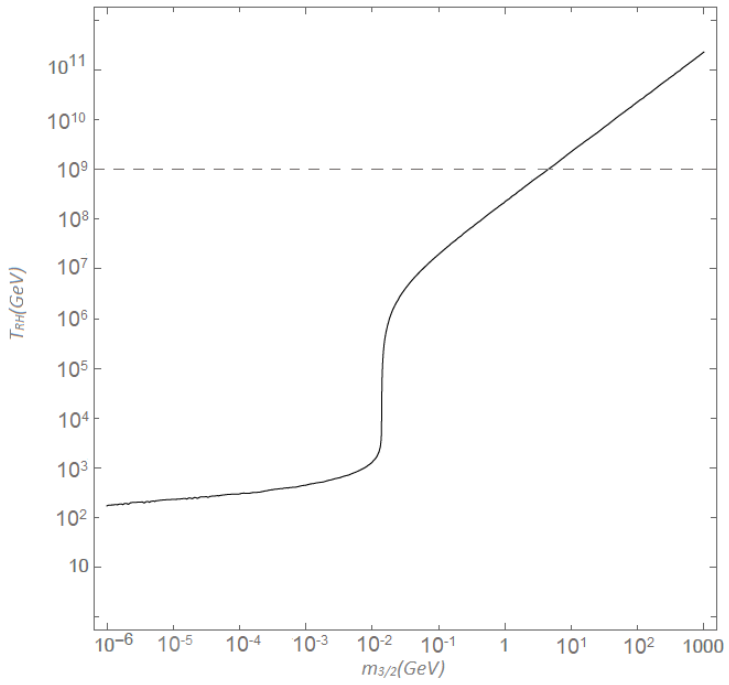

Figure 3.5: Constraint on reheating temperature and gravitino mass due to overproduction problem. The solid line is the contour of $\Omega_{3/2}h^2 = 0.11$. The graph was obtained by using universal scalar masses $m_s = 4$ Tev and unified gaugino masses at Gut scale at $m_{1/2} = 1$Tev.

where $g(T_{dec})$ is the number of effective degrees of freedom at gravitino decoupling (when thermalized), which we'll assume to be $g(T_{dec}) \sim \mathcal{O}(10^2)$.
The critical density constraint assuming negligible photon contribution is therefore:

$$m_{3/2} n_{0,3/2} + n_\nu \sum m_\nu \lesssim \rho_c$$

and assuming also negligible neutrino contribution one gets the constraint on gravitino mass

$$m_{3/2} \lesssim 1KeV \tag{3.28}$$

If gravitino mass is above this bound, one can still avoid the closure problem imposing a limit on T_{RH}.
This was shown at first in [44], using Boltzmann equation

$$\frac{dY_{3/2}}{dT} = -\frac{1}{HT}\left(n_{rad}\langle \sigma^{1/2} v_{rel}\rangle + \sum_i \frac{m_i}{\langle E_i\rangle}\Gamma_i Y_i \right), \tag{3.29}$$

where the first term on the RHS takes into account the scattering production in the sense explained in sec. (3.1) , while the second term stands for production via scalars decay.
The cross section $\sigma^{1/2}$ takes into account processes involving the $\pm 1/2$ helicity modes only, since they are largely dominant in the light gravitino approximation, as explicitly shown in 3.2.

Solution to eq. (3.29) is

$$Y_{3/2}(T) = \frac{g_s^*(T)}{g_s^*(T_{RH})}\left(\bar{Y}_{Scatt} + \bar{Y}_{Dec}\right), \tag{3.30}$$

where

$$\bar{Y}_{Scatt} = \frac{n_{rad}(T_{RH})\langle \sigma v_{rel}\rangle}{H(T_{RH})}, \qquad \bar{Y}_{Dec} = \int_T^{T_{RH}} \frac{dT}{T}\sum_i \frac{m_i \Gamma_i}{\langle E_i\rangle H} Y_i, \tag{3.31}$$

and the prefactor takes into account dilution due to the universe expansion.

The scattering yield grows linearly with T_{RH}, and as seen in sec 3.1 the main contribution comes from gauginos.

The decay yield is instead

$$\bar{Y}_{Dec} \propto \int_{T_0}^{T_{RH}} \frac{dT}{T^3}\sum_i Y_i \frac{m_i}{\langle E_i\rangle},$$

for temperatures much higher than sparticle masses, the Lorentz factor is proportional to T, while Y_i is approximately constant, so that the final result is independent of T_{RH} as long as it is larger than sparticle masses. For smaller temperatures, Y_i becomes rapidly small, being Boltzmann suppressed. The integral rapidly converges to $\mathcal{O}(m_i^{-2})$, for $T_{RH} \gg m_i$, while $\Gamma_i \sim \frac{m_i^5}{6 m_{3/2}^2 M_{Pl}^2}$ so that the final yield is proportional to $m_i^3/(M_{Pl} m_{3/2}^2)$.

For the scattering cross section we used eq. (3.10) keeping into account the correction in eq. (3.26). Annihilation processes where neglected in eq.(3.29), but they are

non-negligible if $\bar{Y}_{Scatt} + \bar{Y}_{Dec} \sim \mathcal{O}(1)$. Authors of [44] used the following trick to take into account annihilation processes: if $\bar{Y}_{Scatt} + \bar{Y}_{Dec} > 3/2$, they considered thermalized gravitino and $\bar{Y}_{Scatt} + \bar{Y}_{Dec} = 3/2$.

The result of the analysis is shown in fig. 3.5; three main regions can be identified in the graph:

- $m_{3/2} \lesssim 1$ KeV: there's no bound on T_{RH}, since gravitino cannot possibly be overproduced.
- 10^{-6} GeV $\lesssim m_{3/2} \lesssim m^*$: sparticles decays are important, and gravitinos are overproduced unless T_{RH} is roughly below scalar masses.
- $m_{3/2} \gtrsim m^*$: scattering processes are dominant and as can be seen from eq.(3.31), the yield is proportional to T_{RH}.

The value m^* depends sensibly on gauginos and scalar masses ratio, in particular it roughly depends on $\frac{m_s^3}{m_{1/2}^2}$.

3.4.2 BBN constraint

Constraints from BBN in the case of LSP gravitino involve mainly NLSP decay, since it can only decay into a gravitino LSP and is hence the longest-lived unstable R-odd particle.
The problem of NLSP decay is that it could easily spoil BBN predictions by photodissociation of light elements. This affects the gravitino mass, providing an upper bound.

The consequences of NLSP decay depend on which particle is the NLSP. We'll here briefly consider the three most likely cases: *sneutrino*, *neutralino* and *stau*.

In the case of a *sneutrino* NLSP, decays cannot produce sufficient photons to considerably affect BBN, hence no upper bound on $m_{3/2}$ is required.

In the case of a *neutralino* or a *stau* NLSP, the relic density has been evaluated in [51] and [58], and it is shown to exceed

$$m_{NLSP} Y_{NLSP} \geq 5.0 \cdot 10^{-11} GeV. \tag{3.32}$$

Taking this value, an overproduction of ${}^3He + D$ occurs unless $\tau_{NLSP} \lesssim 2.6 \cdot 10^6 s$.
Using decay rate, eq. (2.34), one gets

$$\left[\frac{1}{48\pi} \frac{m_{NLSP}^5}{m_{3/2}^2 M_P^2} \left(1 - \left(\frac{m_{3/2}}{m_{NLSP}} \right)^2 \right)^3 \right]^{-1} \lesssim 2.6 \cdot 10^6 s,$$

which for fixed NLSP mass gives a constraint on $m_{3/2}$.

For $m_{NLSP} \leq 1$ TeV, some numerical results are $m_{3/2} \lesssim 1.17$ GeV (6.6 GeV, 245.6 GeV, 715.8 GeV) for $m_{NLSP} = 50$ Gev (100 GeV, 500 Gev, 1 TeV).
For $m_{NLSP} > 1$ TeV the limit becomes more severe, and only a tiny window for $m_{3/2}$ is available.

Chapter 4

Freeze-in mechanism for dark matter production

As the nature of dark matter remains yet unknown, it is also not clear what cosmological mechanism led to a constant comoving number density for one (or more) particle species.

Historically, the most credited and studied mechanism that grants a final relic density which is comparable to that observed for dark matter, is *freeze-out* mechanism, which offers the useful feature to be UV independent. The study of this dark matter genesis mechanism led to the so-called *wimp* miracle: a weak-scale mass particle, which interacts weakly with the visible sector, could account for most DM relic abundance.

Nevertheless freeze-out is not the only available mechanism for DM relic abundance genesis: authors of [59] showed that a novel mechanism they called *freeze-in*, can be a viable way to produce a reasonable relic abundance of *fimp* particles.

Moreover if one extends the dark sector to more than one particle species, a larger variety of mechanisms arises, including the interesting *dark-freeze-out* and *re-annihilation*, which although extremely intriguing, lie outside the aim of this thesis.

In the following we'll review the freeze-in mechanism and its features, specifically in the case in which dark matter is produced via the decay of bath particles, which will be very useful for the rest of this work.

4.1 *Freeze-in* mechanism

Freeze-out was considered the main way of IR-dominated production of dark matter, nevertheless this is not the only way to generate a final abundance that could account for dark matter density.
A new suggestion came in [59], with the proposal of freeze-in mechanism.
This alternative way is somehow opposite to freeze-out, though they share some crucial aspects.

The idea is to have a particle species χ, which interacts so weakly with the bath, that it never achieves thermal equilibrium; together with the assumption that χ primordial density be negligible, for instance due to inflation effects.
Although the interactions are very small, some χ particle can be produced from the thermal plasma, the main production being achieved when temperature drops below the

largest mass, M, involved in an interaction vertex with χ. Due to its extremely small coupling and to relatively small abundance, χ annihilation processes are not active, and the comoving number density after production remains constant.

In order to have a first qualitative idea of what freeze-in main features are, let's suppose particle χ interacts with the thermal plasma with dimensionless interaction strength λ, and let $T \gg m_\chi$ so that particle χ is relativistic. Assuming that the Universe is radiation dominated

$$H^2(T) = \frac{8\pi}{3}\frac{\rho}{M_{Pl}^2} \sim \frac{T^4}{M_{Pl}^2},$$

while the interaction rate of χ particle reads

$$\Gamma \sim n(T)\langle\sigma v\rangle \tag{4.1}$$

where brackets denote an appropriate thermal average. In the case of a massless gauge boson mediated interaction, eq. (4.1) becomes

$$\Gamma \sim T^3\frac{\lambda^2}{T^2} = T\lambda^2. \tag{4.2}$$

To have an idea of what the yield due to freeze-in is, we can simply multiply the interaction rate Γ by the Hubble time $\tau_H \sim H^{-1}$ getting

$$Y(T) = \Gamma(T)H^{-1}(T) \sim \lambda^2\frac{M_{Pl}}{T}. \tag{4.3}$$

We immediately notice that the yield increases with increasing coupling strength; moreover, the yield is temperature-suppressed, hence lower temperatures are favoured. In fact, let m be the largest mass of a particle involved in the χ interaction: for temperatures well above m, the yield is suppressed due to the Hubble rate, while for temperatures below m, it is suppressed due to the fact that the interaction involves a non-relativistic particle whose number density is Boltzmann-suppressed. Therefore, the largest yield will be achieved when $T \sim m$, and from eq. (4.3),

$$Y_{FI} \sim \lambda^2\frac{M_{Pl}}{m}. \tag{4.4}$$

This means that the final freeze-in yield is typically IR-dominated, hence independent of unknown UV quantities that remain experimentally inaccessible. As in the freeze-out case, the relic abundance of a frozen-in particle depends solely on equilibrium quantities and masses involved in the relevant interactions.

For comparison, the freeze-out yield in the case in which DM mass m' is the only mass scale involved in $\langle\sigma v\rangle$, reads

$$Y_{FO} \sim \frac{1}{\lambda'^2}\frac{m'}{M_{Pl}^2},$$

and the *wimp* miracle occurs when a particle of mass $m \sim v$ (where v is the electroweak scale) interacts with $\lambda' \sim 1$, giving

$$Y_{FO} \sim \frac{v}{M_{Pl}}. \tag{4.5}$$

If we suppose that particle χ that undergoes freeze-in has a mass at electroweak scale $m \sim v$, in order to have the same final yield (4.5), the interaction strengthe must be way

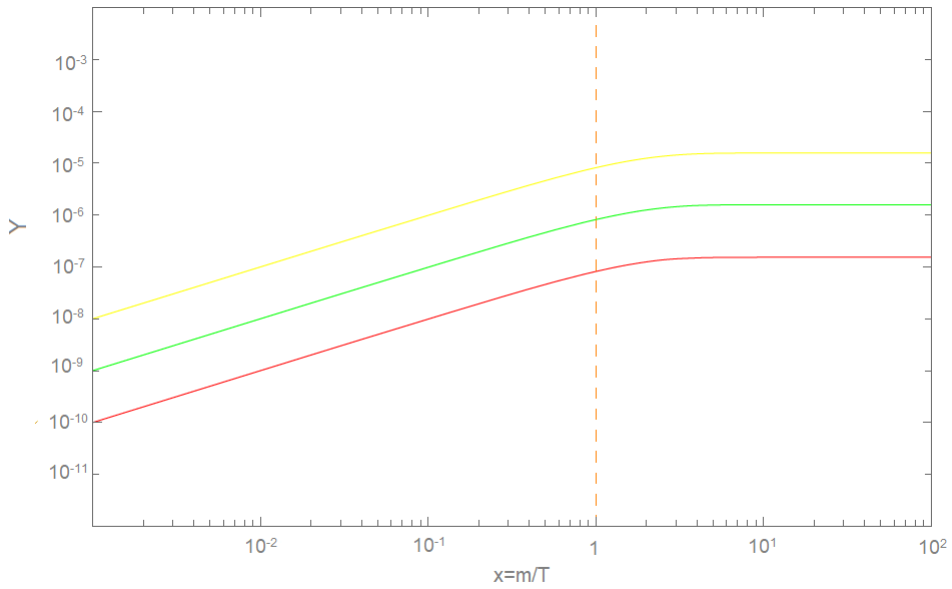

Figure 4.1: Evolution in time of comoving number density of a fimp particle that undergoes freeze-in, for increasing coupling strength, as a function of the ratio between the largest relevant mass to which the fimp couples to and temperature. We see that the comoving number density remains constant for temperatures lower than $(5 \div 10)m$.

smaller than the freeze-out case, namely $\lambda \sim \frac{v}{M_{Pl}}$ (compare eq. 4.4).

Due to the smallness of the required coupling leading to freeze-in, the species that undergoes such a mechanism is referred to as *feebly interacting massive particle*, or simply *fimp*. A sketch of the behaviour of DM yield due to freeze-in is shown in fig. (4.1).
To better understand this new mechanism and to better understand the parametric dependence of the final yield, we'll show some quantitative examples in the following.

4.2 *Fimp* and *losp*: different masses, different scenarios

Fimp is an alternative particle (or group of particles), other than *WIMP*, that could be responsible for DM genesis and relic abundance, nevertheless *fimp* is not necessarily DM itself.

In general we suppose that DM is made stable by a conserved $\mathbb{Z}_2$ discrete symmetry; being the lightest $\mathbb{Z}_2$-odd particle grants stability.

In this case, two kind of particles are of particular interest for our purposes, and could be a good DM candidate: *fimp* itself and the lightest $\mathbb{Z}_2$-odd particle in thermal equilibrium with the bath, referred to as *losp*, *'lightest observable sector particle'*.

Depending on which between *fimp* and *losp* is lighter and on which between freeze-in and freeze-out is the main mode of DM production, we get a different phenomenology (see fig. 4.2):

– **Freeze-in production of dark matter**:

- *fimp* is lighter than *losp* and is itself dark matter (case I of fig 4.2). *losp* undergoes normal freeze-out, and decays to the *fimp*, contributing with a tiny amount to DM relic density
- *losp* is lighter than *fimp*, and it is dark matter (case II of fig 4.2). The main production comes from freeze-in of *fimp*, which later on decays to *losp*. A tiny amount of *losp* DM is generated by freeze-out

– **Freeze-out production of dark matter**:

- Super-WIMP scenario (case III of fig 4.2): *fimp* is lighter than *losp*. In this case the main contribution comes from *losp* freeze-out and subsequent decay to *fimp*. This is called Super-WIMP mechanism because of its analogy with the WIMP DM case.
- WIMP scenario (case IV of fig 4.2): *losp* is lighter than *fimp*, and the main contribution comes from direct *losp* freeze out. A subdominant contribution comes from *fimp* which freezes-in and decays to *losp*. If this contribution is negligible, the old freeze-out result is recovered.

This four cases are schematically depicted in fig. 4.2.

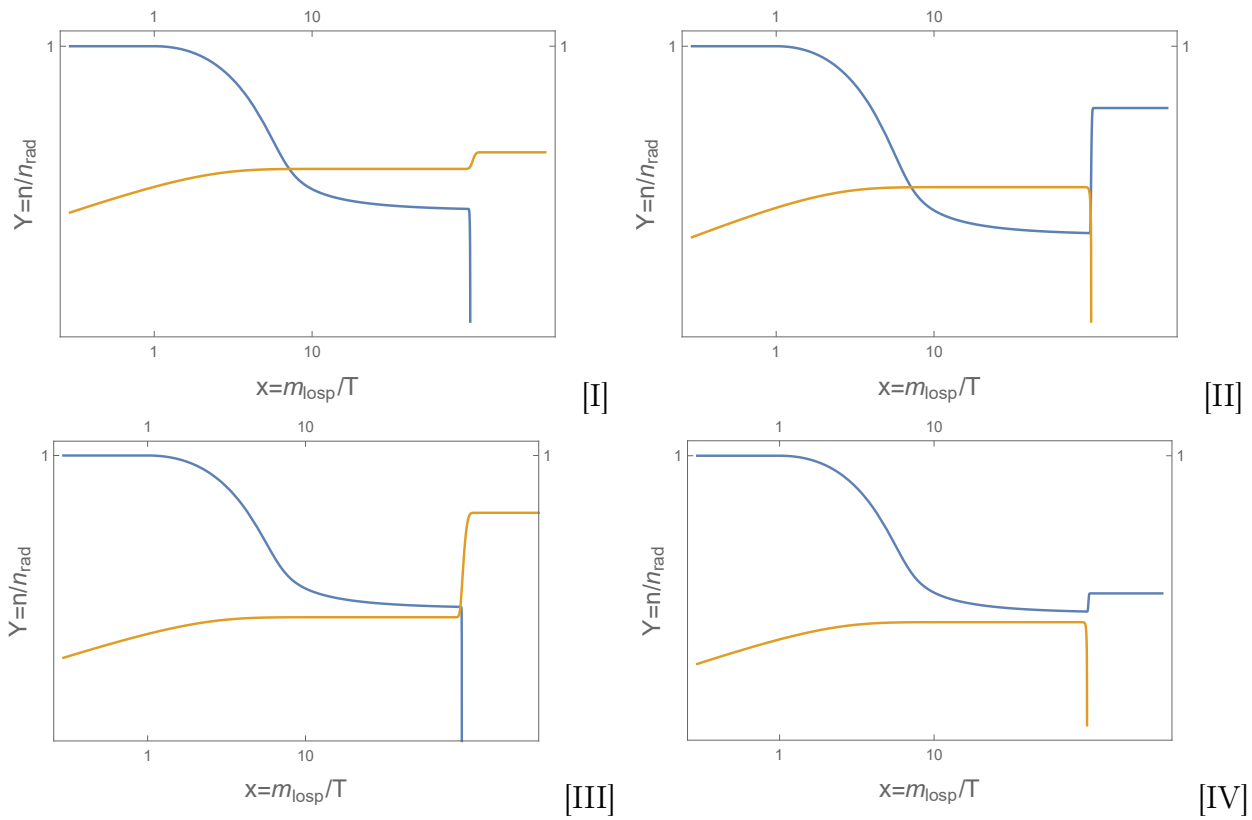

Figure 4.2: We show fimp and losp comoving number densities as a function of m_{losp}/T in the four different cases of DM production: the blue line depicts *losp* abundance, while the green line *fimp* abundance. The main way of production is freeze-in for figures (I) and (II) and freeze-out figures (III) and (IV).

4.3 A simple example: decays of bath particles

In order to point out what are the main features of freeze-in mechanism, we present here a simple direct calculation, namely we show the final yield of particle χ which never achieves thermal equilibrium, but is produced by decays of bath particles.
Although this is not the general case, which could involve for instance $2 \to 2$ scattering processes, freeze-in via decay is the process that we'll need in the following, so we'll limit our considerations to this case.
Let ψ_1 be a particle species which is in thermal equilibrium with the bath in the early universe, an let it interact with particle χ via an interaction term of the type

$$\mathcal{L}_{int} = \lambda \psi_1 \psi_2 \chi. \tag{4.6}$$

We assume a mass spectrum of the type $m_{\psi_1} > m_\chi + m_{\psi_2}$; so that the $\psi_1 \to \psi_2 \chi$ is the main freeze-in mode of production of particle χ.
In order to obtain the final yield we need to solve Boltzmann equation

$$\begin{aligned} s\dot{Y}_\chi = \int & d\Pi_\chi d\Pi_{\psi_1} d\Pi_{\psi_2} (2\pi)^4 \delta^4(p_\chi + p_{\psi_2} - p_{\psi_1}) \\ & \cdot \left(|\mathcal{M}|^2_{\psi_1 \to \psi_2 + \chi} f_{\psi_1}(1 \pm f_\chi)(1 \pm f_{\psi_2}) - |\mathcal{M}|^2_{\psi_2 + \chi \to \psi_1} f_{\psi_2} f_\chi (1 \pm f_{\psi_1}) \right) \end{aligned} \tag{4.7}$$

where s is the entropy density and $d\Pi = \frac{d^3p}{2E(2\pi)^3}$.

We now make the assumption that the initial χ abundance is negligible, allowing us to set $f_\chi = 0$. Moreover we neglect Pauli-blocking and Bose-enhancement effects corresponding to $1 \pm f_{\psi_2} \sim 1$ and assume an equilibrium distribution for ψ_1.

Under these assumptions and using the definition of the decay width Γ_{ψ_1}, Boltzmann equation becomes

$$s\dot{Y} = \int \frac{d^3p}{(2\pi)^3} \frac{f_{\psi_1} \Gamma_{\psi_1}}{\gamma_{\psi_1}}, \tag{4.8}$$

where $\gamma_{\psi_1} = E_{\psi_1}/m_{\psi_1}$ is the Lorentz time dilation factor.
Passing to an integral over energy, eq. (4.8) can be written

$$\begin{aligned} s\dot{Y} =& g_{\psi_1} \frac{m_{\psi_1} \Gamma_{\psi_1}}{2\pi^2} \int_{M_{b1}}^{\infty} (E^2_{\psi_1} - m^2_{\psi_1})^{1/2} e^{-E_{\psi_1}/T} dE_{\psi_1} \\ =& \frac{g_{\psi_1} m^2_{\psi_1} \Gamma_{\psi_1}}{2\pi^2} T \mathcal{K}_1 \left(\frac{m_{\psi_1}}{T} \right), \end{aligned} \tag{4.9}$$

where $\mathcal{K}_1(x)$ is the first modified Bessel function of the second kind. Upon using the variable $x = \frac{m_{\psi_1}}{T}$ and integrating between $x_{min} = 0$ and $x_{max} = \infty$ gives the final result

$$Y_\chi = 4.71 \cdot \frac{45}{4\pi^4 1.66} \frac{\Gamma_{\psi_1} M_{Pl} g_{\psi_1}}{m^2_{\psi_1} g^S \sqrt{g^\rho}} \tag{4.10}$$

Corresponding to final abundance

$$\Omega_\chi h^2 = \frac{1.09 \cdot 10^{27} g_{\psi_1}}{g^S \sqrt{g^\rho}} \frac{m_\chi \Gamma_{\psi_1}}{m^2_{\psi_1}}. \tag{4.11}$$

This is a very simple calculation, but it's crucial for our purposes. Moreover from this example and eq. (4.10) we explicitly see a fundamental feature of freeze in: the final yield

is proportional to interaction cross section, the opposite situation respect to freeze-out case.
This somehow bounds the interaction strength: in fact λ must be sufficiently small so that χ never achieves thermal equilibrium, in order for freeze-in to be the main mode of production (this is a necessary but not sufficient condition, as we'll later show); but still λ must be sufficiently high in order for χ to account for at least part of the DM abundance.
Using eq. (4.11), and assuming for definiteness $\Gamma_{\psi_1} \sim \lambda^2 m_{\psi_1}/8\pi$ and $g^S \sim g^\rho$, demanding $\Omega_\chi h^2 \simeq 0.11$, we get

$$\lambda = 1.6 \cdot 10^{-12} \left(\frac{m_{\psi_1}}{m_\chi}\right)^{1/2} \left(\frac{g_*(m_{\psi_1})}{10^2}\right)^{3/4}. \tag{4.12}$$

From eq. (4.12) we learn that a good candidate for DM, which is produced mainly via freeze-in, needs to have a relatively tiny interaction strength, for this reason we refer to such a species as *fimp*.

For completeness we also show the result in the case in which the particle species that undergoes *freeze-in*, *fimp*, is not dark matter itself,but it rather decays to dark matter after *freeze-in*.
In this case the crucial interaction is again of the type in eq. (4.6), with the only difference in mass spectrum which in this case is set to $m_\chi > m_{\psi_1} + m_{\psi_2}$.
In this case, χ is produced by the inverse decay $\psi_1 + \psi_2 \to \chi$, with a final yield which not surprisingly is of the form of eq. (4.10):

$$Y_\chi = 4.71 \cdot \frac{45}{4\pi^4 1.66} \frac{\Gamma_\chi M_{Pl} g_{\psi_1}}{m_\chi^2 g^S \sqrt{g^\rho}} \tag{4.13}$$

Assuming now that χ decays after ψ_1 *freeze-out*, the final DM abundance is

$$\Omega_{\psi_1} h^2 = \frac{1.09 \cdot 10^{27}}{g^S \sqrt{g^\rho}} \frac{m_{\psi_1} \Gamma_\chi}{m_\chi^2}. \tag{4.14}$$

4.4 Freeze-in phase diagrams

Now that we have some numerical results, we can further analyze for what values of the coupling constant λ the *freeze-in* mechanism is responsible for DM abundance, depending on the parameters of the model.
Again, for future purposes, we'll study the case in which the *fimp* is produced via bath particles decays, namely with an interaction term

$$\mathcal{L}_{int} = \lambda \psi_1 \psi_2 \chi$$

with masses $m_{\psi_1} > m_\chi \gg m_{\psi_2}$.

In a first moment, we'll consider the case in which m_{ψ_1} and m_χ are of the same order of magnitude; we'll later drop this assumption, and let m_χ vary for a given m_{ψ_1}.
This will allow us to understand which range of the coupling constant λ is compatible with the observed dark matter abundance.

Particle χ freezes-in via the allowed decay $\psi_1 \to \psi_2 + \chi$ with final yield given by eq.(4.10). The final yield in this case is roughly

$$Y_{fi,0} \sim 10^{-4}\lambda^2 \left(\frac{M_{pl}}{M_\chi}\right), \tag{4.15}$$

where we've ignored the difference between g^ρ and g^S, and we set both to $g^* = 100$.

Eq. (4.15) shows that the final *freeze-in* yield is $\mathcal{O}(1)$ in the coupling range $\lambda^2 \gtrsim 10^4 \frac{m_\chi}{M_{pl}}$.

This is an important turning point: for this range of coupling constant, χ will reach a full thermal abundance, erasing all information about earlier stages, while for smaller couplings χ never achieves the equilibrium density.

In the $\lambda^2 > 10^4 \frac{m_\chi}{M_{pl}}$ regime, the final abundance of χ will be hence determined by *freeze-out* after thermal number density has been reached via *freeze-in*; decoupling is achieved when the annihilation process $\chi\chi \to \psi_2\psi_2$ becomes no longer effective.
Now we have two possibilities:

- $\lambda^2 > \sqrt{10^4 \frac{m_\chi}{m_{pl}}}$: conventional *freeze-out* will take place, with final abundance given by eq. (1.25) (region I in fig. 4.3),
- $\lambda^2 < \sqrt{10^4 \frac{m_\chi}{m_{pl}}}$: *freeze-out* will take place before χ becomes non-relativistic, hence the final yield is a thermal one (region II in fig . 4.3);

On the other hand for $\lambda^2 < 10^4 \cdot \frac{m_\chi}{M_{pl}}$, thermal density is not achieved, and we again have two possibilities:

- $\lambda^2 > \left(10^4 \frac{m_\chi}{M_{pl}}\right)^2$: *freeze-in* is still able to account for most χ production, corresponding to graph (i) of fig 4.2 and to region III in fig 4.3,
- $\lambda^2 < \left(10^4 \frac{m_\chi}{M_{pl}}\right)^2$: the most contribution comes from ψ_1 *freeze-out* and subsequent decay to χ, corresponding to the graph (iii) of fig 4.2 and to region IV in fig. 4.3.

The contour for $\Omega h^2 = 0.11$ in the four regions are shown in panel (i) of fig. 4.3

By further analysis, it can be shown that the behaviour reported in the left panel of fig. 4.3 seems to be somehow valid in the general case. For renormalizable interactions, independently of particles nature (scalar, fermion or bosons), in the presence of a $\mathbf{Z}_2$ symmetry that makes DM stable, when m_χ and m_{ψ_1} are of the same order of magnitude, the results of fig. 4.3 hold.

As anticipated, we'll now drop the assumption that m_{ψ_1} and m_χ are of the same order of magnitude. For a fixed m_{ψ_1}, we'll let m_χ vary. Limit between *freeze-out* and *freeze-in* regions (I-II and III-IV) is now a bound on λ alone.
If for instance we set $m_\psi = 1$TeV, the result is shown in panel (ii) of fig. 4.3.

If we now keep m_χ fixed and analyze the final abundance as a function of λ (see fig. 4.4, we see that for a large range of λ values there will be an overproduction of DM. In the case of fig. 4.4 where we fixed $m_\chi = 1$TeV, the two regions which are still available are $\lambda \lesssim 10^{-12}$, corresponding to region IV where DM is produced by *LOSP freeze-out* and subsequent decay, and $\lambda \gtrsim 1$, corresponding to region I, where conventional *freeze-out* is responsible for DM relic abundance.

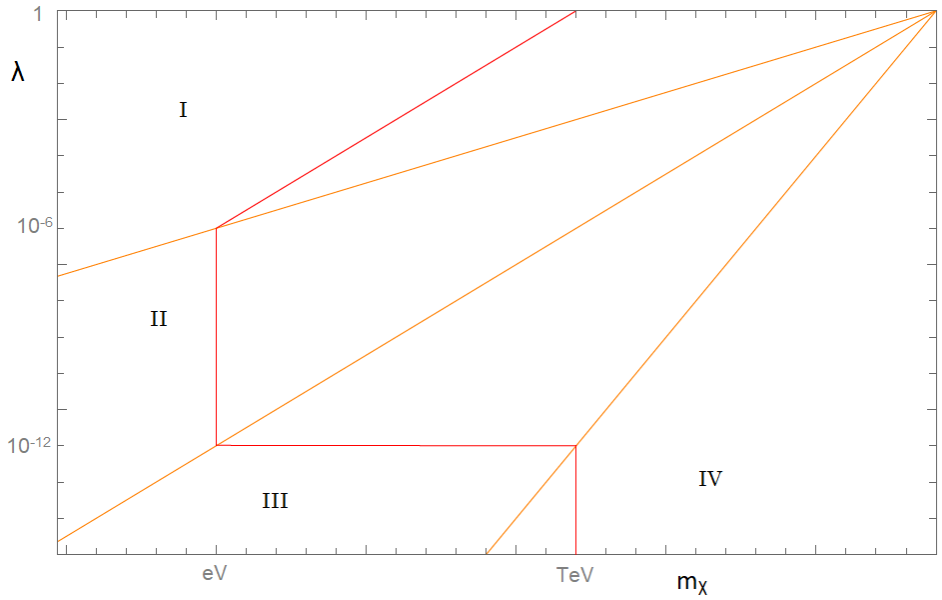

(i)

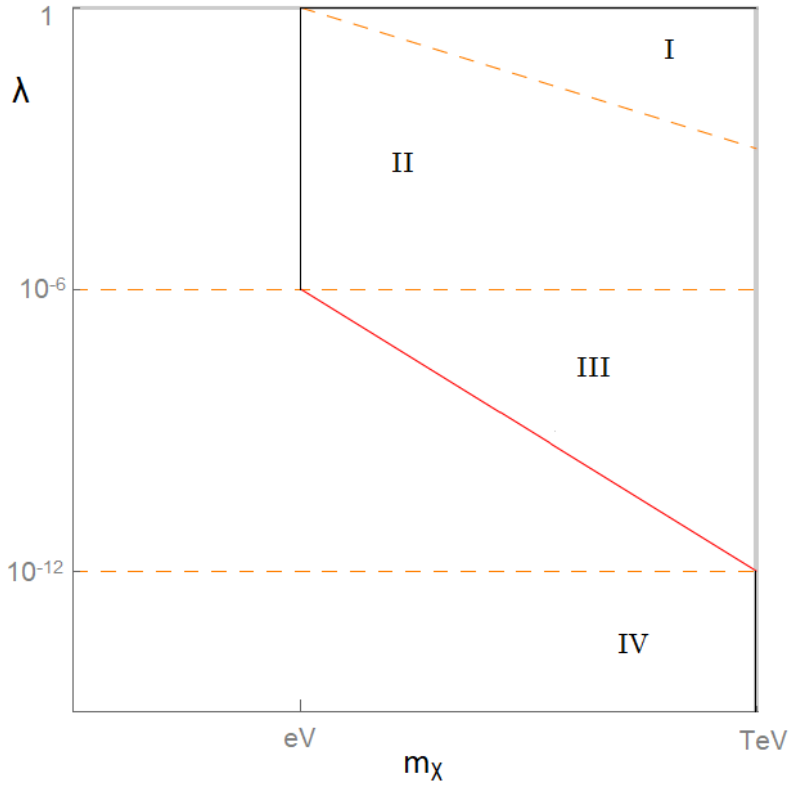

(ii)

Figure 4.3: The two panels show contours for $\Omega h^2 = 0.11$ for different values of λ and m_χ. Panel (i) has $m_\chi \sim m_{\psi_1}$, while for panel (ii) we fixed $m_{\psi_1} = 1\text{TeV}$ and let m_χ vary. Regions I-IV correspond to those in the above analysis.

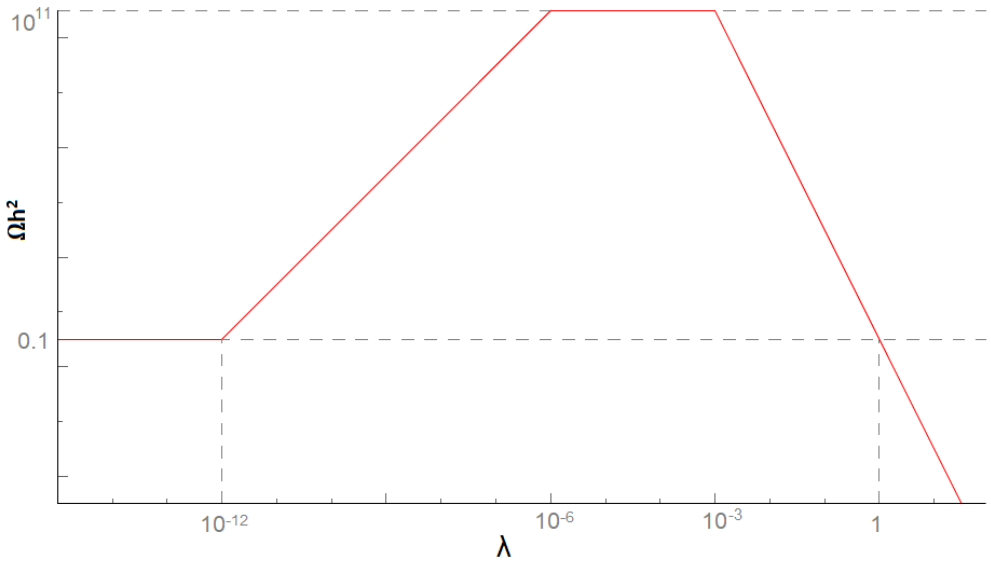

Figure 4.4: In this figure we show the final abundance for a fixed $m_\chi = 1TeV$, as a function of the coupling strength. We immediately see that for most λ range we have an overproduction of χ particles. For m_χ at TeV scale, the regions $\lambda \lesssim 10^{-12}$ and $\lambda > 1$ are compatible with the observed dark matter relic abundance.

4.5 Freeze-in via scattering and UV sensitivity

In the previous section we analyzed freeze-in production via bath particles decay, getting the final yield of eq. (4.10). This result offers us the possibility of quantitative further analysis, and it shows moreover one interesting aspect that the two mechanisms of freeze-out and freeze-in share, namely that the final yield is IR dominated.
We will linger for a moment on this aspect, to give a clarification. The case we analyzed in sec. 4.3, made use of the interaction lagrangian (4.6), which in a general theory could correspond to a renormalizable or non-renormalizable operator. In the case of decay processes, the final yield is of the type (4.11), regardless of the dimension of the relative operator, resulting in a final yield that is proportional to the mass of decaying particle, hence IR dominated.

On the other hand, when dealing with scattering freeze-in production, which we did not quantitatively analyze in this thesis, the situation is quite different.
In fact, for a renormalizable operator, the scattering freeze-in yield remains IR dominated, for definiteness we report the result as obtained in [59]

$$Y_\chi = \frac{135 M_{Pl} \lambda^2}{512 \pi^6 g^S \sqrt{g^\rho} 1.66 m_\chi}, \tag{4.16}$$

where λ is the dimensionless coupling strength and m_χ is the *fimp* mass. It is clear that this result is UV-independent.

On the contrary, let us suppose we have a non-renormalizable operator, namely

$$\mathcal{L}_{int} \sim \Lambda^{d-n} \mathcal{O}_n \tag{4.17}$$

where d=4, and $[\mathcal{O}_n] = [M]^n$, $[\Lambda] = [M]$.
In this case, assuming that the temperature is much higher than the masses of the

particles involved in the interaction, the tree level squared matrix element, relative to $2 \to 2$ scattering processes, is proportional to

$$|\mathcal{M}|^2 \propto \Lambda^{2(d-n)} T^{(n-d)}, \tag{4.18}$$

where s is the center of mass energy of the reaction.
In this way one can show that in the limit in which the temperature is much higher than masses, the final yield is

$$(-HT)SY' \sim T^{4-2(d-n)} \Lambda^{2(d-n)} \tag{4.19}$$

where the $'$ denotes temperature derivative. Since $HTS \propto T^6$ the result is UV-independent as long as $n < 4.5$ hence for renormalizable or super-renormalizable operators.

4.6 Freeze-in during reheating

Across all the discussion above we made the implicit assumption that throughout all the Universe evolution, the expansion is adiabatic; this basically means that we used $H = -\dot{T}/T$ in solving Boltzmann equation, implicitly assuming a relation between the energy content of the universe and temperature.

In the following we'll be interested in studying freeze-in production of dark matter, so that part (or the whole) of the present day dark matter is produced by such a mechanism; in this framework, in order to survive until the present day, dark matter has to go throughout all the Universe history, which does not necessarily mean only adiabatic expansion.
As we already pointed out in the previous chapter, we can safely assert that once the reheating temperature as defined in eq. 3.16 is reached, the universe expands adiabatically, going through an early radiation-domination epoch that turns in matter-domination and to dark-energy domination at late times. Nevertheless, what happens before the end of reheating (i.e. before the moment at which temperature drops to T_{RH}) depends on the cosmological model.

In sec. 3.2 we already mentioned the theoretical setup to study the evolution of relevant quantities during reheating, but we'll briefly recall it here.
In the following we'll follow the most credited cosmological model, according to which the Universe experienced an inflationary phase, led by the slow-roll of a scalar field, inflaton, that ends as the field reaches its minimum and begins oscillating around it. The result of these oscillation is inflaton particle production, that rapidly decay to produce radiation. This phase ends when the reheating temperature is reached; later on inflaton rapidly decays until its abundance is negligibly small, and the standard radiation-dominated epoch begins.
Within this framework, in order to get the right freeze-in final abundance, we need to solve the coupled Boltzmann equations for the inflaton and radiation energy densities, plus the fimp abundance.

In this case one has to solve Boltzmann equations for a general case in which non adia-

batic expansion is allowed

$$\dot{\rho}_\phi + 3H(\rho_\phi, \rho_r)\rho_\phi = -\Gamma_\phi \rho_\phi, \tag{4.20}$$
$$\dot{\rho}_r + 4H(\rho_\phi, \rho_r)\rho_r = \Gamma_\phi \rho_\phi, \tag{4.21}$$
$$H(\rho_\phi, \rho_r) = \sqrt{\frac{8\pi}{3}(\rho_\phi + \rho_r)}\frac{1}{M_{Pl}}, \tag{4.22}$$

where ρ_ϕ and ρ_r are the inflaton and radiation energy density respectively.
Along with those equations we have to add the evolution equation for the fimp number density

$$\dot{n}_{fimp} + 3Hn_{fimp} = \Gamma_\psi \frac{g_\psi}{2\pi^2} m_\psi^2 T(\rho_r) \mathcal{K}_1(\frac{m_\psi}{T(\rho_r)}); \tag{4.23}$$

we called ψ the particles that decay to fimp; in the following for the sake of simplicity we'll set $g_\psi = 2$ and use $\Gamma_\psi = \frac{\lambda^2 m_\psi}{8\pi}$.
In eq. (4.23) we underlined that the bath temperature T is implicitly defined by the radiation energy density via

$$T(\rho_r) = \frac{30}{\pi^2 g^*}^{1/4} \rho_r^{1/4}. \tag{4.24}$$

As a time variable we use $\nu = \Gamma_\phi \cdot t$, and define the reheating temperature

$$\Gamma_\phi M_{Pl} = T_{RH}^2 \left(\frac{8\pi^3 g^*}{90}\right)^{1/2}, \tag{4.25}$$

so that setting the reheating temperature is equivalent to setting Γ_ϕ; moreover we use the average value $g^* \sim 150$, and assume that this is constant in temperature.
We specify that as initial conditions (i.e. right after the end of inflation) we set both fimp and radiation densities to be zero, and an inflaton density obtained using a Starobinsky-like potential $\rho_\phi(0) = 0.175 m_\phi^2 M_{Pl}^2$ with $m_\phi = 10^{-7} M_{Pl}$.

To see how evolution during reheating affects freeze-in, we can write again Boltzmann equation 4.23 as

$$Y'_{fimp} + 3\left(\frac{H}{\Gamma_\phi} + \frac{T'}{T}\right) Y_{fimp} = \alpha T^{-2} \mathcal{K}_1(m_\psi/T), \tag{4.26}$$

where α is a numerical factor and we're using the time variable $\nu = \Gamma_\phi t$.
Borrowing a trick that can be found in [46], we can formally integrate 4.26 to

$$Y_{fimp}(\nu) = \alpha \int_0^\nu T(u)^{-2} \mathcal{K}_1(m_\psi/T(u)) exp\left[-3\int_u^\nu dz \left(\frac{H}{\Gamma_\phi} + \frac{T'}{T}\right)\right] du, \tag{4.27}$$

where the exponential factor provides dilution due to entropy production, and it is unity for the radiation-dominated phase.
We now split the contribution to the integral, evaluating the contribution from the initial (end of inflation) moment to infinity, subtracting the contribution from $u \gg 1$ to infinity, and we get

$$\begin{aligned} Y_{fimp}(\nu) =& \alpha \int_0^\infty T(u)^{-2} \mathcal{K}_1(m_\psi/T(u)) exp\left[-3\int_u^\nu dz \left(\frac{H}{\Gamma_\phi} + \frac{T'}{T}\right)\right] du - \\ & -\alpha \int_{\nu \gg 1}^\infty T(u)^{-2} \mathcal{K}_1(m_\psi/T(u)) du. \end{aligned} \tag{4.28}$$

For reheating temperatures much higher than m_ψ we recover the old freeze-in yield (compare eq. 4.10, see below) while for reheating temperatures smaller than m_ψ the term on the second line of eq. 4.28 can be neglected, since at late times, $\nu \gg 1$, temperature is well below the reheating temperature, hence the presence of $K_1(m_\psi/T)$ strongly suppresses the integral.
On the other hand, the integral on the first line, receives its greatest contribution when $T(u) \sim \mathcal{O}(m_\psi)$, which happens to be earlier in time than the end of reheating, hence fimp number density undergoes a non negligible dilution due to the exponential factor. Only a numerical evaluation can tell us which of the two effects wins.
We are now ready to quantitatively study the behaviour of freeze-in during a generic evolution of the background frame.
In any case, freeze-in by decay gives its dominant contribution at temperature $\mathcal{O}(1 \div 10^{-1} m_\psi)$ hence two case have to be distinguished:

- $T_{RH} \gtrsim m_\psi$: in this case the dominant freeze-in production is achieved well below the reheating temperature, hence in the radiation-dominated epoch. We expect no substantial changes with respect to the previously obtained results

- $T_{RH} < m_\psi$: in this case the dominant freeze-in production could take place during the non-adiabatic phase, and the final yield could be partially washed-out by entropy production, making it necessary to numerically study the result.

We begin with the second case: the fimp yield, which gets its major contribution during the reheating process, is reduced by the residual entropy production, and the final yield is orders of magnitude lower than the 'instantaneous reheating' case. In fig 4.5 we show the final yield for various coupling strengths, and for fixed masses and reheating temperature. Increasing the interaction strength corresponds to an increased final yield, as is to be expected.

On the other hand, if we raise the reheating temperature so that it is higher than m_ψ (or equivalently we lower m_ψ) the result is quite different: now the final yield, see fig. 4.6, is the very same as the fully adiabatic case (see the lower panel of fig. 4.6 for a comparison), even if we see that there is a greater dilution prior to the end of reheating, as is to be expected since $H(\rho_\phi, \rho_r) > H_{adiabatic}$.

Our conclusion is the following: when we'll deal with freeze-in, we have to keep in mind that if the reheating temperature is lower than the mass scale of the decaying particle(s), we need a numerical approach to the problem, since the final result can be many orders of magnitude lower than expected. On the contrary, for a reheating temperature higher than masses of decaying species we're safely allowed to use the results of sec. 4.3.

In this chapter we have presented the freeze-in mechanism as an alternative way to produce dark matter, while keeping the feature of IR production, which grants no dependence on unknown primordial parameters. We have focused on the case in which dark matter is produced via decays of bath particles, since this is the mechanism we'll exploit in the following. Moreover we have seen that for a given mass spectrum, only a tiny range of the parameter space is consistent with freeze-in production, while the rest is still dominated by freeze-out-like mechanisms. In the next chapter we'll apply this new mechanism to a specific model, to show how it can be consistent with observations.

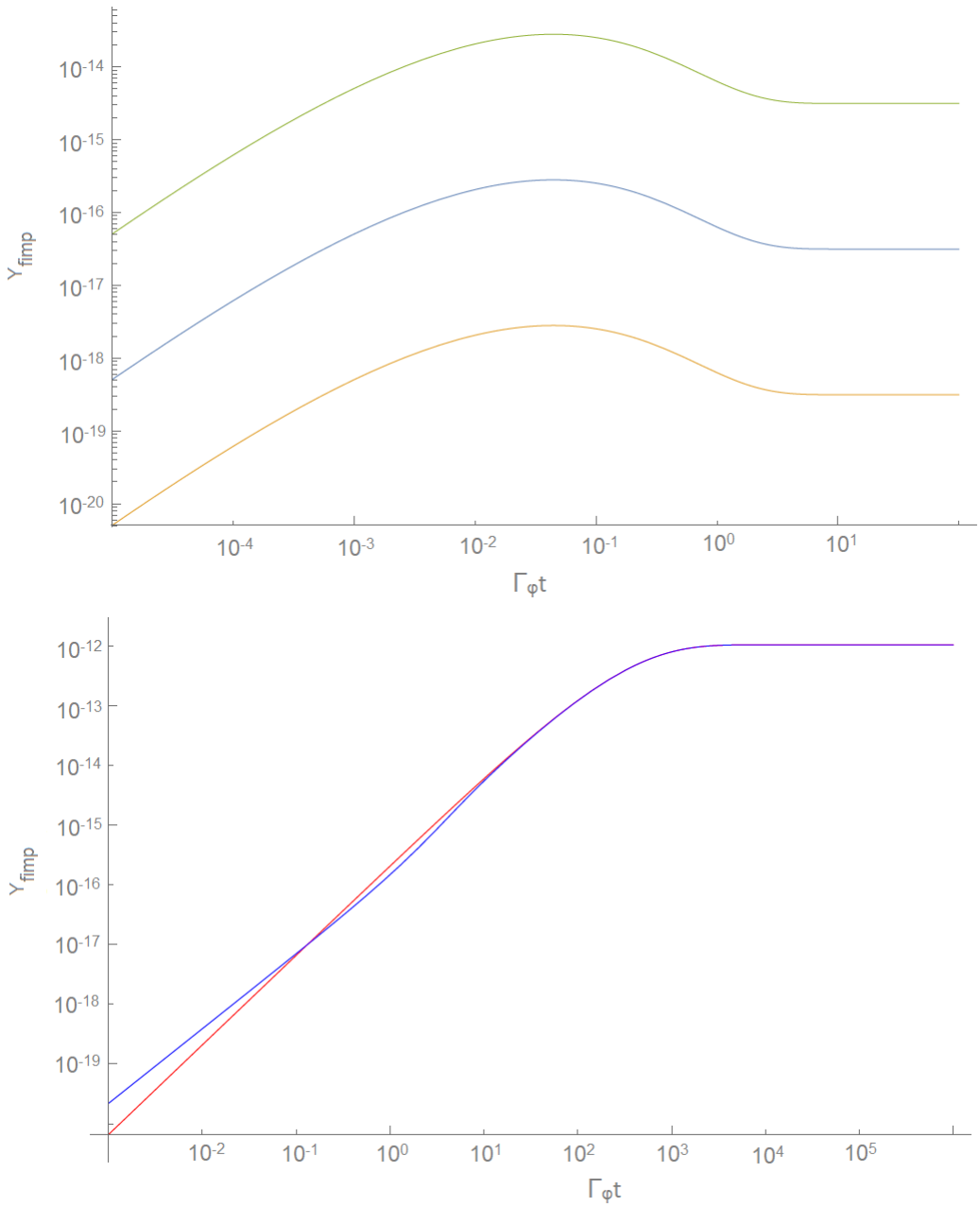

Figure 4.5: In the upper figure we show the evolution of fimp comoving number density for $T_{RH} = 10\text{TeV}$ and $m_\psi = 10^2\text{TeV}$, for increasing coupling strengths $\lambda = (10^{-13}, 10^{-12}, 10^{-11})$ for the (yellow,blue,green) lines respectively. In the lower figure we show the final freeze-in yield for the 'standard' case (i.e. for adiabatic expansion) and for the general case for $\lambda = 10^{-12}$, $m_\psi = 10^3\text{GeV}$ and $T_{RH} = 10^4\text{GeV}$. The final yield is the same; we only spot a tiny difference for $\Gamma_\phi t < 1$ due to the different dilution factors.

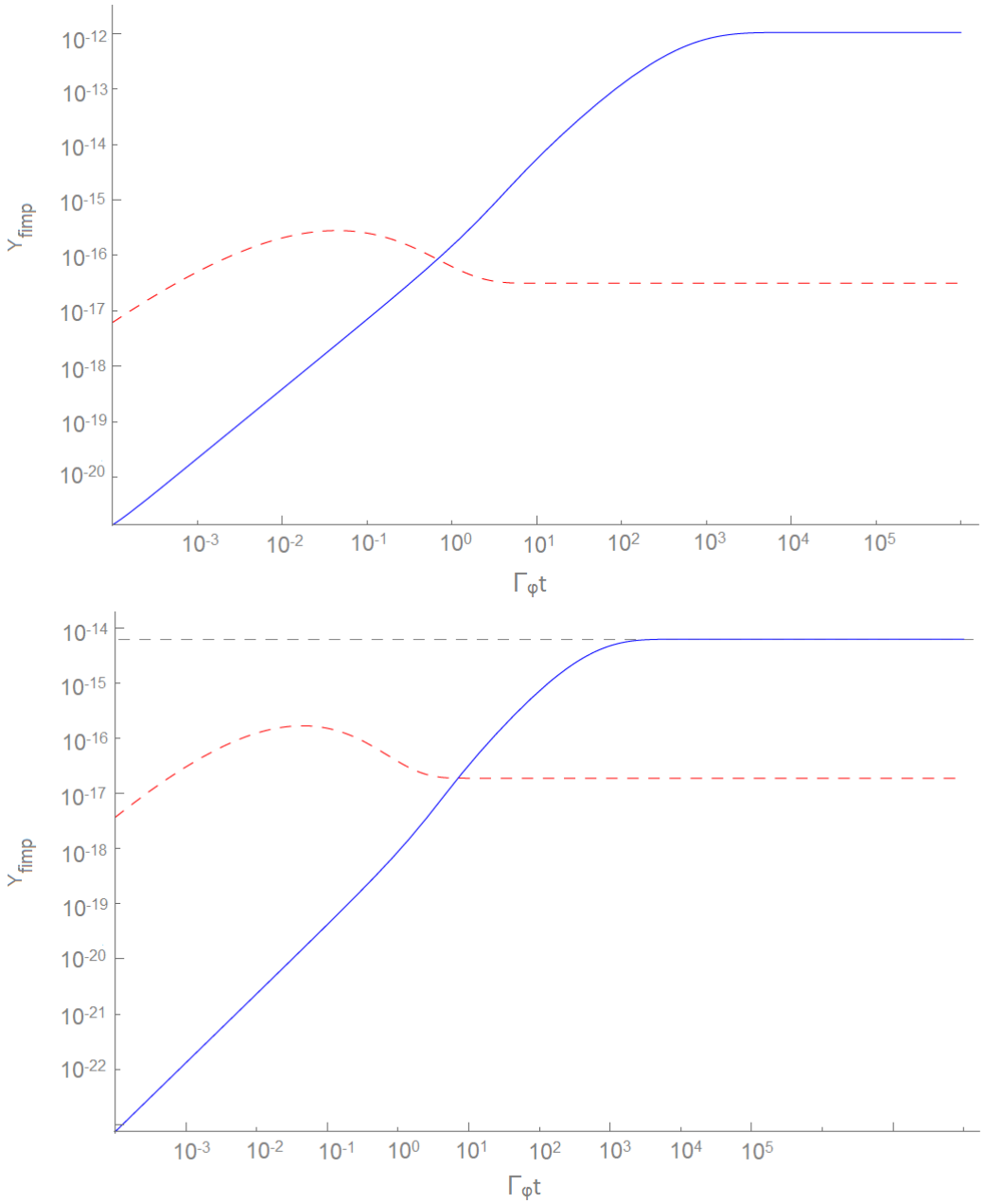

Figure 4.6: The upper panel shows what happens if we keep a fixed reheating temperature $T_{RH} = 10^4$GeV and a fixed interaction strength $\lambda = 10^{-12}$, but we vary the decaying particle mass, here $m_\psi = 10^2$TeV for the dotted line and $m_\psi = 1$TeV for the solid line. In the lower panel instead we keep a fixed mass at $m_\psi = 10^2$TeV and let the reheating temperature vary, in particular $T_{RH} = 1$Tev for the dashed red line, and $T_{RH} = 10^3$TeV for the solid line. The gray dashed line is the freeze-in final yield as obtained from eq. 4.10, with the only caveat that there's a difference of a factor ~ 0.278 since we're here using $Y = n/n_{rad}$ while in eq. 4.10 we had $Y = n/S$.

Chapter 5

Gravitino freeze-in

We are now ready to use the theoretical framework we have developed in the previous chapters and mix the acquired knowledge to present the main topic of this work.
From chapter 2 we learned that under certain conditions, the lightest supersymmetric particle (LSP) is completely stable, which makes that particle a potential candidate for dark matter. Moreover we showed that in the case of gauge-mediated spontaneous breaking of local supersymmetry, the gravitino is easily much lighter than the other superparticles, and is probably the LSP.
Going on, in chapter 3 we listed well known result about thermal production of gravitinos, in particular we derived the scattering cross section for $2 \to 2$ scattering single gravitino production, driven by a non-renormalizable operator and involving gauginos.
Although the presence of a stable gravitino severely bounds reheating temperature, in contrast with thermal processes such as high scale leptogenesis, it was shown that such processes can be achieved at much lower reheating temperature [64, 65, 66] or when we account for finite duration of the reheating process [68, 67].

In chapter 4 we left for a moment the discussion about supersymmetric particles, and in particular about gravitino, to present an alternative mode of dark matter production in the early universe, freeze-in, which could replace the well-known freeze-out paradigm. We showed that freeze-in production of dark matter severely bounds the coupling strength of dark matter sector to the visible sector, and if some conditions are verified, the relic abundance of dark matter is IR dominated.

We are ready to finally sum up all these concepts to present the main idea of [63]: if the gravitino is the LSP, it is a natural candidate for freeze-in produced dark matter.

5.1 Gravitino production: a further analysis

In section 3.4 we already pointed out that the presence of a light stable gravitino can affect cosmology. In particular fig. 3.5 shows that gravitino could easily be overproduced, resulting in an overclosed Universe.
In order to avoid this problem, one needs to set an upper bound on the reheating temperature that seems often in contrast with the commonly accepted fact that T_{RH} should be as high as 10^9GeV in order to allow processes such as thermal leptogenesis.
Looking at fig. 3.5, or equivalently fig 5.1, we see that high reheating temperatures are allowed for relatively heavy gravitino, $m_{3/2} \sim \mathcal{O}(GeV)$, while for a lighter gravitino T_{RH} is severely constrained. Nevertheless what is interesting is that there is an intermediate region, where we lose UV dependence, and T_{RH} is free to vary by many orders of mag-

nitude. This particular region corresponds to gravitino freeze-in.

In order to understand what happens, we borrow the clear and straightforward notation of [69]: as clear from eq. 3.31, gravitino final yield receives two contributions, one from gaugino scattering and one from sparticles decay. While the former involves only gauginos and is UV dominated, the latter involves all superpartners (every $\mathcal{Z}_2$-odd particle must eventually decay into an LSP) and it is this difference that mainly drives gravitino freeze-in.
In particular, gravitino production from sparticles decay, as long as T_{RH} is higher than sparticle masses, has the following form:

$$m_{3/2} Y_{3/2}^{dec} = \frac{405}{4\pi^4} \sqrt{\frac{5}{16\pi}} \frac{M_{Pl}}{g_*^{3/2}} \sum_i \frac{\Gamma_i}{m_i^2}, \tag{5.1}$$

where the sum runs over all superpartners and includes multiplicity factors; this is obtained by simply integrating Boltzmann equation for decay production, we underline again, in the case in which T_{RH} is higher than sparticle masses.
This is indeed a freeze-in-like production of gravitinos, as one can clearly see comparing with the general freeze-in case equation 4.10; this is no surprise, since the gravitino yield equation 5.1 comes from decays of sparticles.

There is one only caveat: as we deeply analyzed in chapter 4, freeze-in mechanism requires specific values for the interaction strength of fimp to other relevant species. In the gravitino case, the interaction strength is contained in Γ_i and (compare eq. 2.35 or lagrangian 2.33) it is proportional to the inverse square mass of the gravitino, and for a fixed spectrum is independent of other quantities. This means that we can arrange the mass spectrum in order to fulfill freeze-in requirements.

For a fixed mass spectrum (except for gravitino mass) this happens for a unique value of the gravitino mass: combining eq. 2.35 for decay width into a gravitino, and equation 4.11 requiring that gravitino freeze-in accounts for all dark matter abundance, we get a value for the gravitino mass

$$\frac{m_{3/2}}{GeV} = 1.12 \cdot 10^{-3} \left(\frac{m_i}{TeV}\right)^3 \left(\frac{g_{bath}}{10^2}\right) \left(\frac{10^2}{g^*(m_i)}\right)^{3/2}. \tag{5.2}$$

where g_{bath} is the multiplicity factor for all decaying sparticles and m_i are sparticle masses. This behaviour is confirmed by contour lines in fig 5.1, as we'll later better explain.

The relative contributions to the final abundance are those of eq. 3.31 and 5.1, and as long as T_{RH} is higher than sparticle masses, the decay production has indeed the form of 4.10; in total one gets

$$Y_{3/2}^{tot} m_{3/2} \sim C_{UV} \frac{T_{RH} m_{1/2}^2}{m_{3/2}} + C_{FI} \frac{n_+^{FI}}{n^{FI}} \frac{m_+^3}{m_{3/2}} \tag{5.3}$$

where $C_{UV} \sim 2.4 \cdot 10^{-4}$, $C_{FI} \sim 3.8 \cdot 10^{-4}$ and we explicitly include multiplicity factors: $n^{FI} = 36+12+9+4 = 61$, while n_+^{FI} is the number of the heaviest superparticles, whose mass is m_+.

We notice the following: while the first contribution (scattering) involves gaugino mass scale and T_{RH}, the second contribution (decay) is largely dominated by the heaviest superpartners, which are in number n_+. This implies that we have to distinguish two cases, namely the case of a split spectrum in the supersymmetric sector, with scalar masses greater than gaugino masses, and the case of a degenerate spectrum (or reversed, with gaugino heavier than scalars).

The two different cases translate in the fact that in the former two mass scales enter equation 5.3, while in the latter only one.

In the following we'll consider the first case only, namely a split spectrum with scalars heavier than gauginos; this will be later better justified, as done also in appendix C.
In this case, from eq. 5.3 we see that scattering contribution will be largely dominant for high T_{RH}, and the two contributions will become comparable at

$$T^*_{RH} = \frac{C_{FI}}{C_{UV}} \frac{n^{FI}_\phi}{n^{FI}} \frac{m^3_\phi}{m^2_{1/2}}, \tag{5.4}$$

and this remains true at least until eq. 5.1 holds, namely until T_{RH} drops to m_ϕ, at which point the integration of Boltzmann equation does not give the freeze-in contribution anymore, which is significant only if $T^*_{RH} > m_\phi$, which is indeed the case for a split spectrum like the one we're considering.

5.2 Dark matter relic density from gravitino freeze-in

We are now ready to show the final result, including all different contributions to gravitino production.
Again, we depict the contour lines for $\Omega_{3/2}h^2 \sim 0.11$, hence in the case in which gravitino production accounts for all dark matter abundance.
The result is reported in fig. 5.1: the general behaviour of the curves resemble that of previous fig. 3.5, although we added some changes, as better explained the following.
We can still recognise the three main behaviours:

$$\begin{cases} T_{RH} \propto m_{3/2} & m_{3/2} > m^* \\ m_\phi \lesssim T_{RH} \lesssim T^*_{RH} & m_{3/2} \sim m^* \\ T_{RH} \lesssim m_\phi & m_{3/2} < m^*, \end{cases}$$

the first corresponding to scattering production and the last to decay production.
In the last case ($m_{3/2} < m^*$) temperature must be less than scalar masses, so that gravitino abundance comes from the Boltzmann-suppressed tail of the scalar number densities, and it's therefore easily limited not to overclose the Universe.

What happens in the middle is exactly freeze-in production: to convince ourselves we can compare values of m^* to find out that they're exactly the ones required for freeze-in production of gravitinos, as observed in eq. 5.2, and they depend as predicted on m^3_ϕ.
Moreover the vertical incline of the contours in those regions underlines UV independence, and this is indeed the case of decay freeze-in: the final gravitino yield is IR dominated and therefore does not depend on T_{RH}, which can freely range in between the values defined in equations 5.2.

If we raise the temperature up to T^*_{RH} we end up in the scattering region, finding the sloped interval of the curves; on the contrary, lowering the temperature down to m_ϕ largely affects the equilibrium distributions of scalar particles, that do depend strongly on temperature. If we step down T^*_{RH}, gravitino abundance will derive from Boltzmann-suppressed tail of the equilibrium distributions of scalars, hence higher coupling strengths are needed to grant a full dark matter final abundance: we're leaving the freeze-in region.

In figure 5.1 we also reported as dotted lines the lines corresponding to $T_{RH} = m_\phi$ and $T_{RH} = T^*_{RH}$, for the right values of the gravitino mass, to show that the freeze-in region, although being relatively small, can be considerably large for some mass spectra, such as those that have scalar masses up to tens of TeV.

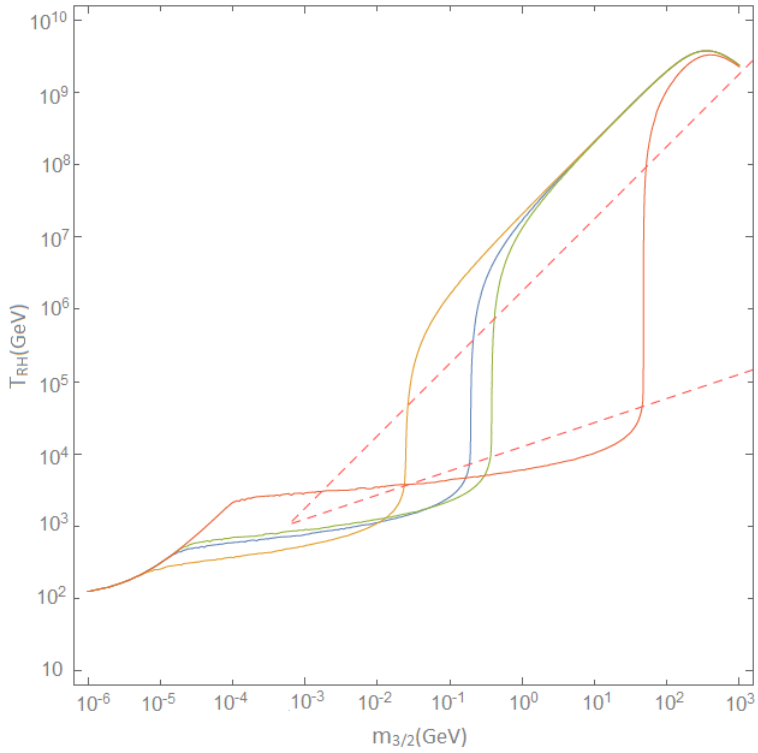

Figure 5.1: The graphic shows again the limit on reheating temperature for different universal scalar masses (4 TeV, 8 Tev, 10 TeV and 20 TeV) assuming gaugino mass unification at $m_{1/2}$ =2 TeV at GUT scale. The red dashed lines delimit the region of parameters where gravitino freeze-in accounts for all dark matter abundance. As we can see, for increasing gravitino mass the available region increases, and it reaches half of the total logarithmic reheating temperature range for scalar masses of $\mathcal{O}$(10 TeV).

Graphs 3.5 and 5.1 represent contours for $\Omega_{dm}h^2 = 0.11$ for different spectra of the supersymmetric sector. The total final abundance of the gravitino LSP is obtained by summing a contribution due to decays and a contribution due to scattering, which are the result of integration of Boltzmann equation

$$Y'_{3/2} = -\frac{n_{rad}(T)\langle\sigma v_{rel}\rangle}{HT} - \sum_i \frac{m_i}{\langle E_i\rangle}\frac{\Gamma_i Y_i}{HT}, \tag{5.5}$$

between T_{RH} and $T \ll T_{RH}$, and Γ_i is the decay width of the i-th superpartner into a gravitino, $m_i/\langle E_i\rangle$ is the Lorentz factor and the scattering cross section is given in eq. (3.10).

The sum on the RHS of eq. (5.5) spans over all superpartners and includes a multiplicity factor for each one of them. After integration, in order to get the final abundance we multiply by the right factor, getting the final result

$$\begin{aligned}\Omega_{dm}(T_0) \stackrel{!}{=} & m_{3/2} Y_{3/2}(T_0) n_{rad}(T_0)/\rho_c(T_0) \\ = & \frac{n_{rad}(T_0)}{\rho_c(T_0)} m_{3/2} \frac{g_S(T_0)}{g_S(T_{RH})} \left(\frac{n_{rad}(T_{RH})}{H(T_{RH})} \langle \sigma v_{rel} \rangle + \int_{T_0}^{T_{RH}} \frac{dT}{T} \sum_i \frac{m_i}{\langle E_i \rangle} \frac{\Gamma_i Y_i}{H(T)} \right),\end{aligned} \tag{5.6}$$

and we used $g_S(T_{RH}) = 915/4$, $g_S(T_0) = 43/11$ and $\rho_c(T_0) \sim 8.1 \cdot 10^{-47} h^2$ GeV^4.

The second term on the RHS is the sparticle decay contribution, and it grows as m_i^3, moreover the integral is sensitive only to temperatures near the sparticle mass scales, due to the high temperature suppression $1/(T^3 \gamma_{lorentz})$ and to the low temperatures exponential suppression due to Y_i

The first term in the brackets on RHS is the scattering contribution: as noted in sec. 3.2 and explicitly shown in appendix B following [50], the result assuming instantaneous reheating at T_{RH} overestimates the final yield by a factor ~ 1.1 with respect to the non-instantaneous reheating case, hence we scaled the final result by the appropriate factor.

Moreover, the scattering thermal averaged cross section as obtained in eq. (3.10) makes the assumption that temperature is much higher than all masses. In this case it correspond to assuming that the range in T_{RH} in which scattering dominates is higher than gluino masses. To show that this is indeed the case, we recall that freeze-in, in the case in which $m_\phi^3 \gg m_{\tilde{g}}^3$, is active from scalar masses, up to T_{RH}^* as defined in eq. (5.4), which is the temperature at which decay and scattering contributions become comparable (for lower T_{RH} decays will dominate). Hence we are left to show that $T_{RH}^* \gg m_{\tilde{g}}$. This is indeed the case, since looking at equation (5.4), the lower temperature at which scattering enters the equations scales as

$$T_{RH}^* \propto \frac{\sum_\phi m_\phi^3}{\sum_{\tilde{g}} m_{\tilde{g}}^2} \tag{5.7}$$

and this is clearly much higher than gluino mass in the $m_\phi^3 \gg m_{\tilde{g}}^3$ regime (note that this is also enhanced by multiplicity factors); therefore we're safely allowed to draw fig. 3.5 and 5.1. A more detailed analysis can be found in appendix C.

5.3 Effects of reheating process on gravitino decay production

As already explained in sec. 3.2, reheating temperature is not the maximum temperature achieved after the end of inflation, it is rather the temperature at which radiation-domination begins.

Before this instant, inflaton was decaying and the Universe was expanding non adiabatically; here we consider the consequences of non-instantaneous reheating on gravitino decay production, focusing first on the freeze-in region and later on the (non-freeze-in) decay region (at far left in fig. 5.1).

Boltzmann equation for gravitino freeze-in is indeed (confront eq. 4.9)

$$\dot{n}_{3/2} + 3Hn_{3/2} = \sum_i \frac{m_i^2 \Gamma_i}{2\pi^2} T \mathcal{K}_1(\frac{m_i}{T}), \tag{5.8}$$

where $\mathcal{K}_1$ is the first modified Bessel function of the second kind, and the sum ranges over all superpartners and includes multiplicity factors.
The study of this equation during a radiation-dominated epoch, results in a final freeze-in abundance such as that in eq. 4.11, and represented in fig. 5.1. From chapter 4, we already know that the dominant contribution to freeze-in is achieved at temperatures $\mathcal{O}(1 \div 10^{-1} m_i)$, where m_i is in the case of fig. 5.1 the mass of scalar particles.

The effect of non-adiabatic expansion could play a relevant role in gravitino freeze-in, if the reheating temperature T_{RH} was lower than scalar masses since freeze-in could take place during inflaton decay, and the final abundance could be washed away due to entropy production. This was explained in much greater detail in sec. 4.6, for the general freeze-in case.
Nevertheless in the case of gravitino freeze-in, we have a clear limit on range of T_{RH} as explained in sec 5.1, in particular $T_{RH} \gtrsim m_\phi$ (see fig. 5.1), therefore the temperature at which the freeze-in process produces most final gravitino abundance will always be below the reheating temperature, allowing us to consider only the adiabatic case. In fact, from numerical simulations such that in fig. 4.6, we showed that the final freeze-in yield is not affected by a non-adiabatic expansion phase whenever the reheating temperature is higher than the decaying particle mass.

On the other hand, the limit on T_{RH} in the range $1KeV \lesssim m_{3/2} \lesssim m_{3/2}^{FI}$, where $m_{3/2}^{FI}$ is the value of the gravitino mass for which freeze-in is active, is precisely $T_{RH} < m_\phi$, so that decay-produced final abundance of gravitino derives from the exponential-suppressed tail of sparticles equilibrium distributions, in order for the Universe not to be overclosed.

In this case, the fact that temperatures higher than T_{RH} can be reached during an early phase could partially change this result, since if the entropy-dilution effect does not win over production via decays, the final gravitino abundance could exceed the one predicted by instantaneous reheating.

To get an idea of what happens, we need to solve the Boltzmann equations for the gravitino comoving number density in the two cases of instantaneous and non-instantaneous reheating.

The decay production, in the case of instantaneous reheating, comes from the Boltzmann suppressed tail of decaying sparticles equilibrium number density, and does not get affected by entropy production.
This means that for a fixed gravitino mass, raising the reheating temperature dramatically raise the final abundance due to the exponential dependence of the equilibrium number density on temperature. This is clear in fig. 5.1: while the gravitino mass ranges for many orders of magnitudes, increasing the interaction strength proportionally, the change in T_{RH} to balance this effect is way smaller, as diminishing T_{RH} of less than an order of magnitude is sufficient to keep the final abundance constant.

On the contrary, in the case of non-instantaneous reheating, increasing the reheating temperature means increasing the maximum reachable temperature, which could dra-

matically boost production via decays. Nevertheless the increased production has to compete with entropy dilution, hence it is not clear which of the two final yields will be the greatest.

In order to understand whether the instantaneous reheating approximation is over or under-estimating the final abundance, we solved Boltzmann equations for a given mass spectrum

$$\rho'_\phi + 3\frac{H(\rho_\phi,\rho_r)}{\Gamma_\phi}\rho_\phi = -\rho_\phi, \tag{5.9}$$

$$\rho'_r + 4\frac{H(\rho_\phi,\rho_r)}{\Gamma_\phi}\rho_r = \rho_\phi \tag{5.10}$$

$$H(\rho_\phi,\rho_r) = \sqrt{\frac{8\pi}{3}(\rho_\phi+\rho_r)}\frac{1}{M_{Pl}} \tag{5.11}$$

$$Y'_{3/2} + 3\left(\frac{H}{\Gamma_\phi}+\frac{T'}{T}\right)Y_{3/2} = \sum_i \Gamma_i \frac{m_i^2}{\zeta(3)g^*(T)}T^{-2}\mathcal{K}_1(m_i/T)\frac{1}{\Gamma_\phi} \tag{5.12}$$

where the prime denotes derivative with respect to rescaled time $\nu = \Gamma_\phi t$, we use the constant value $g^* \sim 150$ and the sum includes multiplicity factors.

We're interested mainly in the asymptotic value of the gravitino comoving number density for late times; since the difference occurs for the non-freeze-in region (low gravitino mass), we're only interested in the case $T_{RH} < m_i$, since we already know that if $T_{RH} \gtrsim m_i$ the results is unchanged.
For this reason, most of decay production will be achieved during reheating, and we can simply confront the gravitino number density for $\nu \gg 1$ with the instantaneous reheating case.

We report the result in fig. 5.2: what happens is that for reheating temperatures close enough (one order of magnitude) to the decaying particle mass, the results of instantaneous reheating overestimates the final result by a varying factor (which is ~ 1.68 at most), while for lower reheating temperatures the instantaneous reheating yield greatly underestimates the final abundance.

This means that for reheating temperatures lower than the decaying particle mass by a factor ~ 20, the possibility to reach higher temperatures allowed by the continuous reheating process, wins over the dilution effect.
In turn, the limit on reheating temperature in fig. 5.1 changes: as long as T_{RH} is close to scalar masses, the final abundance with continuous reheating is lower, hence higher reheating temperature are allowed (by a factor ~ 1.68) for a fixed final abundance.
On the contrary, as T_{RH} falls due to the raising of the coupling strength, the final yield for continuous reheating is actually higher, hence lower reheating temperatures are needed, for a fixed final abundance.

5.4 Evidences of frozen-in gravitino

When talking about freeze-in, we deal with extremely tiny interaction strength, which make detection of *fimp* particles very difficult [70, 71, 72].
Nevertheless, tiny interaction strength translates into relatively long lifetimes. In the

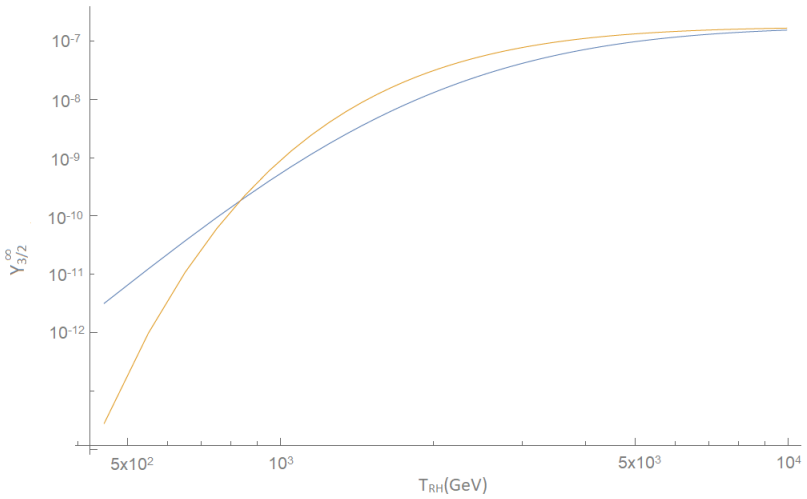

Figure 5.2: We show the gravitino final abundance for a fixed mass spectrum, $m_\phi = 10$ TeV and $m_{3/2} = 10^{-2}$GeV, for varying reheating temperatures in the case of instantaneous and non-instantaneous reheating. We see that as T_{RH} approaches m_ϕ the two results tend to converge, while we get two different behaviours for lower reheating temperatures.

case of gravitino freeze-in, using the language of chapter 4, the *losp* is the lightest supersymmetric particle which is in thermal equilibrium with the bath, i.e. the NLSP (which we'll assume to be in thermal equilibrium).
Therefore, eq. (4.11) can be rearranged to obtain an expression for the NLSP lifetime.

In the case of gravitino, assuming that all the final relic density is entirely achieved by freeze-in, we get from eq. (4.11)

$$m_{3/2} Y_{3/2}^{dec} = \frac{405}{4\pi^4}\sqrt{\frac{5}{16\pi}}\frac{M_{Pl}}{g_*^{3/2}}\sum_i \frac{\Gamma_i}{m_i^2} \tag{5.13}$$

where index i runs over all superparticles and the sum implicitly includes the degrees of freedom of particle i.
Using now eq. (2.34) and (2.35), we normalize all the decay widths to the NLSP decay width

$$\Gamma_i = \Gamma_{NLSP}\frac{m_i^5}{m_{NLSP}^5}, \tag{5.14}$$

in this way we can rearrange eq. (5.13) in the following way

$$m_{3/2} Y_{3/2} \sim \frac{0.13}{g_*^{3/2}}\sqrt{\frac{m_{NLSP}}{\tau_{NLSP}}}\sum_i \left(\frac{m_i^3}{m_{NLSP}^3}\right). \tag{5.15}$$

Assuming that the gravitino LSP dark matter accounts for the observed relic density, namely $m_{3/2} Y_{3/2} s_0/\rho_c = 0.11$, and that the largest contributions to RHS of eq. (5.13) come from squarks and gluinos, we can constrain mass spectrum

$$\tau_{NLSP} = 1.5\cdot 10^{-7} s \left(\frac{150}{g_*}\right)^3 \left(\frac{TeV}{m_{NLSP}}\right)^5 \left[\frac{9}{11}\left(\frac{m_{\tilde{q}}}{TeV}\right)^3 + \frac{2}{11}\left(\frac{m_{\tilde{g}}}{TeV}\right)^3\right]^2 \tag{5.16}$$

which for varying τ_{NLSP} correspond to curves of fig. 5.3. This means that in the case of frozen-in gravitino, we have a relation between the mass spectrum and the NLSP lifetime, therefore if we were able to measure both, that could produce a strong evidence eventually supporting gravitino dark matter.

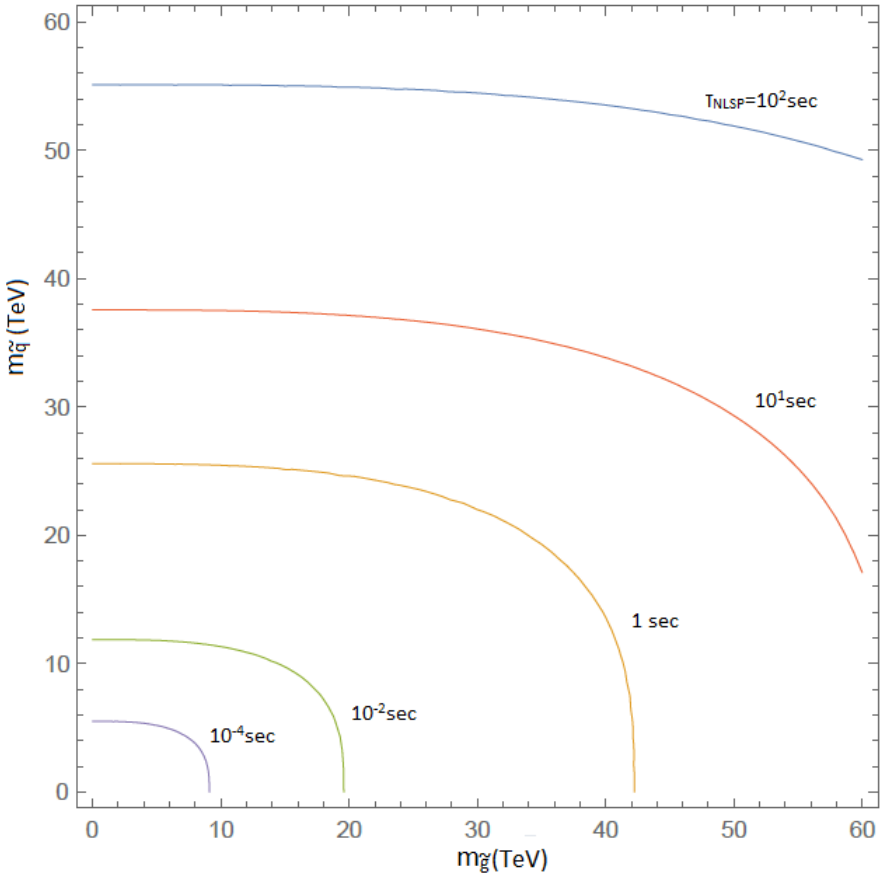

Figure 5.3: Gluino and squarks masses constraint for different NLSP lifetimes. The result was obtained for m_{NLSP} =2 TeV, assuming that all dark matter relic density is generated by gravitino freeze-in, and assuming that the largest contributions to the sum in eq. (5.15) are due to squarks and gluinos. For masses of $\mathcal{O}(10TeV)$ lifetime of NLSP is $\mathcal{O}(10^{-3}s)$. For increasing NLSP mass, lager gluinos and squarks masses are allowed.

Chapter 6

Gravitino freeze-in with extremely split spectra

In last chapter we explored in detail the possibility of having dark matter relic density generated by gravitino freeze-in via sparticles decay, in particular we focused on the split mass spectrum case, with universal scalar masses larger than gaugino masses.

In this last chapter we're ready to show the main result of this thesis, namely gravitino freeze-in enhancement in the case in which the mass spectrum is extremely split, with scalars orders of magnitude heavier than gauginos. Such spectra have been studied in detail and it was shown they can be realizable [73, 74, 75].

As we'll see, in this case, freeze-in production of gravitino spans many orders of magnitude in reheating temperature range, making freeze-in the main mode of production of gravitinos.

6.1 The case of split spectra

All along this work, we underlined that the final gravitino yield receives mainly three contributions, which dominate for different gravitino masses.
For large masses the main mode of production is via gaugino scattering, and the final yield is proportional to the reheating temperature, while for low gravitino masses decays dominate the production, and the reheating temperature is bound to stay below sparticle masses. In between these two regions we have the freeze-in area.

For gravitino mass at the TeV scale (namely at gaugino mass scales, in our case mainly $(1 \div 10)$TeV scale) the production of $\pm 3/2$ purely gravitino modes begins to be important, and sums to the $\pm 1/2$ goldstino modes, making the reheating temperature quickly fall. This can be seen for instance in figure 5.1 for gravitino mass at TeV scale: in this case the turnover gravitino mass stays constant since it depends solely on gaugino masses, which we kept fixed.

On the other hand, for low gravitino mass, decay production dominates, and we see that T_{RH} is bound to be below sparticle masses. Nevertheless, we also notice a little jump in temperature dependence, corresponding to various gravitino gravitino masses, but typically around 10^{-5}GeV.

This effect is due to the gaugino decay contribution: even if we consider a split spectrum

in which scalars are much heavier than gauginos, for some regions of the parameter space gaugino contribution to decay production can reach the same order of magnitude of the scalar contribution, and since the two sum together the reheating temperature needs to be lowered in order to keep a fixed final gravitino yield.

This can be seen in the following way: as we explained in great detail in chapter 5, scattering production is active down to temperature

$$T^*_{RH} \propto \frac{\sum_\phi m^3_\phi}{\sum_i m^2_i}. \tag{6.1}$$

which in our case is higher than universal scalar masses.
At this temperature, since the decay yield reads

$$Y^{decay}_{3/2} \propto \sum_i \frac{m^3_i}{m^2_{Pl} m^2_{3/2}} \int_{m_i/T_{RH}}^{\infty} dx x^3 \mathcal{K}_1(x), \tag{6.2}$$

where the sum runs over all superpartners and includes multiplicity factors, scalar superpartners will provide the majority of the gravitino abundance, both enhanced by a factor m^3_ϕ and granted by the fact that $T^*_{RH} > m_\phi$.

From T^*_{RH} down, decay production will dominate over scattering production, and the ratio between the gaugino and scalar contributions reads

$$\mathcal{R} \sim \frac{m^3_{1/2} g_{1/2} \int_{m_{1/2}/T_{RH}}^{\infty} dx x^3 \mathcal{K}_1(x)}{m^3_\phi g_\phi \int_{m_\phi/T_{RH}}^{\infty} dx x^3 \mathcal{K}_1(x)}, \tag{6.3}$$

where $n_{1/2} = 8 + 4$ is the number of gauginos and $n_\phi = 36 + 12$ is the number of scalar sparticles.
The ratio 6.3 varies with varying mass spectra and with temperature, except for a degenerate spectrum, in which case it is fixed at $\mathcal{R} \sim 0.23$ and gauginos contribute proportionally to the final yield.
For the case of a split spectrum, the behaviour of the ratio $\mathcal{R}$ is not trivial. Although there is a mass cube factor that enhances the final result, and in our case would favour scalar decays, the non-trivial dependence of the integral on temperature makes thing a little more involved.

Since gravitino freeze-in via scalar decays is active from temperatures as high as T^*_{RH} down to temperatures $T_{RH} \sim m_\phi$, as long as the freeze-in region ends, the integral in the denominator of 6.3 begins to sharply fall due to the exponential Boltzmann suppression of the number density of scalar particles contained in the Bessel function $\mathcal{K}_1$ (see also appendix D).
In the meanwhile gaugino are still relativistic, and their contribution to decay production is not affected by the exponential suppression, but only by a Lorentz factor: the integral relative to gaugino contribution is still constant.

As we lower gravitino mass, hence raising the coupling strength and in turn having a greater production (see eq. 6.2), we need to lower the reheating temperature to keep the gravitino yield fixed, thus diminish the value of the integral in eq. 6.3. As we proceed till the limit $m_{3/2} \sim 10^{-6}$GeV, if the scalar masses are sufficiently higher than gaugino masses, the integral in the denominator of 6.3 can become so small that the m^3_ϕ enhancement is no more sufficient to compete with gaugino contribution, which although

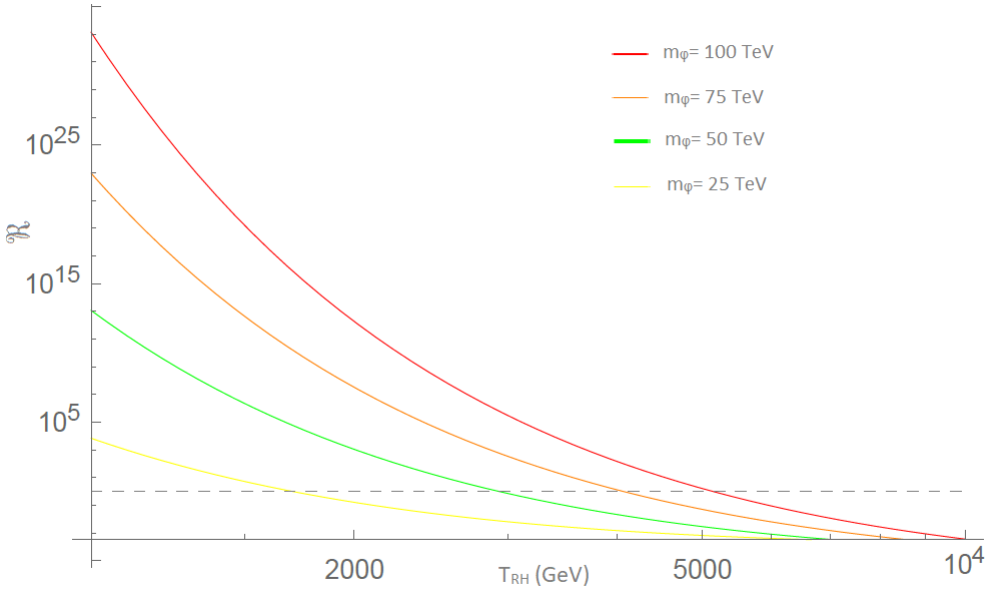

Figure 6.1: We show the behaviour of the ratio $\mathcal{R}$ as defined in 6.3 for different scalar masses as a function of the reheating temperature. We fixed $m_{1/2} = 2$ TeV, the dashed line is $\mathcal{R} = 1$.

proportional to $m_{1/2}^3$ only, can count on a considerable contribution from the integral in the nominator of 6.3.

We'll call $\bar{T}_{RH}$ the reheating temperature for which $\mathcal{R}(T < \bar{T}_{RH}) > 1$. It is important to notice that it is not obvious that $\bar{T}_{RH}$ exist for all mass spectra: in particular, as noted above, for a degenerate mass spectrum it does not exists at all, and in general we expect it to exist only if $m_\phi \gg m_{1/2}$.
This happens because when lowering gravitino mass, $\bar{T}_{RH}$ is not necessarily reached before $m_{3/2} \sim 10^{-6}$ GeV, hence $\mathcal{R}$ could be always smaller than 1 in the range we're interested in.

To understand how $\bar{T}_{RH}$ changes with the mass spectrum we need to numerically integrate eq. 6.3. We show the result in fig. 6.1, reporting the value of $\mathcal{R}$ for different spectra as a function of the reheating temperature.

As we expected, for growing m_ϕ at fixed $m_{1/2}$, $\bar{T}_{RH}$ increases, eventually entering the interesting region of graph 5.1. In fact, the condition to have a freeze-in region due to gaugino decays, is $\bar{T}_{RH} > m_{1/2}$, and for this reason we need an extremely split spectrum to get a contribution from gaugino decays.

6.2 Gravitino freeze-in enhancement

So why if this effect is realizable it doesn't take place in normal gravitino freeze-in?
The answer is that freeze-in is not so easy to occur, as we saw for instance in fig. 5.1. Although it is present, it only ranges over a small T_{RH} region unless scalar masses are very large; moreover freeze-in requires a specific value of gravitino mass for a given mass spectrum, as we learn from eq. 5.2.

For this reason, when we deal with normal freeze-in, it is very unlikely to observe another freeze-in region.

In order for gaugino decay production to achieve a freeze-in phase, what has to happen is that the mass $\bar{m}_{3/2}$ at which $\mathcal{R} \gtrsim 1$ must be at the same time the gravitino mass required for gaugino decay freeze-in, that we already know from equation 5.2 to be

$$\frac{\bar{m}_{3/2}}{GeV} \sim 1.12 \cdot 10^{-3} \left(\frac{m_{1/2}}{TeV}\right)^3 \left(\frac{g_{1/2}}{10^2}\right) \left(\frac{10^2}{g^*(m_i)}\right)^{3/2}. \tag{6.4}$$

In principle, while we can always arrange the mass spectrum so that the reheating temperature $\bar{T}_{RH}$ is reached, as we showed before, it is not obvious whether we can make this occur exactly at $\bar{m}_{3/2}$ defined by equation 6.4.

On the other hand for increasing scalar masses and for a fixed value of gaugino masses, $\bar{T}_{3/2}$ increases, and since in the decay region T_{RH} is a monotonous growing function of $m_{3/2}$, $\bar{m}_{3/2}$ increases as well.
For this reason, we expect that as $\mathcal{R} \gtrsim 1$ is achieved, we can again increase scalar masses to get condition 6.4 satisfied, while $\mathcal{R} \gtrsim 1$ is automatically satisfied, because we're not lowering scalar masses.
This is indeed confirmed by numerical evaluation, which we postpone to the next section.

We're ready to show the final result for a very split spectrum, in which scalar masses are orders of magnitude larger than gaugino masses.

We show results for fixed gaugino masses and varying scalar masses in fig. 6.2.

As we expected, if the ratio $m_\phi/m_{1/2}$ is not large enough, we recover the old single freeze-in results that we had in fig. 5.1. On the other hand, for increasing scalar masses, a shy freeze-in pattern starts to emerge, and when m_ϕ is about two orders of magnitude larger than $m_{1/2}$ we get a satisfying full freeze-in region, which ranges in reheating temperatures from $\bar{T}_{RH}$ down to $m_{1/2}$, analogously to the primary freeze-in region with the due substitutions $\bar{T}_{RH} \to T^*_{RH}, \quad m_{1/2} \to m_\phi$.

Moreover we observe that the gravitino mass scale at which the smaller freeze-in region appears is precisely the one predicted by via eq. 6.4.

The reheating temperature range of the smaller freeze-in region is not as wide as the scalar decay region, and this is because $\bar{T}_{RH}$ is typically not much higher than $m_{1/2}$. Moreover we have the condition $\bar{T}_{RH} < m_\phi$, since we must be out of the scalar freeze-in region.
Also, as we learn from fig. 6.1, T_{RH} increases weakly with increasing m_ϕ.

For these reasons, the smaller freeze-in region is not so interesting on its own, rather it has a role when we look the whole picture.
In fact, as we see from fig. 6.2, when scalar masses are large enough, freeze-in is the main mode of production of gravitinos, and the two freeze-in regions helps to extend freeze-in to almost all reheating temperatures above the TeV scale.

This happens for the following reason: the primary freeze-in region ranges from T^*_{RH}

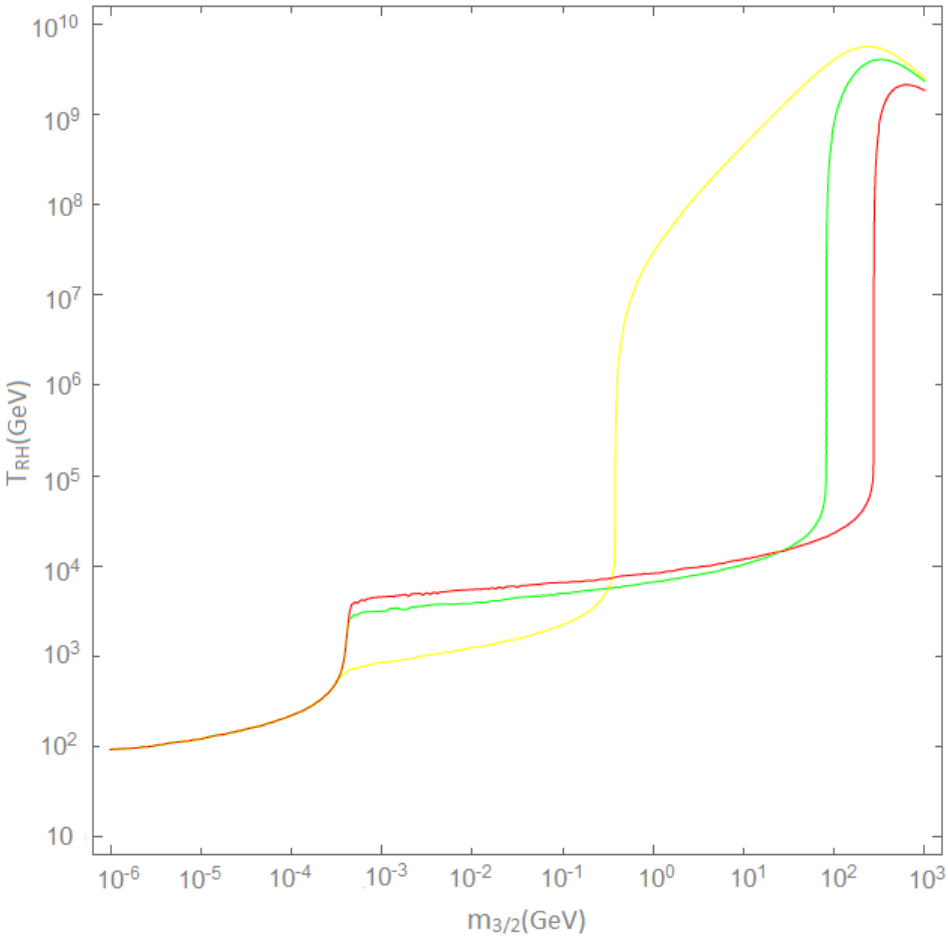

Figure 6.2: We show here the contours for $\Omega_{3/2}h^2 = 0.11$ for fixed gaugino unified masses at 1 TeV, and for increasing scalar masses. We set $m_\phi = (10, 60, 80)$TeV for the (yellow,green,red) lines respectively. We see that as scalar masses approach the 10^2TeV scale, a smaller freeze-in region begins to appear, while for $m_\phi \sim 10$ TeV it disappears completely. Unfortunately we cannot raise scalar masses too much, if we want the largest freeze-in region to appear for gravitino masses below the TeV scale. Nevertheless we see that for $m_\phi \sim 80$ TeV freeze-in is by far the main way of gravitino production.

down to m_ϕ, and we recall

$$T^*_{RH} \propto \frac{\sum_\phi m^3_\phi}{\sum_i m^2_i}, \tag{6.5}$$

where the sum at the denominator ranges over gauginos and includes multiplicity factors. Therefore, having a larger m_ϕ not only raises $\bar{T}_{RH}$, favouring the smaller freeze-in region, but it also favours the scalar freeze-in region, pushing scattering production to higher gravitino masses (eventually to the TeV scale).

Therefore, if such a split spectrum is realized, freeze-in is the relevant way of gravitino production from T^*_{RH} to $T_{RH} \sim m_\phi$ and from $\bar{T}_{RH}$ to $T_{RH} \sim m_{1/2}$. For gaugino masses at the TeV scale, we typically have $\bar{T}_{RH} = \mathcal{O}(10^{-1} m_\phi)$, so that if we exclude that narrow region between $m_{1/2}$ and $\bar{T}_{RH}$, and reheating temperatures below the TeV scale, freeze-in is the only other way of gravitino production.

In conclusion, we have seen that in the case of split spectra, a freeze-in region eventually appears, which is generated by the heaviest superparticles decay to a single gravitino.

The freeze-in region typically spans many orders of magnitude in reheating temperature range for very split spectra, getting to cover almost half of available reheating temperatures between TeV scale to 10^{10} GeV. This is however enhanced in the case of an extremely split mass spectrum as we have shown in detail throughout this chapter, as freeze-in could in principle become the main way of gravitino production, leaving space to scattering and usual decay only in a very narrow region of reheating temperatures. This means that in these cases, freeze-in is most likely the way in which gravitino relic density was produced, offering a completely UV-independent solution to the dark matter problem.

Conclusions

Supersymmetry could solve many of the problems of modern physics if realized in nature, moreover it significantly enlarges the particle content of the theory. Throughout this work we have shown the basis of this framework, showing in particular how the gravity supermultiplets arises and how the gravitino acquires mass after the breaking of local supersymmetry. We explored the various possibilities of achieving supersymmetry breaking, pointing out in which cases the gravitino is easily the lightest supersymmetric particle. In this case, we obtained the thermal production rate in the early Universe, showing how two different kind of interactions, decay and scattering, take part to the process. Of these two, the decay of bath particles could also play a relevant role in the achievement of the gravitino relic abundance via the freeze-in mechanism.
We studied in detail this alternative process generalizing the results to the case of non-instantaneous reheating process, numerically solving the complete Boltzmann equations, showing how this affects the final gravitino yield. Beyond reviewing the results about scattering production, we concluded that reheating process effects can affect decay production depending on the mass spectrum of the theory, while leaving unvaried freeze-in production. This result suggests that the final yield achieved via freeze-in depends only on the mass spectrum of the theory, granting the general validity of the results obtained in the instantaneous reheating approximation.

We have shown that for a split spectrum, freeze-in is by far the most active way of gravitino relic density production, ranging in reheating temperatures from TeV scale to 10^9 GeV. This suggests that in most cases, if supersymmetry is realized in nature and the gravitino is the LSP, which we showed to be easily obtained, freeze-in is very likely to be the mechanism of relic abundance achievement.
The framework of frozen-in gravitino also provides a relation between superparticle masses and NLSP lifetime, which if experimentally measured could provide an evidence supporting the theory.

In conclusion, we have shown how the framework of gravitino freeze-in provides a powerful alternative to the solution of the missing matter problem, and that the final result depends mainly on the mass spectra of the theory. The conclusions of this work are based on the assumption that supersymmetry is a local symmetry of nature and that the breaking symmetry is gauge-mediated, which is the main constraint of validity of the final results. Unfortunately by far collider experiments did not show any evidence of the presence of sparticles, typically confining their masses above the TeV scale.

Future experiments, exploring farther regions in parameter space, could eventually find the sought-for and long-waited evidence and the search for displaced vertices could also give information about the NLSP lifetime, since this special particle is likely to decay within the accelerator detector at LHC. This could in turn provide a strong evidence favouring or disfavouring gravitino freeze-in as a solution for the missing matter problem.

Appendix A

Gravitino wave function and polarization tensor

We briefly report results about spin-3/2 particles, which are crucial to perform calculation of diagrams including gravitinos.
The gravitino is a spin-3/2 fermion, hence it obeys Rarita-Schwinger equation, with lagrangian density:

$$\mathcal{L}_{RS} = -\frac{1}{2}\epsilon^{\mu\nu\rho\ \sigma}\psi^{\dagger}_{\mu}\sigma_{\nu}\partial_{\rho}\psi_{\sigma} - \frac{1}{4}m_{3/2}\psi_{\nu}(\bar{\sigma}_{\mu}\sigma_{\nu} - \bar{\sigma}_{\nu}\sigma_{\mu})\psi_{\nu} + h.c. \tag{A.1}$$

The equation of motion for the free gravitino obtained from lagrangian (A.1) read:

$$\begin{aligned} \bar{\sigma}^{\mu}\psi_{\mu} &= 0, \\ \partial^{\mu}\psi_{\mu} &= 0, \\ (i\bar{\sigma}^{\nu}\partial_{\nu} - m_{3/2})\psi_{\mu} &= 0. \end{aligned} \tag{A.2}$$

Solution to the above equations can be built using the wave function u_L for the spin-1/2 field and the polarization vector ϵ_{μ} for the spin-1 field.
In momentum space, where $\psi_{\mu} \sim e^{-ipx}\tilde{\psi}_{\mu}$, the solution reads

$$\tilde{\psi}_{\mu}(p,\lambda) = \sum_{s,m} \left\langle \left(\frac{1}{2},\frac{s}{2}\right)(1,m) \middle| \left(\frac{3}{2},\lambda\right) \right\rangle u_L(p,s)\epsilon_{\mu}(p,m), \tag{A.3}$$

where $u_L(p,s) = \sqrt{p^0+m}\chi^{(s)}$, $\chi^{+} = (1,0)^t$ and $\chi^{-} = (0,1)^t$,is an eigenstate of the helicity operator

$$n^i\sigma_i u(p,s) = s u(p,s)$$

where $n^i = p^i/|\vec{p}|$, and satisfies Dirac equation

$$(\bar{\sigma}^{\mu}p_{\mu} - m_{3/2})u(p,s) = 0.$$

The coefficients in eq. (A.3) are listed in tab A.1.

The helicity sum for the gravitino in momentum space reads

$$\Pi_{\mu\nu}(P) = -(\bar{\sigma}^{\rho}p_{\rho} + m_{3/2}) \cdot (\pi_{\mu\nu} - \frac{1}{3}\pi_{\mu\eta}\pi_{\nu\lambda}\bar{\sigma}^{\eta}\sigma^{\lambda}), \tag{A.4}$$

where $\pi_{\mu\nu} = g_{\mu\nu} - \frac{p_{\mu}p_{\nu}}{m^2_{3/2}}$.
Since in the text we're interested in gravitino production at energies much larger than

	m=-1	m=0	m=+1
s=-1	1	$\sqrt{\frac{2}{3}}$	$\sqrt{\frac{1}{3}}$
s=+1	$\sqrt{\frac{1}{3}}$	$\sqrt{\frac{2}{3}}$	1

Table A.1: Clebsch-Gordan coefficients for $\lambda = \frac{s}{2} + m$. The other coefficients vanish.

gravitino mass, we take this limit in equation A.4, and assuming that the supercurrent to which the gravitino couples is conserved one gets

$$\Pi_{\mu\nu} \simeq -\bar{\sigma}_\rho p^\rho g_{\mu\nu} + \frac{2}{3}\bar{\sigma}_\rho p^\rho \frac{p_\mu p_\nu}{m_{3/2}^2}, \tag{A.5}$$

where the first term on the RHS is the sum over the $\pm 3/2$ helicity modes, and the second is the sum over $\pm 1/2$ helicity modes.

Decay width into light gravitino

In the case of a light gravitino, interaction lagrangian in well approximated by lagrangian (2.33). From the interaction terms involving gauge and chiral supermultiplets we can derive decay widths, neglecting masses of the $\mathcal{R}$-even particles.
For the following calculation only we'll go back to 4x4 γ matrices notation, since for the trace evaluation we used the *FeynCalc* package for *Mathematica* software, which directly implements such objects.
In the case of a chiral supermultiplet, the matrix element reads

$$\mathcal{M} = \frac{-im_\phi^2}{2\sqrt{3}m_{3/2}M}\phi\bar{\chi}(1-\gamma^5)\psi \tag{A.6}$$

hence, mediating over iniital helicity states and summing over final

$$\begin{aligned}\sum_{s,l,l',s'} |M|^2 =& \frac{m_\phi^4}{12m_{3/2}^2M^2}\sum_{l,s,l',s'} Tr\left(\bar{\chi}_l(1-\gamma^5)\psi_l\bar{\psi}_{l'}(1+\gamma^5)\chi_{s'}\right) \\ =& \frac{m_\phi^4}{6m_{3/2}^2M^2} Tr\left(\not{k}(1-\gamma^5)(\not{p}+m_{3/2})\right)\end{aligned} \tag{A.7}$$

which in the rest frame of the decaying particle

$$\begin{pmatrix} m_\phi \\ 0 \end{pmatrix} \quad \rightarrow \quad \begin{pmatrix} k \\ \vec{k} \end{pmatrix} \quad + \quad \begin{pmatrix} E_{3/2} \\ \vec{p} = -\vec{k} \end{pmatrix} \tag{A.8}$$

becomes

$$|\bar{\mathcal{M}}|^2 = \frac{2}{3}\frac{m_\phi^4}{m_{3/2}^2M^2}(k\cdot p). \tag{A.9}$$

Now using the definition of decay width $\Gamma = \frac{|\bar{\mathcal{M}}|^2}{8\pi}\frac{k}{m_{phi}^2}$ and the fact that $k\cdot p = -\frac{1}{2}(m_\phi^2 - m_{3/2}^2)$ we get the final result

$$\Gamma(\phi \rightarrow \psi + \chi) = \frac{1}{48\pi}\frac{m_\phi^5}{m_{3/2}^2M^2}\left(1-\left(\frac{m_{3/2}}{m_\phi}\right)^2\right)^2. \tag{A.10}$$

In the case of the gauge term, the calculation is a little bit more involved. the matrix element squared, when averaged on initial states and summed over final states reads

$$|\bar{\mathcal{M}}|^2 = \frac{-m_\lambda^2}{48 m_{3/2}^2 M^2} k^\beta k^\rho Tr\left((\not{p} + m_{3/2})[\gamma^\rho, \gamma^\sigma] g_{\sigma\alpha}(\not{q} + m_\lambda)[\gamma^\alpha, \gamma^\beta]\right) \tag{A.11}$$

where p and q are gravitino and gaugino momenta, while k is the massless gauge boson momentum.
For the evaluation of the Dirac trace we made use of the *FeynCalc* package for *Mathematica* software.
The evaluation of the trace gives

$$Tr\left((\not{p} + m_{3/2})[\gamma^\rho, \gamma^\sigma] g_{\sigma\alpha}(\not{q} + m_\lambda)[\gamma^\alpha, \gamma^\beta]\right) = 16\left((3 m_{3/2} m_\lambda + p\cdot q) g^{\beta\rho} - 2p^\beta q^\rho - 2p^\rho q^\beta\right), \tag{A.12}$$

and when contracted with the k outgoing momenta leaves(see eq. A.11)

$$|\bar{\mathcal{M}}|^2 = \frac{4}{3}\frac{m_\lambda^2}{m_{3/2}^2 M^2}[(p\cdot k)(q\cdot k)]. \tag{A.13}$$

The two scalar products contribute each one with a factor $\pm\frac{m_\lambda^2}{2}(1 - \frac{m_{3/2}^2}{m_\lambda^2})$, and using the definition of decay width we conclude

$$\Gamma(\lambda \to \psi + A_\mu) = \frac{1}{48\pi}\frac{m_\lambda^5}{m_{3/2}^2 M^2}\left(1 - \left(\frac{m_{3/2}}{m_\lambda}\right)^2\right)^3. \tag{A.14}$$

Appendix B

Solution of the Boltzmann equation during reheating

In this appendix we want to justify result in eq. (3.26);to this end we'll follow the results of [50].
We will first solve the Boltzmann equation for the gravitino number density assuming adiabatic expansion, negligible dependence of effective degrees of freedom on temperature and instantaneous reheating at

$$T_{RH} = \left(\frac{40}{g(T_{RH})\pi^2}\right)^{1/4} \left(\frac{\Gamma_\phi M_P}{c}\right), \tag{B.1}$$

where the constant c depends on the inflation model.
The solution to Boltzmann equation is

$$Y_{3/2} = \frac{n_{rad}(T_{RH})\langle\sigma_{tot}v_{rel}\rangle}{H(T_{RH})} \cdot \frac{g(T_0)}{g(T_{RH})}, \tag{B.2}$$

which upon using eq. (B.1) and cross section in eq. (3.10) becomes

$$Y_{3/2} \simeq \frac{0.00398}{\sqrt{c}} \left(\frac{\Gamma_\phi}{M_P}\right)^{1/2} \left(1 + 0.588\frac{m_{1/2}^2}{m_{3/2}^2}\right). \tag{B.3}$$

We shall now drop the instantaneous reheating hypothesis an re-derive the final gravitino yield.

The Boltzmann equation for the gravitino production, dropping the hypothesis of adiabatic expansion, which is not valid during reheating, is

$$\dot{Y}_{3/2} + 3\left(H + \frac{\dot{T}}{T}\right) Y_{3/2} = \langle\sigma_{tot}v_{rel}\rangle n_{rad}. \tag{B.4}$$

Using the new time variable

$$v = \Gamma_\phi(t - t_{end}) \tag{B.5}$$

and the definitions

$$\hat{H} = \frac{H}{\Gamma_\phi}, \qquad \hat{T} = \frac{T}{(\Gamma_\phi M_P)^{1/2}}, \qquad \hat{n}_{rad} = \frac{n_{rad}}{(\Gamma_\phi M_P)^{3/2}}, \qquad \hat{\Sigma} = \langle\sigma_{tot}v_{rel}\rangle M_P^2,$$

equation (B.4) becomes

$$Y'_{3/2} + 3\left(\hat{H} + \frac{\hat{T}'}{\hat{T}}\right) Y_{3/2} = \left(\frac{\Gamma_\phi}{M_P}\right)^{1/2} \hat{\Sigma}\hat{n}_{rad}. \tag{B.6}$$

The exact solution for the energy density during the reheating phase is

$$\rho(v) = \rho_{end}\left(1 + (1+\bar{w})(\frac{v}{A})\right)^{-2} \tag{B.7}$$

where

$$A = \frac{\Gamma_\phi}{m}\left(\frac{3}{4}\frac{\rho_{end}}{m^2 M_P^2}\right)^{-1/2}.$$

The constant A is $\mathcal{O}(\Gamma_\phi/m)$ for most models of inflation, and Γ_ϕ is many order of magnitude smaller than m. It is hence safe to consider the $v \gg A$ case, which eventually excludes times extremely close to the end of inflation.
During inflation, the parameter $w = \frac{P}{\rho}$ of the fluid varies, and in eq. (B.7) it was substituted with its average value $\bar{w}(t_{rh})$ at the moment of reheating end, which is defined as the moment at which the ratio between the inflaton energy density to the total falls below some $\delta \ll 1$ (for $\delta = 2 \cdot 10^{-3}$, $\bar{w} = 0.273$).
Using an iterative method, one can better define the average parameter $\bar{w}$ as

$$\bar{w}(v) = \frac{1}{3v}\int_0^v \frac{\boldsymbol{\gamma}(\frac{5}{3}, u)}{\boldsymbol{\gamma}(\frac{5}{3}) + u^{2/3}e^{-u}}du, \tag{B.8}$$

where $\boldsymbol{\gamma}$ is the lower incomplete gamma function.
In the $v \gg A$ limit

$$\rho(v) \sim \frac{4}{3}\left(\frac{M_P\Gamma_\phi}{(1+\bar{w})v}\right)^2 \equiv (\Gamma_\phi M_P)^2\hat{\rho}(v). \tag{B.9}$$

From definition in eq. (B.9) we link the adimensional temperature and radiation energy density

$$\hat{T}^3 = \left(\frac{30\hat{\rho}_\gamma}{\pi^2 g}\right)^{3/4}$$

and eq. (B.6) becomes

$$Y'_{3/2} + 3\left[\left(\frac{\hat{\rho}_\phi + \hat{\rho}_\gamma}{3}\right)^{1/2} + \frac{\hat{\rho}'_\gamma}{4\hat{\rho}\gamma}\right]Y_{3/2} = \hat{T}^3\left(\frac{\Gamma_\phi}{M_P^2}\right)^{1/2}\hat{\Sigma}\frac{\pi^2}{\zeta(3)}$$

which ignoring temperature dependence of the cross section integrates to

$$Y_{3/2}(v) = \int_o^v \hat{T}^3(u)exp\left[-3\int_u^v\left[\left(\frac{\hat{\rho}_\phi(z) + \hat{\rho}_\gamma(z)}{3}\right)^{1/2} + \frac{\hat{\rho}'_\gamma(z)}{4\hat{\rho}_\gamma(z)}\right]dz\right]du \cdot \left(\frac{\Gamma_\phi}{M_P}\right)^{1/2}\frac{\hat{\Sigma}\pi^2}{\zeta(3)}.$$

The integral in dz keeps into account the entropy production during the reheating phase, and can partially wash away the final result; the exponential inside the integral indeed vanishes during radiation dominated era, signaling adiabatic expansion from there on.
The integrand gives the contribution from time 0 to time u to gravitino yield at time v, which has to be rescaled considering entropy production between time u and v.
For times $v \gg 1$ we can split the integral exploiting the fact that in radiation dominated era, the exponential is 1, since no dilution is occurring. We split the integral in u into one between 0 and ∞, and then we subtract the contribution with no exponential factor between v and ∞. The result is

$$\begin{aligned}\int_o^v \hat{T}^3(u)exp\left[-3\int_u^v\left[\left(\frac{\hat{\rho}_\phi(z) + \hat{\rho}_\gamma(z)}{3}\right)^{1/2} + \frac{\hat{\rho}'_\gamma(z)}{4\hat{\rho}\gamma(z)}\right]dz\right]du \\ = \int_o^\infty \hat{T}^3(u)exp\left[-3\int_u^\infty\left[\left(\frac{\hat{\rho}_\phi(z) + \hat{\rho}_\gamma(z)}{3}\right)^{1/2} + \frac{\hat{\rho}'_\gamma(z)}{4\hat{\rho}\gamma(z)}\right]dz\right]du - 2\left(\frac{90}{4\pi^2 g}\right)^{3/4}v^{-1/2}.\end{aligned} \tag{B.10}$$

Using this trick and eq. (B.8) in eq. (B.7), the yield is

$$Y_{3/2}(T) \simeq (0.233 - 0.221 v^{-1/2}) g(T_{RH})^{-3/4} \left(\frac{\Gamma_\phi}{M_P}\right)^{1/2} 2.04 \cdot \hat{\Sigma}. \tag{B.11}$$

For late times the result simplyfies to

$$Y_{3/2} \simeq 0.00363 \left(1 + 0.558 \frac{m_{1/2}^2}{m_{3/2}^2}\right) \left(\frac{\Gamma_\phi}{M_P}\right)^{1/2}. \tag{B.12}$$

Finally, confronting eq. (B.3) with eq. (B.12), we get that for $c = 1$ the result for instantaneous reheating exceeds the one here calculated of about 1.1, while the two results are equivalent for $c \sim 1.2$.

Appendix C

Validity range of gaugino scattering cross section

All along chapter 5 we implicitly assumed that eq. 3.10 for gaugino scattering cross section holds. Actually, the expression we used was borrowed form [49], where authors assume that the energy of the reactions is much larger than masses involved; hence if we fail this hypothesis we're in principle not allowed to use the result in eq. 3.10.

Here we'll briefly show that for our purposes the assumption under which eq. 3.10 holds are verified, studying here only the gluino scattering case, while the generalization to all gauginos is straightforward.
In fact, in the case of gravitino freeze-in, the energy scale at which scattering processes take place is comparable to T_{RH}, and such processes remain the dominant way of gravitino production until decay contribution becomes important.

To show this we borrow the clear and straightforward notation of [69]: the curves of fig. 5.1 are the contours for $Y^{tot}_{3/2} m_{3/2} = c$ where $c \propto \Omega_{dm} h^2$ and $Y^{tot}_{3/2}$ receives three different contributions so that

$$Y^{tot}_{3/2} m_{3/2} \sim C_{UV} \frac{T_{RH} M_3^2}{m_{3/2}} + C_{FI} \frac{n_+^{FI}}{n^{FI}} \frac{m_+^3}{m_{3/2}} + Y_{FO} m_{3/2}, \tag{C.1}$$

where Y_{FO} is the NLSP freeze-out and decay contribution which we can now safely neglect, $C_{UV} \sim 2.4 \cdot 10^{-4}$, $C_{FI} \sim 3.8 \cdot 10^{-4}$; the decay contribution is largely dominated by the heaviest superpartner(s), hence here we explicitly include multiplicity factors: $n^{FI} = 36 + 12 + 9 + 4 = 61$, while n_+^{FI} is the number of the heaviest superparticles.

We need to distinguish here two different cases, namely the case in which scalars are heavier than gaugino and the opposite. From eq. C.1 it is clear that the two contributions (decay and scattering) become comparable at

$$T^*_{RH} \sim \alpha M_+^3 / M_3^2 \tag{C.2}$$

with $\alpha \sim 1.6 \frac{n_+^{FI}}{n^{FI}}$.
In order for the use of expression 3.10 to be justified, we need $T^*_{RH} \gg M_3$, so that the energy scales at which scattering processes take place is much greater than masses playing a role in the processes, while for lower temperatures and energies freeze-in takes over.

In fact, if $T^*_{RH} \lesssim M_3$, scattering processes remain active and relevant down to temperatures below or comparable to gluino masses, and we can no longer use an expression

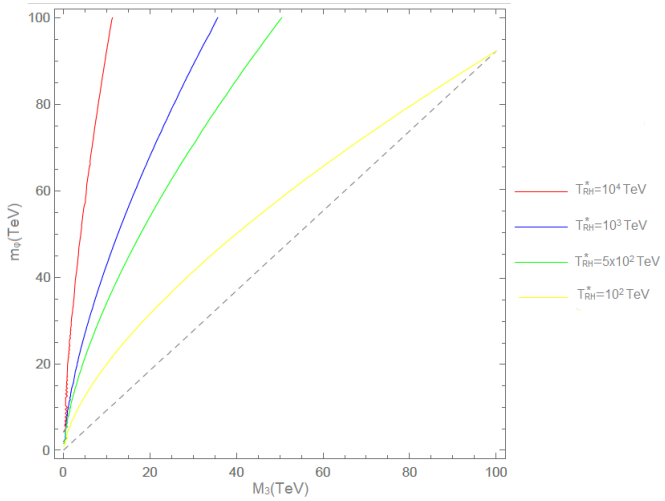

Figure C.1: In this figure we show the contours for a fixed T^*_{RH} as a function of the scalar and gluino masses, m_ϕ and M_3 respectively. The dashed line depicts the critical limit $T^*_{RH} = M_3$, hence the region below the dashed line is excluded. The solid lines represent contours for fixed T^*_{RH}, and show that it is easy to set masses so that $T^*_{RH} \gg M_3$. In particular, for the case of gravitino freeze-in, T^*_{RH} ranges from 10^2TeV up to 10^6TeV, and the problem can be safely avoided.

for the cross section that is based on the assumption that the particles that scatter are effectively massless.

Luckily, in our case, for a large range of mass spectra, as long as we have a split spectrum with scalar masses greater than gluino mass, the problem is avoided, as T^*_{RH} is much greater than gluino masses.
Numerical results are reported in fig. C.1, where we show the region in parameter space where we are not able to use cross section as reported in 3.10, which we exclude from our analysis; moreover we learn that for masses choices such as those of chapter 5 we are allowed to use eq. 3.10.

On the contrary, if gluino is the heaviest particle, T^*_{RH} is automatically lower (or at most equal) to gluino mass.
In this case $n^{FI}_+ = 8$, and from eq. C.2 we get $T^*_{RH} \sim 0.2 M_3$.
Moreover in this case freeze-in is not a relevant way of production of gravitino, since scattering production immediately leaves the place to decay production without the intermediate step of freeze-in due to the fact that the mass scale that enter freeze-in production and scattering production is now the same; hence we exclude that region of parameter space from this work.

Appendix D

Modified Bessel functions and decay production of fimp particles

Throughout chapters 4 and 5 we made large use of the modified Bessel functions of the second kind $\mathcal{K}_1$ and $\mathcal{K}_2$ when dealing with decay production of particles.
It's easy to lose the physical meaning of evaluated quantities when we make use of definitions of such mathematical objects, and being decay production of particles one of the main subjects of this work, we want to spend a page in explaining better what's the function of those objects, recovering for a moment the physical interpretation.

By definition, the equilibrium number density of a particle species X is

$$n_X = \frac{g_X}{8\pi^3}\int d^3p f_X, \tag{D.1}$$

where g_X are the internal degrees of freedom of particle X and f_X is the equilibrium phase space distribution

$$f_X = \frac{1}{e^{E/T}\pm 1}, \tag{D.2}$$

where the minus (plus) holds for Bose-Einstein (Fermi-Dirac) distribution. Approximating the phase space distribution with a Boltzmann distribution, $f_X \sim e^{-E/T}$, and changing the variable of integration to energy, we get

$$n_X = \frac{g_X}{2\pi^2}\int dE E\sqrt{E^2-m_X^2}e^{-E/T}, \tag{D.3}$$

which by definition of modified Bessel function of the second kind

$$m_X^2 T\mathcal{K}_2(m_X/T) = \int_{m_X}^{\infty} dE E\sqrt{E^2-m_X^2}e^{-E/T}, \tag{D.4}$$

gives

$$n_X = \frac{g_X}{2\pi^2}m_X^2 T\mathcal{K}_2(m_x/T). \tag{D.5}$$

Most of the time we'll be interested in solving Boltzmann equation for decay production of fimp particles (confront equations 4.7 and 4.8). In this case we have the product of the equilibrium phase space density f_X times the decay width of particle X into a fimp particle, Γ_X, which carries a Lorentz factor γ_X to account for time dilation.
In this case, considering the rest decay width a constant, the integral we need to perform to solve Boltzmann equation is of the form

$$\sim g_X\int \frac{d^3p}{8\pi^3}\frac{f_X}{\gamma_X}, \tag{D.6}$$

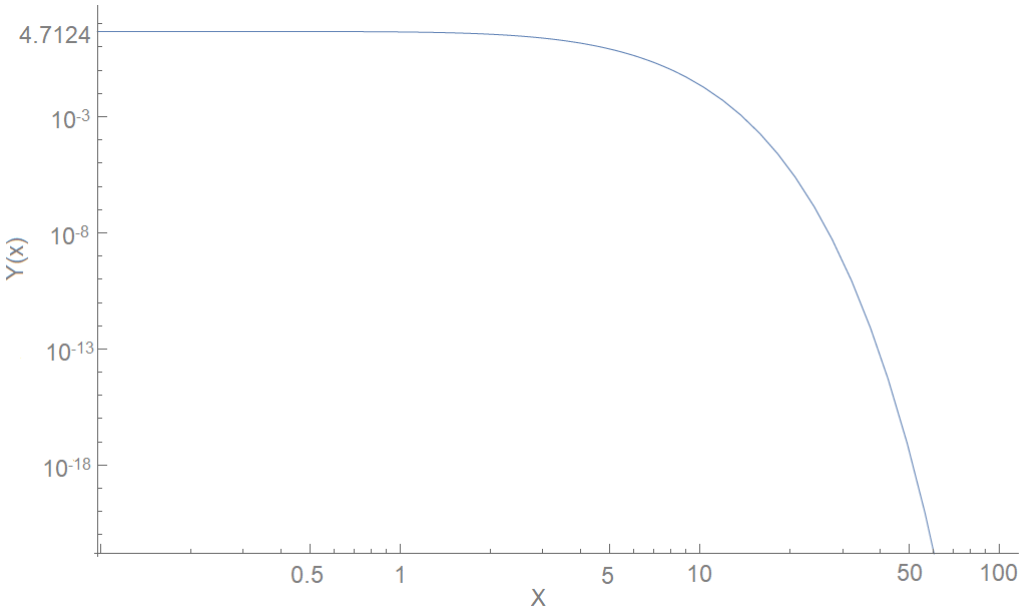

Figure D.1: We show the result of integration $y(x) = \int_x^\infty dz z^3 \mathcal{K}_1(z)$ for varying x. In the case of freeze-in, the final yiled is proportional to $y(x)$ and it is strongly temperature dependent. In fact, in our case, the extreme of integration x is the quantity m_X/T_{RH} where m_X is the decaying particle mass. As we learn from this graph, as long as $T_{RH} m_X$, the integral remains constant, while as soon as T_{RH} drops below m_X, the integral begins to sharply fall; this is due to the fact that if $T_{RH} < m_X$, X number density is Boltzmann suppressed, resulting in a lower final yield.

which upon changing variable to energy reads

$$\frac{g_X}{2\pi^2} m_X \int dE \sqrt{E^2 - m_X^2} e^{-E/T}, \tag{D.7}$$

which by definition of modified Bessel function of the first kind

$$m_X T \mathcal{K}_1(m_X/T) = \int_{m_X}^\infty dE \sqrt{E^2 - m_X^2} e^{-E/T}, \tag{D.8}$$

gives

$$g_X \int \frac{d^3p}{8\pi^3} \frac{f_X}{\gamma_X} = \frac{g_X}{2\pi^2} m_X^2 T \mathcal{K}_1(m_X/T). \tag{D.9}$$

This means that when we use the function $\mathcal{K}_2$ we're using the equilibrium number density of a particle species, while when we use the $\mathcal{K}_1$ we're including a Lorentz factor in our integral (which is most of the time throughout this work).

To conclude, we show in fig. D.1 the behaviour of the useful integral

$$y(x) = \int_x^\infty dz z^3 \mathcal{K}_1(z), \tag{D.10}$$

to make it clear that there is a strong dependence of the decay yield on the reheating temperature.
In the case of chapter 4, the lower integration extreme corresponds to m_X/T_{RH} where m_X is the decaying particle mass.

Bibliography

[1] W. Thomson, Baron Kelvin, "Baltimore Lectures on Molecular Dynamics and the Wave Theory of Light" London, C.J. Clay and Sons; Baltimore, Publication agency of the Johns Hopkins University. (1904)

[2] F. Zwicky, "The redshift of extragalactic nebulae", Helvetica Physica Acta, Vol. 6, p. 110-127. (1933)

[3] K. C. Freeman, "On the disk of spiral and S0 galaxies," Astrophysical Journal, vol. 160, p.811 (1970)

[4] Vera C. Rubin, W. Kent Jr. Ford, "Rotation of the Andromeda Nebula from a Spectroscopic Survey of Emission Regions," Astrophysical Journal Letters, Vol. 159, p. 379,(1970)

[5] D. H. Rogstad, G. S. Shostak "Gross Properties of Five Scd Galaxies as Determined from 21-CENTIMETER Observations," Astrophysical Journal, vol. 176, p.315 (1972)

[6] M. S. Roberts, R. N. Whitehurst "The rotation curve and geometry of M31 at large galactocentric distances" Astrophysical Journal, Vol. 201, p. 327-346 (1975)

[7] Babcock Horace W. "The rotation of the Andromeda Nebula" Lick Observatory bulletin ; no. 498; Lick Observatory bulletins ; no. 498., Berkeley : University of California Press (1939)

[8] C. Carignan et al. "Extended HI Rotation Curve and Mass Distribution of M31" Astrophys.J.641:L109-L112 (2006) [arXiv:astro-ph/0603143]

[9] J. Ostriker, P. Peebles and A. Yahil, "The size and mass of galaxies, and the mass of the universe," Astrophys. J. Lett. **193** (1974),

[10] P. J. E. Peebles, R. B. Partridge, "Upper Limit on the Mean Mass Density due to Galaxies," Astrophysical Journal, vol. 148, p.713 (1966)

[11] A. H. Guth, "The Inflationary Universe: A Possible Solution to the Horizon and Flatness Problems," Adv. Ser. Astrophys. Cosmol. **3** (1987), 139-148

[12] V. Springel, *et al.*, "Simulating the joint evolution of quasars, galaxies and their large-scale distribution," Nature **435** (2005), 629-636 [arXiv:astro-ph/0504097 [astro-ph]].

[13] M. Bauer and T. Plehn, "Yet Another Introduction to Dark Matter," Lect. Notes Phys. **959** (2019), pp. [arXiv:1705.01987 [hep-ph]].

[14] N. Aghanim *et al.* [Planck], "Planck 2018 results. VI. Cosmological parameters," [arXiv:1807.06209 [astro-ph.CO]].

[15] P. Tisserand *et al.* [EROS-2], "Limits on the Macho Content of the Galactic Halo from the EROS-2 Survey of the Magellanic Clouds," Astron. Astrophys. **469** (2007), 387-404 [arXiv:astro-ph/0607207 [astro-ph]].

[16] M. Aker *et al.* [KATRIN], "Improved Upper Limit on the Neutrino Mass from a Direct Kinematic Method by KATRIN," Phys. Rev. Lett. **123** (2019) no.22, 221802 [arXiv:1909.06048 [hep-ex]].

[17] P. Bode, J. P. Ostriker and N. Turok, "Halo formation in warm dark matter models," Astrophys. J. **556** (2001), 93-107 [arXiv:astro-ph/0010389 [astro-ph]].

[18] N. Banik, J. Bovy, G. Bertone, D. Erkal and T. J. L. de Boer, "Novel constraints on the particle nature of dark matter from stellar streams," [arXiv:1911.02663 [astro-ph.GA]].

[19] S. Tremaine , J. E. Gunn, Phys. Rev. Lett. 42, 407 (1979).

[20] B. D. Wandelt, R. Dave, G. R. Farrar, P. C. McGuire, D. N. Spergel and P. J. Steinhardt, "Selfinteracting dark matter," [arXiv:astro-ph/0006344 [astro-ph]].

[21] E. D. Carlson, M. E. Machacek and L. J. Hall, "Self-interacting dark matter," Astrophys. J. **398** (1992), 43-52

[22] D. N. Spergel and P. J. Steinhardt, "Observational evidence for selfinteracting cold dark matter," Phys. Rev. Lett. **84** (2000), 3760-3763 [arXiv:astro-ph/9909386 [astro-ph]].

[23] V. A. Acciari *et al.*, "Constraining Dark Matter lifetime with a deep gamma-ray survey of the Perseus Galaxy Cluster with MAGIC," Phys. Dark Univ. **22** (2018), 38-47 [arXiv:1806.11063 [astro-ph.HE]].

[24] B. Audren, J. Lesgourgues, G. Mangano, P. D. Serpico and T. Tram, "Strongest model-independent bound on the lifetime of Dark Matter," JCAP **12** (2014), 028 [arXiv:1407.2418 [astro-ph.CO]].

[25] N. Afshordi, P. McDonald and D. N. Spergel, "Primordial black holes as dark matter: The Power spectrum and evaporation of early structures," Astrophys. J. Lett. **594** (2003), L71-L74 [arXiv:astro-ph/0302035 [astro-ph]].

[26] A. Robertson, R. Massey and V. Eke, "What does the Bullet Cluster tell us about self-interacting dark matter?," Mon. Not. Roy. Astron. Soc. **465** (2017) no.1, 569-587 [arXiv:1605.04307 [astro-ph.CO]].

[27] H. J. Mo and S. Mao, "Tully-fisher relation and its implications for halo density profile and self-interacting dark matter," Mon. Not. Roy. Astron. Soc. **318** (2000), 163 [arXiv:astro-ph/0002451 [astro-ph]].

[28] T. Falk, K. A. Olive and M. Srednicki, "Heavy sneutrinos as dark matter," Phys. Lett. B **339** (1994), 248-251 [arXiv:hep-ph/9409270 [hep-ph]].

[29] C. Arina, "Sneutrino cold dark matter in extended MSSM models," [arXiv:0805.1991 [hep-ph]].

[30] L. Delle Rose, S. Khalil, S. King, J.D., S. Kulkarni, C. Marzo, S. Moretti and C. S. Un, "Sneutrino Dark Matter, Constraints and Perspectives," [arXiv:1804.07753 [hep-ph]].

[31] R. D. Peccei and H. R. Quinn, "CP Conservation in the Presence of Pseudoparticles," Phys. Rev. Lett. **38** (1977), 1440-1443

[32] G. Bertone and D. Hooper, "History of dark matter," Rev. Mod. Phys. **90** (2018) no.4, 045002 [arXiv:1605.04909 [astro-ph.CO]].

[33] B. Fields and S. Sarkar, "Big-Bang nucleosynthesis (2006 Particle Data Group mini-review)," [arXiv:astro-ph/0601514].

[34] M. Aaboud *et al.* [ATLAS], "Measurement of the Higgs boson mass in the $H \to ZZ^* \to 4\ell$ and $H \to \gamma\gamma$ channels with $\sqrt{s} = 13$ TeV pp collisions using the ATLAS detector," Phys. Lett. B **784** (2018), 345-366 [arXiv:1806.00242 [hep-ex]].

[35] U. Lindstrom, "Supersymmetry, a biased review," Rend. Circ. Mat. Palermo S **71** (2003), 41-66 [arXiv:hep-th/0204016 [hep-th]].

[36] S. P. Martin, "A Supersymmetry primer," Adv. Ser. Direct. High Energy Phys. **21** (2010) [hep-ph/9709356].

[37] T. Moroi, "Effects of the gravitino on the inflationary universe," [hep-ph/9503210].

[38] E. W. Kolb and M. S. Turner, "The Early Universe," Front. Phys. **69** (1990) 1.

[39] G. F. Giudice and A. Masiero, "A Natural Solution to the mu Problem in Supergravity Theories," Phys. Lett. B **206** (1988), 480-484

[40] J. E. Kim and H. P. Nilles, "The mu Problem and the Strong CP Problem," Phys. Lett. B **138** (1984), 150-154

[41] G. Jungman, M. Kamionkowski and K. Griest, "Supersymmetric dark matter," Phys. Rept. **267** (1996) 195 [hep-ph/9506380].

[42] J. Polonyi, *Preprint KFK-1977-93* (1997)

[43] H. Pagels and J. R. Primack, "Supersymmetry, Cosmology and New TeV Physics," Phys. Rev. Lett. **48** (1982) 223.

[44] T. Moroi, H. Murayama and M. Yamaguchi, "Cosmological constraints on the light stable gravitino," Phys. Lett. B **303** (1993) 289.

[45] M. Bolz, A. Brandenburg and W. Buchmuller, "Thermal Production of Gravitinos," [hep-ph/0012052] (revised version)

[46] J. Ellis, M. A. G. Garcia, D. V. Nanopoulos, K. A. Olive and M. Peloso, "Post-Inflationary Gravitino Production Revisited," JCAP **1603** (2016) 008 [astro-ph/1512.05701].

[47] J. Pradler and F. D. Steffen, "Thermal gravitino production and collider tests of leptogenesis," Phys. Rev. D **75** (2007) 023509 [hep-ph/0608344].

[48] M. Bolz, W. Buchmuller and M. Plumacher, "Baryon asymmetry and dark matter," Phys. Lett. B **443** (1998) 209 [hep-ph/9809381].

[49] V. S. Rychkov and A. Strumia, "Thermal production of gravitinos," Phys. Rev. D **75** (2007) 075011 [hep-ph/0701104].

[50] M. A. G. Garcia, Y. Mambrini, K. A. Olive and M. Peloso, "Enhancement of the Dark Matter Abundance Before Reheating: Applications to Gravitino Dark Matter," Phys. Rev. D **96** (2017) no.10, 103510 [arXiv:1709.01549].

[51] M. Drees and M. M. Nojiri, "The Neutralino relic density in minimal $N = 1$ supergravity," Phys. Rev. D **47** (1993), 376-408 [arXiv:hep-ph/9207234].

[52] K. Kohri, T. Moroi and A. Yotsuyanagi, "Big-bang nucleosynthesis with unstable gravitino and upper bound on the reheating temperature," Phys. Rev. D **73** (2006), 123511 [arXiv:hep-ph/0507245 [hep-ph]].

[53] J. Ellis, D. V. Nanopoulos, K. A. Olive and S. J. Rey, "On the thermal regeneration rate for light gravitinos in the early universe," Astropart. Phys. **4** (1996), 371-386 [arXiv:hep-ph/9505438 [hep-ph]].

[54] G. Giudice, A. Riotto and I. Tkachev, "Thermal and nonthermal production of gravitinos in the early universe," JHEP **11** (1999), 036 [arXiv:hep-ph/9911302 [hep-ph]].

[55] F. D. Steffen, "Gravitino dark matter and cosmological constraints," JCAP **09** (2006), 001 [arXiv:hep-ph/0605306 [hep-ph]].

[56] J. Ellis, J. E. Kim, D.V. Nanopoulos, "Cosmological gravitino regeneration and decay," Physics Letters B, **145**, Issues 3–4, 181-186 (1984).

[57] J. R. Ellis, J. Hagelin, D. V. Nanopoulos, K. A. Olive and M. Srednicki, "Supersymmetric Relics from the Big Bang," Nucl. Phys. B **238** (1984), 453-476

[58] T. Asaka, K. Hamaguchi and K. Suzuki, "Cosmological gravitino problem in gauge mediated supersymmetry breaking models," Phys. Lett. B **490** (2000) 136 [hep-ph/0005136].

[59] L. J. Hall, K. Jedamzik, J. March-Russell and S. M. West, "Freeze-In Production of FIMP Dark Matter," JHEP **1003** (2010) 080 [hep-ph/0911.1120].

[60] N. Bernal, M. Heikinheimo, T. Tenkanen, K. Tuominen and V. Vaskonen, "The Dawn of FIMP Dark Matter: A Review of Models and Constraints," Int. J. Mod. Phys. A **32** (2017) no.27, 1730023 [arXiv:1706.07442 [hep-ph]].

[61] J. McDonald, "Thermally generated gauge singlet scalars as selfinteracting dark matter," Phys. Rev. Lett. **88** (2002), 091304 [arXiv:hep-ph/0106249 [hep-ph]].

[62] R. T. Co, F. D'Eramo, L. J. Hall and D. Pappadopulo, "Freeze-In Dark Matter with Displaced Signatures at Colliders," JCAP **12** (2015), 024 [arXiv:1506.07532 [hep-ph]].

[63] C. Cheung, G. Elor and L. Hall, "Gravitino Freeze-In," Phys. Rev. D **84** (2011), 115021 [arXiv:1103.4394 [hep-ph]].

[64] Y. Grossman, T. Kashti, Y. Nir and E. Roulet, "New ways to soft leptogenesis," JHEP **11** (2004), 080 [arXiv:hep-ph/0407063 [hep-ph]].

[65] G. D'Ambrosio, G. F. Giudice and M. Raidal, "Soft leptogenesis," Phys. Lett. B **575** (2003), 75-84 [arXiv:hep-ph/0308031 [hep-ph]].

[66] C. S. Fong, M. Gonzalez-Garcia and E. Nardi, "Leptogenesis from Soft Supersymmetry Breaking (Soft Leptogenesis)," Int. J. Mod. Phys. A **26** (2011), 3491-3604 [arXiv:1107.5312 [hep-ph]].

[67] S. Davidson, M. Losada and A. Riotto, "A New perspective on baryogenesis," Phys. Rev. Lett. **84** (2000), 4284-4287 [arXiv:hep-ph/0001301 [hep-ph]].

[68] R. Rangarajan and N. Sahu, "Perturbative Reheating and Gravitino Production in Inflationary Models," Phys. Rev. D **79** (2009), 103534 [arXiv:0811.1866 [hep-ph]].

[69] L. J. Hall, J. T. Ruderman and T. Volansky, "A Cosmological Upper Bound on Superpartner Masses," JHEP **02** (2015), 094 [arXiv:1302.2620 [hep-ph]].

[70] C. Cheung, G. Elor, L. J. Hall and P. Kumar, "Origins of Hidden Sector Dark Matter II: Collider Physics," JHEP **03** (2011), 085 [arXiv:1010.0024 [hep-ph]].

[71] C. E. Yaguna, "The Singlet Scalar as FIMP Dark Matter," JHEP **08** (2011), 060 [arXiv:1105.1654 [hep-ph]].

[72] W. Buchmuller, K. Hamaguchi, M. Ratz and T. Yanagida, "Supergravity at colliders," Phys. Lett. B **588** (2004), 90-98 [arXiv:hep-ph/0402179 [hep-ph]].

[73] G. Giudice and A. Romanino, "Split supersymmetry," Nucl. Phys. B **699** (2004), 65-89 [arXiv:hep-ph/0406088 [hep-ph]].

[74] N. Arkani-Hamed, S. Dimopoulos, G. Giudice and A. Romanino, "Aspects of split supersymmetry," Nucl. Phys. B **709** (2005), 3-46 [arXiv:hep-ph/0409232 [hep-ph]].

[75] N. Haba and N. Okada, "Structure of split supersymmetry and simple models," Prog. Theor. Phys. **114** (2006), 1057-1068 [arXiv:hep-ph/0502213 [hep-ph]].

Ringraziamenti

Al termine di questo lungo percorso desidero ringraziare le persone che mi hanno accompagnato.
Ringrazio chi ha reso possibile lo sviluppo di questo lavoro di tesi, in particolare i professori Francesco D'Eramo e Marco Peloso.

Ringrazio la mia famigia per il supporto offertomi durante questi anni, mia mamma e mia sorella, i miei nonni, mio babbo e i miei zii Angela e Pino.
Ringrazio gli amici di lunga data Giacomo, Ela, Lavinia, Margherita, Silvia, Chiara che mi hanno accompagnato in molti traguardi, e che ancora mi accompagnano oggi in questo importante momento.
Ringrazio Paolo, Francesco e Fabio, che nonostante il tempo ci abbia allontanati sono ancora qua.
Ringrazio i compagni Riccardo M. (e le diete ipocaloriche e proteiche), Alessandro (er capitano), Aldo (e i sottomarini russi) e Giulia, Matteo T. (e i sprisseti), Jan (e i sprisseti de novo), Marco Benedetto (er manetta, a cui chiedo scusa per avergli soffiato tutte le ragazze), Anna coibbluggins, Isabella volgarotta, Luca Biasolino, Chiara superTurpe, Giorgia e Elena.
Ringrazio i miei coinquilini di qeusti anni (Aldo di nuovo!), Michele e Maria, che nonstante la breve convivenza sono stati SUPER.

Un ringaziamento speciale ai colleghi del Diemme, che mi hanno accompagnato giorno dopo giorno, con i quali mi sono divertito da morire ogni minuto passato insieme: Benedetta che per gli amici c'è sempre qualcosa, Anna che te copa se non vai in f..., Giovanni antifa, Marianna che spacca tutto, Monzi che è bella solo lei, Mattia e Francesca. Per finire ringrazio er capoccia Davide e di nuovo Marianna, per aver creduto in me sin dall'inizio ed avremi offerto una bellissima possibilità di crescita. Porterò sempre con me il tempo passato con queste splendide persone, e ricorderò sempre con goia i giorni passati a correre tra i tavoli.

Un ringraziamento particolare a Marta che mi ha accompagnato in quest'ultimo strano anno, e con la quale ho condiviso momenti piacevoli.
Ringrazio lo staff del circolo Nadir e dell'osteria del Re Fosco per le serate musicali che hanno riscaldato i freddi inverni Padovani.

Ringrazio tutti coloro che mi hanno accompagnato nei cammini, insegnandomi che la fatica sparisce in compagnia, in particolare Nina.

Ricordo con profondo affetto Riccardo, a cui dedico questo importante traguardo, nell'attesa di incontrarci ancora.
Amen.